CENTRO INTERNACIONAL DE ESTUDOS
DE DOUTORAMENTO E AVANZADOS
DA USC (CIEDUS)

TESIS DE DOCTORADO

PV SYSTEMS DESIGN OPTIMIZATION AS FUNCTION OF THE CLIMATIC CONDITIONS

Cristina Cabo Landeira

ESCUELA DE DOCTORADO INTERNACIONAL

PROGRAMA DE DOCTORADO EN ENERGÍAS RENOVABLES Y SOSTENIBILIDAD ENERGÉTICA

SANTIAGO DE COMPOSTELA

2018

USC
UNIVERSIDADE
DE SANTIAGO
DE COMPOSTELA

DECLARACIÓN DEL AUTOR DE LA TESIS

PV SYSTEMS DESIGN OPTIMIZATION AS FUNCTION OF THE CLIMATIC CONDITIONS

Dña. Cristina Cabo Landeira

Presento mi tesis, siguiendo el procedimiento adecuado al Reglamento, y declaro que:

1) La tesis abarca los resultados de la elaboración de mi trabajo.
2) En su caso, en la tesis se hace referencia a las colaboraciones que tuvo este trabajo.
3) La tesis es la versión definitiva presentada para su defensa y coincide con la versión enviada en formato electrónico.
4) Confirmo que la tesis no incurre en ningún tipo de plagio de otros autores ni de trabajos presentados por mí para la obtención de otros títulos.

En Santiago de Compostela, 16 de Abril de 2018

Fdo. Cristina Cabo Landeira

USC
UNIVERSIDADE
DE SANTIAGO
DE COMPOSTELA

AUTORIZACIÓN DEL DIRECTOR/A DE LA TESIS

PV systems design optimization as function of the climatic conditions

D./Dª. Ángeles López Agüera

INFORMA:

Que la presente tesis, se corresponde con el trabajo realizado por D/Dª. Cristina Cabo Landeira, bajo mi dirección, y autorizo su presentación, considerando que reúne los requisitos exigidos en el Reglamento de Estudios de Doctorado de la USC, y que como director de esta no incurre en las causas de abstención establecidas en la Ley 40/2015.

De acuerdo con el artículo 41 del Reglamento de Estudios de Doctorado, declara también que la presente tesis doctoral es idónea para ser defendida en base a la modalidad de COMPENDIO DE PUBLICACIONES, en los que la participación del doctorando/a fue decisiva para su elaboración.

La utilización de estos artículos en esta memoria, está en conocimiento de los coautores, tanto doctores como no doctores. Además, estos últimos tienen conocimiento de que ninguno de los trabajos aquí reunidos podrá ser presentado en ninguna otra tesis doctoral.

En Santiago de Compostela, 16 de Abril de 2018

Fdo. Ángeles López Agüera

USC
UNIVERSIDADE
DE SANTIAGO
DE COMPOSTELA

"(Wo)Men of science have made abundant mistakes of every kind;
their knowledge has improved only because of their gradual
abandonment of ancient errors, poor approximations and premature conclusions"

George Sarton (1884-1956)

USC
UNIVERSIDADE
DE SANTIAGO
DE COMPOSTELA

A Dani y Pipo

USC
UNIVERSIDADE
DE SANTIAGO
DE COMPOSTELA

Agradecimientos

Esta tesis es algo que mi yo del pasado no se creería. Si he llegado aquí es, principalmente, gracias a Juan, que me dio el primer empujón para volver. Pero sin Dani y mis padres, tampoco podría haber sido posible. Su apoyo diario, junto con el de Pipo, han sido fundamentales para seguir adelante.

Este trabajo ha sido posible gracias a la colaboración del CLRLA (*Committee Local & Regional Leaders Appointment*) de UNESCO, de Norvento Enerxía, de Vitín Lema y de mis compañeros del grupo SEAG. En particular, es un poquito de Alejandro por las horas compartidas, las frustraciones y las risas.

También tengo que dar las gracias a los amigos que me han acompañado en este camino y me han animado a seguir adelante, ¡ya no os voy a dar más la lata con esto!

Y quiero acordarme también de los amigos de Bilbao y de parties, de la gente de Internet (gracias, ARM3DS) y, en representación de mi gran pasión, agradezco a Shigeru Miyamoto las horas de evasión que me ha dado.

Por último, agradecer a Qki que me haya demostrado que sí que podía. Te debo un millón de cafés.

USC
UNIVERSIDADE
DE SANTIAGO
DE COMPOSTELA

List of papers

This PhD thesis is based on the following papers:

1. C. Cabo Landeira and Á. López-Agüera, “PV Tracker System Net Gain Associated o the Local Climatic Conditions,” *Int. J. Res. Appl. Sci. Eng. Technol.*, vol. 6, no. I, pp. 185–193, 2018.

   https://www.ijraset.com/fileserve.php?FID=12677

2. C. Cabo Landeira and Á. López-Agüera, “Net benefit evaluation method for solar tracker connected PV systems,” *Int. J. Res. Appl. Sci. Eng. Technol.*, vol. 6, no. I, pp. 2638–2645, 2018.

   https://www.ijraset.com/fileserve.php?FID=13052

3. A. Braña Lopez, C. Cabo Landeira, A. Lopez Aguera, and R. Pernas Leiro, “Optimal PV technology selection depending on climatic conditions,” *Int. J. Res. Appl. Sci. Eng. Technol.*, vol. 5, no. XI, pp. 2962–2970, 2017.

   https://www.ijraset.com/fileserve.php?FID=11399

4. C. Cabo Landeira, Á. López-Agüera, and F. Núñez Sánchez, “Loss of Load Probability method applicability limits as function of consumption types and climate conditions in stand-alone PV systems,” *Int. Res. J. Eng. Technol.*, vol. 5, no. 3, pp. 2036–2043, 2018.

   https://irjet.net/archives/V5/i3/IRJET-V5I3474.pdf

USC
UNIVERSIDADE
DE SANTIAGO
DE COMPOSTELA

Index

List of abbreviations

AEMET	Agencia Estatal de Meteorología
a-Si	Amorphous silicon
B	Beam Horizontal Irradiance
C_A	Array capacity
CIS	Copper-Indium-Selenide
CM-SAF	Climate Monitoring Satellite Application Facilities
C_S	Storage capacity
DF	Diffuse Fraction
DHI	Diffuse Horizontal Irradiance
DNI	Direct Normal Irradiance
DoD	Depth of Discharge
ECMWF	European Centre for Medium-Range Weather Forecasts
E_{DC}	Energy production of a PV module
EPBT	Energy Payback Time
GHG	Greenhouse Gas
GHI	Global Horizontal Irradiance
GIS	Geographic information system
IEA	International Energy Agency
IMP_{CC}	Input Mitigation Potential in terms of Climate Change
IRR	Internal Rate of Return
I_{SC}	Short-circuit current
K_T	Clearness Index
LCA	Life Cycle Assessment
LCC	Lifecycle Cost
LLP	Loss of Load Probability
MDG	Millennium Development Goals
m-Si	Monocrystalline silicon
NASA-POWER	National Aeronautics and Space Administration - Prediction of Worldwide Energy Resource
NASA-SSE	National Aeronautics and Space Administration - Surface Meteorology and Solar Energy
NPV	Net Present Value
NREL	National Renewable Energy Laboratory
P_{max}	Maximum power
PR	Performance Ratio
PSH	Peak Sun Hours
p-Si	Polycrystalline silicon
PSM	Physical Solar Model
PV	Photovoltaics
QE	Emergency charge
RE	Renewable Energy
SDG	Sustainable Development Goals
STC	Standard Test Conditions
SUNY	State University of New York/Albany
UMG	Upgraded Metallurgical Grade polycrystalline silicon
V_{no}	Nominal output voltage
V_{OC}	Open-circuit voltage
WMM	Worst Month method
Y_f	Yield Factor
Y_r	Reference Yield

USC
UNIVERSIDADE
DE SANTIAGO
DE COMPOSTELA

ABSTRACT

The adequate sustainable development is defined as the one that, meeting the present needs, do not compromise the future generation's capability to satisfy their own needs. This concept was one of the premises for the Rio Summit in 1992, the first international attempt to develop global plans and strategies for a sustainable development. As action plans, within the framework of the United Nations, two initiatives to end the world poverty in its multiple dimensions have been developed: The Millennium Development Goals (2000-2015), and the Sustainable Development Goals (2015-2030).

The 17 Sustainable Development Goals aim to end the world hunger and poverty, protect the planet and ensure the peace and prosperity by the year 2030. Among them, the goal 7 seeks to ensure the access to sustainable, safe and reliable energy for all, including the increase of the renewable energies share in the world's energy mix.

Within the renewable energy sources, the solar photovoltaics, PV, constitutes a good alternative to the conventional power production systems. Its main strengths are the resource availability, its modularity and its competitive costs. Besides, and like the other renewable energies, it decreases the greenhouse gas emissions and reduces the external energy dependence. Its suitability increases when considering that the most vulnerable regions are those with the higher solar resource. Last, but not least, its scalability makes the solar PV suitable for small installations to large-scale centralized power generation systems.

However, there are weaknesses and threats related to the PV technology implementation. In this context, it has to be considered the technical adaptation to the new deployment scenario of highly irradiated regions with extreme climate variations and lower technical sophistication. This means that to ensure an adequate growth of the PV market, not only the different PV modules technologies response have to be assessed, but the different sizing methods and the adequate designs. And this study has to be extended to every region on the planet.

To ensure the sustainability and suitability of any energy production system, after the UN Paris Agreement in the year 2015 the need to carry out a Life Cycle Assessment, LCA, was established. Therefore, inside the new energy transition paradigm, the gain analysis of a PV system requires considering both its power production as well as the economic and environmental costs.

The evaluation of the potential impacts associated with the production, use and end of life of any product is mandatory. For it, the LCA is used to evaluate the economic, energetic and environmental impacts of an installation from the raw materials extraction process, the element's manufacturing and the transportation-associated logistics to its reuse, recycle or waste disposal.

The present work aims to provide answers to some of the questions arising from the adequate and sustainable implementation of PV installations. For that end, independent and

dedicated analysis of the design modes, sizing methods and most suitable commercial PV technologies selection have been carried. The studies have been developed as function of the climate conditions and considering the response in terms of life cycle assessment. For the climate characteristics analysis, the Köppen climate classification has been used together with the diffuse fraction of the solar radiation, DF. For the life cycle assessment, the economic impacts have been measured using the Internal Rate of Return, IRR, which measures the required time to amortize the economic investment. The energetic impacts have been evaluated with the Energy Payback Time, EPBT, which measures the required time to recover the energy used in all the PV life stages. Additional impacts, as the environmental Input Mitigation Potential, IMP, strongly depend on the regional regulations. Hence, they are not considered in the present work.

As a difference with respect to previous studies and intending to minimise the meteorological and climate models' dependence, validated experimental data are used. Likewise, all the carried studies are based on experimental setups conformed of mature commercial-phase PV technologies. In some cases, the studies have been complemented with dedicated laboratory tests, always under real sun conditions.

Thereby, **Chapter 2** evaluates the suitability of solar tracker systems, also known as trackers, with respect to fixed-tilt PV systems as function of the climate conditions. These devices are designed to maximise the PV system's power production by continuously following the sun's path. On the other hand, the fixed-tilt PV systems design are the cheapest option, but do not optimise their performance along the year.

Currently, the grid-connected centralised PV systems represent the main share of the systems in operation, with a forecast of a 5% annual growth in the next decade. The result of this research has been published in Volume 6, Issue I of the *International Journal for Research in Applied Science & Engineering Technology* with the title "*PV tracker system net gain associated to the local climatic conditions*".

On this chapter, the analysis of two identical PV systems is presented. The same-technology, same-manufacturer arrays are installed in a PV field owned by Norvento Enerxía in Lugo (Spain). While one of the PV arrays is equipped with a tracker, the other is installed with a fixed tilt. The analysis shows a production increase of the 60% for the tracker on a fully sunny day with high solar irradiation. By contrast, a study carried in overcast conditions shows no difference in production between both arrays. This high variation creates the need to carry out a detailed study as function of the climatic conditions.

To relate the production difference between both arrays the diffuse fraction, DF, is used as it measures the cloudiness levels as the ratio between the diffuse and the global radiation. The solar radiation values are obtained in the PV field and from a close meteorological station. The difficulty arising is that these stations do not measure diffuse solar radiation. Due to the distance to the closest meteorological station with diffuse radiation experimental values, Meteogalicia-EOAS, a criterion is developed to compare both locations in climate conditions terms. This criterion includes conditions over the global radiation's average daily values and daily total sum, as well as over the global radiation spectra along the day.

For the days verifying the criterion, the Performance Ratio, PR, of each array is used to avoid location or seasonality biases. This allows calculating the net gain of the tracker-equipped array compared to the fixed-tilt PV system as function of the DF value.

The variation of the Performance Ratio variation between both PV systems, σ(PR), shows a linear decreasing response with the increasing DF. When DF tends to zero, this gain is almost 80%. In overcast conditions, with DF tending to one, it is compatible to zero.

The tracker gain cannot be assessed considering only its production increase. Besides the required maintenance and the power consumption, for its profitability analysis the economic and energetic costs must be assessed due to the raw materials and manufacturing processes increasement compared to a fixed-tilt system. For a tracker-equipped system, the EPBT is double than for a fixed-tilt system, while the IRR is a 50% higher for the tracker. Both costs show a positive slope with the DF due to the increasing number of required years to compensate the energetic and economic investments associated to the tracker installation.

The sum of the economic and energetic costs is measured with the Cost Variation, σ(CV). Thus, σ(PR) and σ(CV) allow to define the required climate conditions to obtain a net gain for installing a tracker. On average, the DF limit value for gain is 0.41; higher values make a tracker non-profitable. Considering a 2σ standard deviation, this value varies between 0.14 and 0.68.

The obtained results offer an interesting opportunity: Extrapolate the analysis to anywhere on the planet. This is the goal of **Chapter 3**, published in Volume 6, Issue I of the *International Journal for Research in Applied Science & Engineering Technology* titled as "*Net benefit evaluation method for solar tracker connected PV systems*".

The challenge of extent this method is finding a reliable data source with solar global and diffuse radiation values for any location. While there are several databases for solar global radiation, the main obstacle is the lack of experimental diffuse radiation values.

For this analysis, the initial hypothesis is the existence of a climate classification which allows characterizing the climates as function of the DF. Besides, it is considered that the previously obtained experimental relations can be extended to an annual basis and that the annual average DF value of each climate is adequate for the study.

Extending the method to any location requires finding a suitable solar radiation database and a data grouping system. For that, the Köppen-Geiger climate classification is selected. This classification numerically defines the climates as function of temperatures and precipitations. With five main climate categories, it defines subtypes according to the temperature and precipitation seasonality.

Once defined the cataloguing system, the radiation database is selected. Due to the lack of sufficient meteorological stations with experimental solar radiation values to characterize any world location, the NASA-SSE database is selected. Besides the solar global and diffuse radiation values for a location, this satellite database provides temperature and precipitation values.

The NASA-SSE database is validated with experimental solar global and diffuse radiation values from AEMET. The low difference between both databases allows to consider the NASA-SSE as a valid data source for the solar radiation values. With this, the climatic database is created with over 35000 representative values of the 29 existing Köppen climates.

The analysis of the monthly diffuse fraction values for each climate allows to confirm the initial hypothesis that the DF describes the different climates and its seasonality. The statistical analysis shows the results validity.

Since the PV production analyses are done on an annual basis, the tracker gain is assessed using the annual average DF value for each climate. The results are compatible with the published by different authors. However, it can be seen the tracker production gain is limited to certain climates.

When, in addition to the production increase, the economic costs are accounted, all the climates but the polar show a positive gain. The analysis of the environmental costs allows calculating the net gain, σ(PRN), as the difference between the production variation, σ(PR), and the associated costs, σ(CV). This net gain varies, on average, from the 27% to the -50% depending on the climate.

Due to the high errors associated with the method, tendencies are analysed. The advised climates are mainly savannah, semi-arid, desert and Mediterranean or continental climates with hot summers. A positive tendency appears in dry tropical and Mediterranean temperate climates. As a general tendency, it can be seen that the installation of trackers is not advised for latitudes over 40ºN.

These results allow to primarily assess the solar tracker suitability. But, in addition to the design analysis, the optimization of a PV system requires the PV modules technology to be adequate. This selection has to be analysed for all kind of PV installations to ensure the minimum environmental cost for the system.

The adequate selection of the optimal PV modules as function of the climate is another detected weakness in the PV technology implementation. The **Chapter 4** is dedicated to this analysis and its results are published in Volume 5, Issue XI of the *International Journal for Research in Applied Science & Engineering Technology* with the title "*Optimal PV technology selection depending on climatic conditions*".

When designing a PV system, it is common to select the modules after its price, availability and expected lifetime. Nevertheless, the efficiency of a PV technology depends on the irradiation levels on the system's location and on the module's temperature.

For the analysis, two experimental setups measured under real sun conditions are used. In one, the module's temperature and the solar irradiation are controlled values, while the other is measured under standard operation conditions. The results comparison allows to evaluate the analysed commercial PV technologies response and validate the results.

The relevance of this analysis is that no previous studies of degradation have been carried under real sun conditions in highly irradiated regions. The existing studies are limited to

temperate climate conditions or based on simulations. Besides, extreme irradiation conditions are not considered for the PV modules certification.

The controlled conditions setup analyses brand-new commercial PV modules of monocrystalline (m-Si), polycrystalline (p-Si), upgraded metallurgical grade polycrystalline (UMG) and Copper-Indium-Selenide (CIS) technologies. This setup allows to separately measure each technology response under fixed temperature or irradiation conditions. Using a curve tracer, production values are obtained at fixed module temperature with irradiation variation, and also at fixed irradiation values with module temperature variation. Besides, this setup allows to calculate the temperature coefficients for each technology.

The standard conditions setup is a grid-connected PV field with different silicon-based PV technologies; amorphous (a-Si), monocrystalline (m-Si) and polycrystalline (p-Si). The period of analysis is selected to avoid modules ageing effects and focuses on highly irradiated months.

The analysis of the PV technologies in controlled and standard conditions allows determining which are the optimal technologies as function of the solar irradiation levels and temperature. The main results show a better performance with the temperature and a great stability along the full radiation spectra for the p-Si. Nevertheless, the UMG shows also a good response. The m-Si is more efficient for medium to high radiation levels.

The climatic analysis of the results shows that the p-Si is the optimal PV technology for desert, semi-arid, and hot and dry summer climates. The p-Si and UMG technologies are advised for hot, humid climates, like tropical and monsoon climates. For temperate and cool summer continental climates, the m-Si, p-Si and UMG technologies are adequate. Highland and polar climates allow to install any silicon-based PV technology.

Against this backdrop of PV systems expansion, the stand-alone PV systems are increasing its market share due to the energetic independence they provide to users anywhere in the world. Thus, **Chapter 5** analyses the stand-alone PV systems sizing considering its economic and environmental costs. The results have been published on Volume 5, Issue III of the *International Research Journal of Engineering and Technology* with the title "*Loss of Load probability method applicability limits as function of consumption types and climate conditions in stand-alone PV systems*".

Unlike the grid-connected PV systems, the stand-alone PV systems sizing requires calculating the number of PV modules of the array and the required batteries system to ensure its autonomy. This sizing is suitable if, besides fulfilling the user's expected comfort levels, the final product is economically affordable and has the minimum possible environmental impacts.

On this final chapter the limitations of some of the most frequent sizing methods are analysed and, after them, a reliability-based sizing method is proposed.

The Worst Month method, WMM, is one of the most used sizing methods despite its conservative character. For the calculation, the month with the higher energy demand and the lower available radiation are used. This generates a system oversizing, especially relevant in high seasonality climates.

An alternative to the WMM is the LLP method, Loss of Load Probability. Its main hypothesis is that the reliability of a PV system, defined as the ratio between the energy deficit and demand, can be fixed. For its use, the PV array and battery system are sized and, for a fixed reliability, the battery-array pairs represent an isoreliability curve. For the calculation, the LLP method considers a constant energy demand provided by the batteries, besides of using the average solar radiation value.

However, these hypotheses are inadequate as they do not reflect the real power consumption scenarios nor allow to distinguish mainly diurnal or nocturnal energy demands, besides of not representing the climates seasonality.

To include this variability on the system's sizing, a reliability-based sizing method is proposed. The developed program is based on the battery system's state of charge calculation and, unlike the previous methods, allows to analyse different power consumption types and the climate seasonality.

This program is used with the experimental solar radiation and power consumption values of a single-family home disconnected from the grid in December 2015. The PV system sizing was done using the WMM considering 3 days of autonomy for the system. The use of the program over the power consumption values allows to determine the PV system's reliability as a 99.75%.

Besides its use for sizing new PV systems, the proposed method allows to analyse existing PV systems to increase the reliability or assess its capability to withstand the ageing effects. For it, a simple algorithm, which can be used in any scenario, has been designed to evaluate the associated economic and energetic costs. As an example, the analysis of the used PV system to increase its reliability to a 99.9%, shows that it can be done with a 20% increase in batteries or a 17% in modules.

A 20% decrease in the batteries capacity and the array power production is estimated at the PV system's end of life. The analysis shows that the studied system, with its current configuration, can assume even higher decreases maintaining a 99% reliability, adequate for the domestic use.

The developed work shows the possibility of developing new lines of work, both with research centres and technology companies for commercial products development.

RESUMEN

El desarrollo sostenible adecuado se define como aquel que, satisfaciendo las necesidades del presente, no compromete la capacidad de las futuras generaciones para satisfacer sus propias necesidades. Este concepto fue una de las premisas utilizadas en la Cumbre de Río de 1992, primer intento internacional de desarrollar planes y estrategias globales para un desarrollo sostenible. Como planes de acción, en el marco de las Naciones Unidas se han desarrollado dos iniciativas dedicadas a acabar con la pobreza mundial en sus múltiples dimensiones: los Objetivos de Desarrollo del Milenio (2000-2015) y los Objetivos del Desarrollo Sostenible (2015-2030).

Los 17 Objetivos del Desarrollo Sostenible tienen como objetivo erradicar el hambre y la pobreza del mundo, proteger el planeta y asegurar la paz y prosperidad de todos los habitantes para el año 2030. De entre ellos, el objetivo 7 busca asegurar el acceso a energía sostenible, segura y asequible para todos, incluyendo el incremento del porcentaje de las energías renovables dentro del mixing energético mundial.

Dentro de las fuentes energéticas renovables, la energía solar fotovoltaica, PV, constituye una buena alternativa a los sistemas de producción eléctrica convencionales, siendo sus principales fortalezas la disponibilidad de recurso, su modularidad y sus costes competitivos. Además, al igual que el resto de las energías renovables, disminuye las emisiones de gases de efecto invernadero y reduce la dependencia energética externa. Su idoneidad aumenta si se tiene en cuenta que las zonas en mayor riesgo de exclusión son aquellas que disponen de mayor recurso solar. Por último, aunque no menos importante, su escalabilidad hace que resulte oportuna tanto para pequeñas instalaciones como para sistemas de generación centralizados a gran escala.

Sin embargo, también existen debilidades y amenazas asociadas a la implementación de esta tecnología. En este ámbito, hay que considerar la adecuación de la técnica al nuevo escenario de explotación con niveles más altos de recurso solar, variaciones climáticas extremas y menos sofisticado tecnológicamente. Esto implica que, para asegurar un adecuado crecimiento del mercado PV, han de analizarse cuidadosamente no solo la respuesta de las múltiples tecnologías de módulos PV, sino los diferentes métodos de dimensionado y diseños más adecuados. Y este estudio ha de extenderse a cada región del planeta.

Para asegurar la sostenibilidad y adecuación de cualquier sistema de producción energética, en el acuerdo de París de Naciones Unidas del año 2015, se estableció la necesidad de realizar un análisis del ciclo de vida, LCA (*Life Cycle Assessment*). Por tanto, dentro del nuevo paradigma de transición energética, el análisis de rentabilidad de un sistema PV ha de tener en cuenta tanto su producción eléctrica como los costes económicos y medioambientales asociados.

La evaluación de los potenciales impactos asociados a la producción, uso y fin de la vida útil de cualquier producto es esencial. Para ello, se utiliza el LCA, que evalúa los impactos

económicos, energéticos y medioambientales de una instalación desde el proceso de extracción de materias primas, fabricación de los elementos y logística asociada al transporte hasta su reutilización, reciclado o eliminación de desechos.

El trabajo que se presenta tiene como objetivo dar respuesta a algunas de las cuestiones abiertas en el campo de la implantación adecuada y sostenible de instalaciones fotovoltaicas. Para ello, se han realizado análisis dedicados e independientes de los modos de diseño, métodos de dimensionado y selección de las tecnologías comerciales más apropiadas. En cada uno de los casos el trabajo se ha desarrollado en función de las condiciones climáticas y atendiendo a la respuesta en términos de ciclo de vida. Para el análisis de las características climáticas, se han utilizado la clasificación de Köppen y la correspondiente fracción de componente difusa de la radiación solar, DF. En cuanto al ciclo de vida, el impacto económico se ha medido usando el *Internal Rate of Return,* IRR, que evalúa el tiempo necesario para amortizar la inversión. El impacto energético se ha evaluado mediante el *Energy Payback Time*, EPBT, que mide el tiempo requerido para recuperar la energía consumida en todas las etapas de la vida de la instalación. El resto de los impactos, como el potencial de mitigación de impactos medioambientales, IMP (*Input Mitigation Potential*), dependen fuertemente de regulaciones regionales. Por tanto, no serán objeto de estudio en este trabajo.

Como hecho diferencial respecto a estudios previos, y con el fin de disminuir en lo posible la dependencia de modelos climáticos y meteorológicos, se han utilizado datos experimentales validados. Asimismo, todos los estudios están basados en dispositivos experimentales construidos con tecnologías fotovoltaicas maduras y en fase comercial. En algunos casos, los estudios han sido completados realizando test dedicados de laboratorio, siempre en condiciones de sol real.

Así, en el **Capítulo 2** se evalúa la idoneidad de los sistemas con seguimiento solar, también conocidos como *trackers*, respecto de sistemas PV a ángulo fijo en función de las condiciones climáticas. Estos sistemas, que siguen de forma continua la trayectoria del sol, se diseñan para maximizar la producción eléctrica del sistema PV. Por el contrario, los diseños de sistemas a ángulo fijo son más económicos pero no optimizan su rendimiento a lo largo del año. En la actualidad, los sistemas PV centralizados y conectados a red representan un gran porcentaje de los sistemas en operación, con una previsión de crecimiento del 5% anual para la siguiente década. El resultado de este estudio ha sido publicado en el Volumen 6, Número I de la revista *International Journal for Research in Applied Science & Engineering Technology* con el título "*PV tracker system net gain associated to the local climatic conditions*".

En el presente capítulo, se presenta el análisis realizado sobre dos dispositivos experimentales idénticos, de la misma tecnología y mismo fabricante, instalados en un campo de producción fotovoltaica propiedad de Norvento Enerxía en Lugo (España). Uno de ellos está equipado con un tracker mientras que el otro está instalado a ángulo fijo. El análisis muestra un incremento en producción del 60% a favor del tracker en un día completamente soleado y con alta radiación solar. Por el contrario, un estudio realizado en días nublados muestra diferencias nulas en producción entre ambos dispositivos. Esta alta variación motiva la necesidad de un estudio más profundo en función de las condiciones climáticas.

Para relacionar la diferencia en producción entre ambos sistemas se utiliza la fracción de difusa, DF, que mide el nivel de nubosidad como cociente entre radiación difusa y global. Los

datos de radiación solar utilizados en el estudio proceden del propio campo PV y de una estación meteorológica cercana. La dificultad que surge es que ninguna de ellas dispone de medidas de radiación difusa. Debido a la distancia a la estación más cercana con valores experimentales de radiación difusa, Meteogalicia-EOAS, se desarrolla un criterio para comparar ambas ubicaciones en términos de condiciones climáticas. Este criterio incluye condiciones sobre los valores promedio diario y suma total diaria de radiación global, así como sobre el espectro de radiación a lo largo del día.

Para los días que verifican el criterio, se calcula el Performance Ratio, PR, de cada sistema para evitar sesgos asociados a la ubicación o época del año. Esto permite calcular la ganancia neta del sistema con tracker respecto del instalado a ángulo fijo en función de la DF.

La variación del Performance Ratio entre ambos sistemas, σ(PR), muestra un comportamiento lineal decreciente con el incremento de DF. Cuando DF tiende a cero, esta ganancia se acerca al 80%. En condiciones de nubosidad, con DF tendiendo a uno, es compatible con cero.

La ganancia de un tracker no puede evaluarse considerando solo su incremento en producción. Además del mantenimiento necesario y su consumo de energía, para el análisis de su rentabilidad es necesario evaluar sus costes energéticos y económicos debido al mayor uso de materias primas y procesos de fabricación respecto de un sistema a ángulo fijo. El EPBT para un sistema con tracker es el doble que a ángulo fijo, mientras que el IRR es un 50% mayor para el tracker. Ambos costes muestran una pendiente positiva respecto de DF debido al creciente número de años necesarios para compensar la energía e inversión asociadas a la instalación del tracker.

La unión de ambos costes se mide con el Cost Variation, σ(CV). Así, σ(PR) y σ(CV) permiten definir las condiciones climáticas necesarias para obtener ganancia neta al instalar un tracker. En promedio, el valor límite de DF para tener ganancia es 0.41; valores superiores hacen que un tracker no sea rentable. Considerando 2σ de desviación estándar, este valor de DF varía entre 0.14 y 0.68.

Los resultados obtenidos ofrecen una interesante oportunidad: Extrapolar el análisis a cualquier lugar del planeta. Ese es el objetivo del **Capítulo 3**, publicado en el Volumen 6, Número I de la revista *International Journal for Research in Applied Science & Engineering Technology* bajo el título "*Net benefit evaluation method for solar tracker connected PV systems*".

El reto de extender este método es disponer de una fuente de datos de radiación global y difusa localmente fiable. Mientras que para los valores de radiación solar global existen múltiples bases de datos, el principal obstáculo es la ausencia de datos experimentales de radiación difusa.

Para este análisis, se plantea como hipótesis inicial que existe alguna clasificación climática que permite caracterizar los climas en función de la fracción de difusa. Además, se considera que las relaciones experimentales anteriormente obtenidas pueden extenderse a una base anual y que el promedio anual de la DF de cada clima es adecuado para este estudio.

Extender el método a cualquier ubicación requiere encontrar una base de datos de radiación solar adecuada y un sistema que agrupe los datos. Para esto, se elige la clasificación climática de Köppen-Geiger, que define numéricamente los climas en función de temperaturas y precipitaciones. Partiendo de cinco grupos climáticos principales, define distintos subtipos en función de la estacionalidad de precipitaciones y temperaturas.

Definido el sistema de catalogación, se selecciona la base de datos de radiación. Debido a la ausencia de suficientes estaciones meteorológicas con valores experimentales de radiación para caracterizar cualquier ubicación, se selecciona la base de datos NASA-SSE. Además de valores de radiación global y difusa para un lugar, esta base de datos satelital proporciona valores de temperatura y precipitación.

La base de datos NASA-SSE se valida con valores experimentales de radiación solar global y difusa de AEMET. La baja diferencia entre ambas bases de datos permite considerar NASA-SSE como una fuente de datos válida para los valores de radiación solar. Con esto se construye la base de datos climática, con más de 35000 valores representativos de los 29 climas Köppen existentes.

El análisis del comportamiento mensual de la fracción de difusa para cada clima permite confirmar la hipótesis inicial de que DF describe los diferentes climas y su estacionalidad. El análisis estadístico muestra la validez de los datos.

Debido a que los análisis de producción PV se realizan en base anual, se evalúa la ganancia asociada a la instalación de un tracker utilizando el promedio anual de DF de cada clima. Los resultados obtenidos son compatibles con los publicados por diferentes autores. Sin embargo, se observa que los incrementos de producción se limitan a algunos climas.

Cuando además del incremento en producción se tienen en cuenta los costes económicos asociados, todos los climas excepto los polares, muestran una ganancia positiva. Al tener en cuenta los costes medioambientales, se puede calcular la ganancia neta del sistema, $\sigma(PRN)$, como diferencia entre la variación de producción, $\sigma(PR)$, y los costes asociados, $\sigma(CV)$. Esta ganancia neta varía, en promedio, del 27% al -50% dependiendo del clima.

Debido a los altos errores asociados al método, se analizan tendencias de comportamiento. Los climas recomendados son principalmente de sabana, semiáridos, desérticos, y mediterráneos y continentales con veranos cálidos. Se presenta una tendencia positiva en climas tropicales secos y mediterráneos templados. En general, se observa que para latitudes superiores a 40° la instalación de un tracker es poco recomendable.

Estos resultados permiten evaluar de forma primaria la idoneidad de instalar un tracker. Pero además del análisis del diseño, la optimización de un sistema PV requiere que la tecnología de módulos PV sea adecuada. Esta selección ha de ser analizada en todo tipo de instalaciones PV para asegurar el menor coste medioambiental del sistema.

Otra de las debilidades detectadas en la implantación de la tecnología fotovoltaica es realizar una adecuada selección de los módulos PV óptimos en función del clima. Este estudio, al que se dedica el **Capítulo 4**, ha sido publicado en el Volumen 5, Número XI de la revista

International Journal for Research in Applied Science & Engineering Technology y titulado "*Optimal PV technology selection depending on climatic conditions*".

Al diseñar un sistema PV, es habitual seleccionar los módulos en base a precio, disponibilidad y tiempo de vida esperado. Sin embargo, la eficiencia de una tecnología PV depende de los niveles de radiación en la ubicación y de la temperatura del módulo. Por tanto, la optimización de un sistema PV requiere seleccionar la tecnología más adecuada en función de las condiciones de temperatura e irradiación para la ubicación.

Para este análisis se utilizan dos montajes experimentales medidos en condiciones de sol real. En uno de ellos se controlan temperatura de módulo e irradiación solar, mientras que el otro se mide en condiciones estándar de operación. La comparación de los resultados permite evaluar el comportamiento de las tecnologías PV comerciales analizadas y validar los resultados.

La relevancia de este análisis radica en la ausencia de estudios previos de degradación en condiciones de sol real en zonas altamente irradiadas. Los estudios existentes suelen limitarse a condiciones climáticas intermedias o estar basados en simulaciones. Además, las condiciones extremas no se consideran en la certificación de módulos PV.

El montaje en condiciones controladas analiza módulos PV comerciales nuevos de tecnologías monocristalina (m-Si), policristalina (p-Si), policristalina de calidad metalúrgica (UMG) y Cobre-Indio-Selenio (CIS). Este montaje permite medir separadamente la respuesta de cada tecnología en condiciones de temperatura o irradiación fijas. Con el uso de un trazador de curvas se obtienen datos de producción a temperaturas de módulo fijas con irradiación variable, y a irradiación fija con variación de temperatura del módulo. Además, permite calcular los coeficientes de temperatura para cada tecnología.

El montaje en condiciones estándar es un campo de producción PV conectado a red con diferentes tecnologías PV basadas en silicio; amorfo (a-Si), monocristalino (m-Si) y policristalino (p-Si). El período de análisis evita efectos asociados al envejecimiento de módulos y se centra en meses altamente irradiados.

El análisis de tecnologías PV en condiciones controladas y en condiciones estándar permite determinar cuáles son las tecnologías óptimas en función de los niveles de radiación solar. Los resultados generales muestran un mejor comportamiento con la temperatura y una gran estabilidad del p-Si en todo el espectro de radiación. No obstante, el UMG muestra también una buena respuesta. El m-Si es más eficiente en radiaciones medias a altas.

Realizando un análisis climático de los resultados, el p-Si aparece como la tecnología PV óptima para climas desérticos, semiáridos o con veranos cálidos y secos. Las tecnologías p-Si y UMG están recomendadas para climas húmedos y cálidos, como tropicales y monzónicos. En climas templados y continentales de veranos frescos, las tecnologías m-Si, p-Si y UMG resultan adecuadas. Climas polares y de alta montaña permiten instalar cualquier tecnología PV basada en silicio.

En el actual escenario de expansión de los sistemas PV, los sistemas aislados cuentan con una creciente presencia debido a la independencia energética que ofrecen a usuarios en

cualquier lugar del planeta. Por ello, el **Capítulo 5** se centra en el análisis del dimensionado de los sistemas PV aislados teniendo en cuenta sus costes económicos y medioambientales. Los resultados de este análisis han sido publicados en el Volumen 5, Número III de la revista *International Research Journal of Engineering and Technology* bajo el título "*Loss of Load probability method applicability limits as function of consumption types and climate conditions in stand-alone PV systems*".

A diferencia de los sistemas conectados a red, el dimensionado de sistemas aislados requiere calcular el número de módulos que conformarán el array PV y el sistema de baterías necesarios para asegurar su autonomía. Este dimensionado será adecuado si, además de cumplir los niveles de confort esperados por el usuario, el producto final es económicamente asequible y el impacto medioambiental asociado es mínimo.

En este último capítulo se analizan las limitaciones de algunos de los métodos de dimensionado más comunes y, a partir de ellas, se propone un método de dimensionado basado en fiabilidad.

El método de dimensionado del peor mes, WMM (*Worst Month Method*), es uno de los más utilizados a pesar de su carácter conservador. Al considerar para el cálculo el mes de mayor demanda energética y el de menor radiación disponible, se genera un sobredimensionamiento que es especialmente relevante en climas con alta estacionalidad.

Una alternativa al WMM es el método LLP (*Loss of Load Probability*). Su hipótesis básica es que la fiabilidad de un sistema PV, definida como el cociente entre déficit y demanda de energía del sistema, puede ser fijada. Para su aplicación, se realiza el dimensionado del array PV y del sistema de baterías y, para una fiabilidad definida, los pares de valores batería-array representan una curva de isofiabilidad. Las distintas propuestas de este método consideran para el cálculo una demanda de energía constante y procedente de las baterías, así como el uso del valor promedio de la radiación solar.

Sin embargo, estas hipótesis resultan inadecuadas ya que no reflejan los escenarios de reales consumo ni permite diferenciar consumos predominantemente diurnos o nocturnos, además de no representar la estacionalidad de los climas.

Para incluir esta variabilidad en el dimensionado se propone un método basado en fiabilidad. El programa desarrollado está basado en el cálculo del estado de carga del sistema de baterías y, a diferencia de los métodos anteriores, permite analizar diferentes tipos de consumo y la estacionalidad climática.

Se utiliza este programa sobre los datos experimentales de radiación solar y consumo de una vivienda unifamiliar desconectada de la red eléctrica en diciembre de 2015. El dimensionado del sistema PV se realizó utilizando el WMM y considerando 3 días de autonomía. El uso del programa sobre los datos de consumo ha permitido determinar la fiabilidad del sistema PV en un 99.75%.

Además de su uso para el dimensionado de nuevos sistemas PV, el método propuesto permite realizar análisis de sistemas existentes para incrementar su fiabilidad o estudiar su capacidad para resistir los efectos del envejecimiento. Para ello, se ha diseñado un algoritmo de

evaluación simple de los costes económicos y energéticos asociados que puede ser utilizado de forma simple en cualquier escenario. Como ejemplo, el análisis del sistema PV utilizado para aumentar su fiabilidad a un 99.9% indica que se podría lograr con un incremento de un 20% en baterías o de un 17% en paneles.

Se estima en un 20% la disminución de capacidad de baterías y de producción del array al final de la vida útil del sistema PV. El análisis muestra que el sistema en estudio, con su dimensionado actual, puede asumir disminuciones incluso mayores manteniendo una fiabilidad del 99%, adecuada para el uso doméstico.

El trabajo realizado ofrece la posibilidad de abrir nuevas líneas de trabajo, tanto con centros de investigación como con empresas tecnológicas para el desarrollo de productos comerciales.

USC
UNIVERSIDADE
DE SANTIAGO
DE COMPOSTELA

Chapter 1 - Introduction

The sustainable development was defined in 1987 in the Brundtland Report as “the development that meets the needs of the present without compromising the ability of future generations to meet their own needs" [1][2]. This report, often known as Our Common Future, was developed by the World Commission on Environment and Development to investigate the growing concerns about the environment. It focused on the severe and negative impacts of the human activity on the planet and the unsustainability of the pattern of growth and development.

The concept of sustainable development was the base for the United Nations Conference on Environment and Development held in Rio de Janeiro in 1992 [3]. This summit, attended by over 100 Heads of State and representatives from 178 national governments, was the first international attempt to develop plans and strategies for a more sustainable development as the major world challenge. To evaluate the advances after the Rio summit, the World Summit on Sustainable Development was held in Johannesburg in 2002 [4]. This summit, attended by 191 national governments, United Nations agencies and other major groups, led to key commitments on sustainable consumption and production, water, sanitation and energy.

As action plans, the United Nations has developed the two major initiatives to end the world poverty in its multiple dimensions: The Millennium Development summit, in the year 2000, and the Sustainable Development summit, in the year 2015.

The Millennium Development Goals (MDG) summit was the first attempt to globally meet 8 goals to end the world’s poverty by the year 2015 [5]. Despite not including clean energy or electricity access as a goal, the goal 7 was focused to ensure the environmental sustainability. The results, published in the year 2015, showed a variable success on the different objectives.

Against this backdrop, the 17 Sustainable Development Goals (SDG) [6] are defined to go further on the MDG. The goals to be reached by 2030 include ending the world hunger and poverty, protect the planet and ensure the peace and prosperity. The goal 7 aims to **“**ensure access to affordable, reliable, sustainable and modern energy for all” [7]. Inside this goal, the targets include increase the share of renewable energy and supply sustainable energy services for all, particularly focusing on developing countries.

The renewable energies (RE) are clean, inexhaustible and increasingly cost-competitive with the conventional fossil fuels. Its utilization plays a key role in the climate change mitigation as the RE implementation decrease the greenhouse gas (GHG) emissions [8]. In addition, the RE reduce the external energy dependence, particularly favourable when considering the fossil fuels variable costs [9]. Among the RE, the solar energy is one of the best candidates for power production due to the resource availability and competitive costs with conventional energy sources.

The utilization of solar photovoltaics (PV) for electrical power generation is general across the world due to its availability and competitive cost. Figure 1.1a-b respectively show the solar

resource availability and the energy deficit during night-time in the world. The comparison of both maps shows that the higher solar resource availability areas have the lower night illumination access. Even though some of these regions are uninhabited, these high-resource regions include populated areas without proper electricity access despite the high solar potential. Its global availability makes the solar energy a sustainable alternative to the conventional power production systems. But its adequateness is higher when the regions in energy deficit are also considered as these regions show the most abundant solar resource.

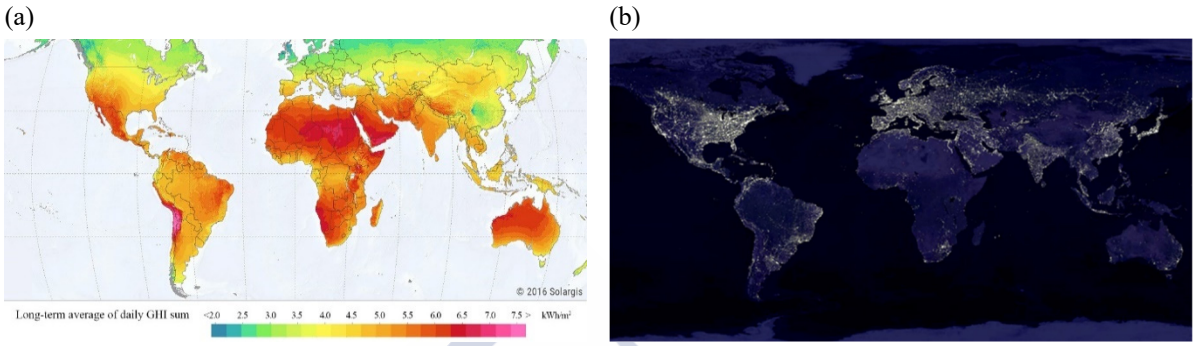

Figure 1.1. (a) Solar resource availability and (b) night power availability [10][11]

A simple SWOT (Strengths, Weaknesses, Opportunities, and Threats) analysis of the current and future perspectives for the PV massive deployment shows its main **strengths**; the technology robustness and its maturity level in the energy market. Following the Swanson's law [12], the solar PV modules tend to decrease a 20% for every doubling of the cumulative installed power. At present rates, the costs halve about every 10 years. In fact, the price of PV cells shows an almost constant price drop (Figure 1.2). This pricing fall is related to the silicon price decrease [13], crucial since PV panels prevalent technologies are silicon-based, with over 90% of market share [14].

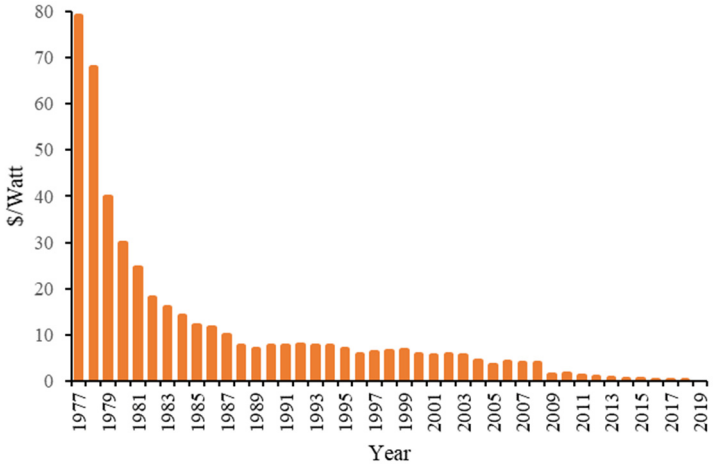

Figure 1.2. Evolution of silicon PV cells price [15][16]

These positive perspectives favour the **opportunity** to expand the PV technology. The PV deployment is mainly a consequence of its scalability, which makes it suitable for small installations to large-scale centralized power generation systems.

On this PV market growth scenario, the uncontrolled proliferation of new technologies in early maturity level represent some **threats** and **weaknesses**. Most of them are related to the rapid growth of the technology, with multiple solar panel technologies and increasingly sophisticated designs. An example of these complex designs are the solar tracker systems for power production maximization.

The major development of PV systems is focused on temperate climate regions with intermediate radiation levels. Therefore, the commercially available PV technologies have not been properly tested under extreme climate conditions. This is a weakness on the PV expansion since the greatest potential for the future PV technology deployment are the third countries, climatically characterized by a high solar irradiation and extreme temperatures. The evaluation of the technologies response under these extreme conditions is mandatory as it is known that high levels of temperature and radiation affect to the system's efficiency and accelerate the degradation [17][18][19].

Choosing the optimal design is another relevant issue. The decision of include a tracker system to increase the solar catchment requires evaluating its effect in terms of economic cost and maintenance. Even if this increase strongly depends on the climate conditions, the published studies are biased to results in a given location climate or depend on microphysics models [20][21].

Last but not least, it must be noticed that, until a few years ago, the impact of a technology on the climate change was not considered. But the climate change mitigation has also to be accounted. The lifecycle analysis, LCA, allows to evaluate the environmental impacts associated with an energy production system. After the UN Paris Agreement in the year 2015 [22], and inside the new energy transition paradigm, these environmental costs cannot be ignored [23][24].

The motivation behind the present work is to provide answers to some of the questions that arise from the presented threats. After the already presented main challenges for the PV market development, Figure 1.3 sums the photovoltaic energy evolution. After the early PV development, the silicon price drop led to an increasing presence of PV systems with the appearance of new technologies, not always as mature as required for the new markets. But also, the new users require higher reliability on their PV systems. These topics will be the subject of study in the present work.

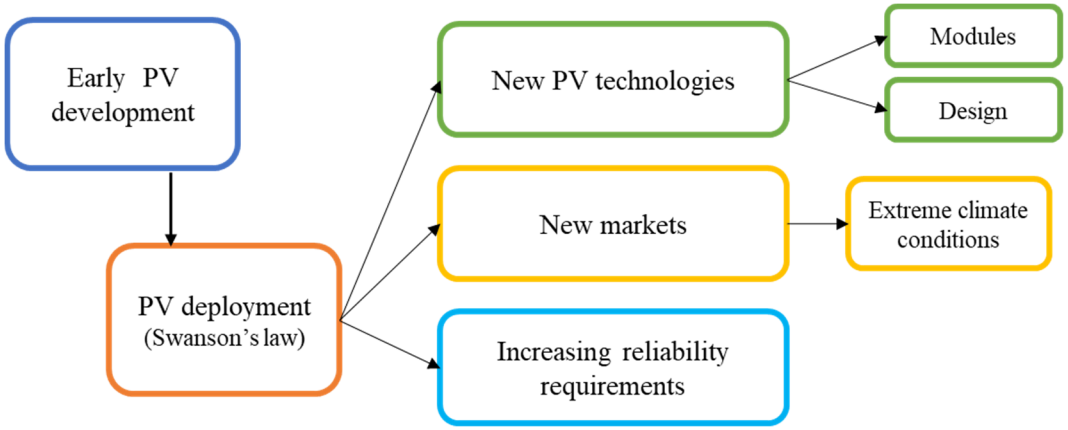

Figure 1.3. Scheme of PV deployment consequences

The optimal design of a PV system as function of the climate conditions is analysed in Chapter 2. The current trend of installing solar tracking systems shows variable responses, hence, including these systems on the design must be carefully evaluated. To that end, and after experimental data, a relation between the net gain of a tracker-equipped PV system compared to a fixed-tilt system is obtained as function of the climate conditions. This net gain considers both the power production as well as the economic and energetic associated costs.

The Chapter 3 goes further into the study of the climate conditions. Also, an extended analysis of the tracker suitability as function of the climate is carried out. This study is developed after the experimental relation obtained in Chapter 2. As result, a decision table to evaluate the suitability of the tracker system as the optimal PV design is presented.

The selection of the optimal PV technology as function of the climate conditions is evaluated in Chapter 4. This topic is crucial to ensure the optimum performance of the PV system. To that end, the response of different silicon-based and thin-film commercial PV technologies is evaluated. Experimental power production data are used to determine the optimal technology. For the analysis, two setups are evaluated under real sun conditions: Grid-connected arrays under standard operation conditions plus modules measured under controlled conditions on a laboratory to separately characterize the technologies response in temperature and irradiation. After the results, a decision table for the technology selection is presented.

The sizing of a stand-alone PV system is analysed in Chapter 5 in terms of reliability. For this, a high-reliability sizing method based on isoreliability curves is used. The optimal sizing is evaluated as function of the consumption types, which can be classified according to their mode, frequency and reliability. The effect of the different consumption types and the economic and energetic associated costs are assessed after the data analysis of an existing stand-alone PV system. As result, the PV system sizing is evaluated as function of the expected system reliability.

To facilitate the core knowledge, this introduction presents hereafter a brief discussion of the general concepts that will be used throughout the work. In addition to a definition of solar cells, the PV technologies generations are presented. Also, the variables used to measure the PV production are introduced.

1.1. GENERAL CONCEPTS ON PHOTOVOLTAIC SOLAR ENERGY

This section provides the basic information on how the solar energy is converted into electricity. The working principle of the solar cells, the basic unit of the PV modules is briefly presented, as well as the commercially available PV technologies. Also, the production variables are defined.

1.1.1. Solar cells

The solar cell is the basic element of a solar photovoltaic module. The solar cells directly convert the solar light into electricity through the photovoltaic effect [25]. This effect is related to the photoelectric effect [26], but requires a semiconductor structure to appear (even other materials such as polymers or organic cells can be used) [27].

The working principle of a solar cell is shown in Figure 1.4. The sunlight photons with energy to free electrons and, thus, create an electron-hole pair, generate a charge imbalance. Due to the electric field created by the union of the type P and N materials on the cell, this pair is separated before the recombination process can occur, creating an electric potential.

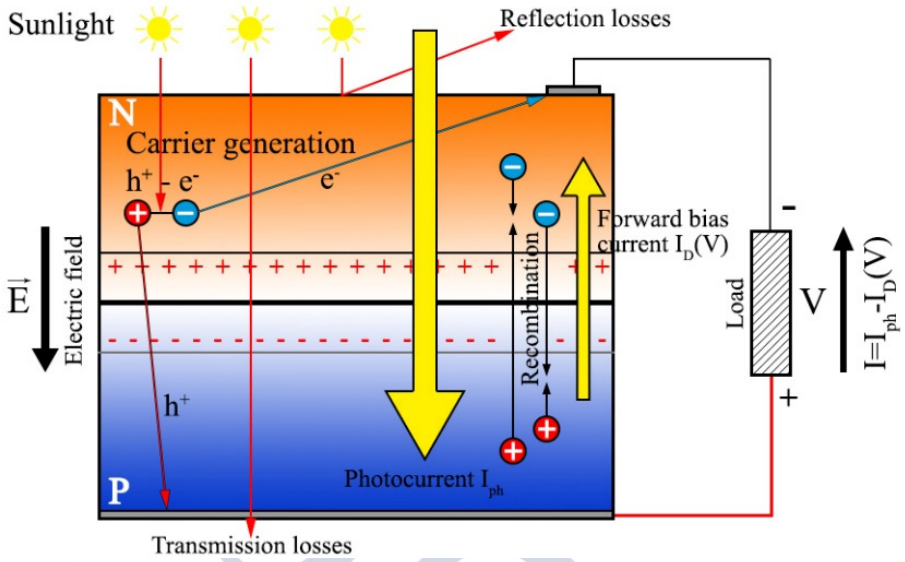

Figure 1.4. Solar photovoltaic working principle [28]

1.1.2. Photovoltaic technologies

The photovoltaic solar modules assembly consists on a series of photovoltaic cells electrically connected to each other. The union of several PV modules constitute an PV array. The different commercially available PV modules are usually divided into three main groups according to the manufacturing technology. This classification introduces the first, second and third generation [29][30]:

- **First generation:** Includes the crystalline silicon-based PV modules. Within this group, the monocrystalline (m-Si), polycrystalline (p-Si) and ribbon/sheet-defined film growth (ribbon/sheet-Si) technologies are included.
- **Second generation:** Intending to reduce the raw materials usage, the thin film-based PV technologies appeared. This group includes amorphous silicon (a-Si), Cadmium Telluride (CdTe), Copper-Indium-Selenide (CIS) and Copper-Indium-Gallium-Selenide (CIGS).
- **Third generation:** Comprises the new PV technologies in experimental phase or entering the market. This group includes the advanced inorganic thin films, the organic solar cells and the thermo-PV cells used in heat and power systems. These technologies are intended to achieve efficiency increase as well as reduction of manufacturing costs.

First generation PV technologies are the most mature and frequent (see Figure 1.5). This is not only for their maturity but for their high efficiency and relatively low price.

On the present work, commercial PV modules of first and second generation will be considered. Monocrystalline (m-Si), polycrystalline (p-Si), amorphous silicon (a-Si), upgraded metallurgical grade silicon (UMG) and Copper-Indium-Selenide (CIS) will be analysed under real sun conditions.

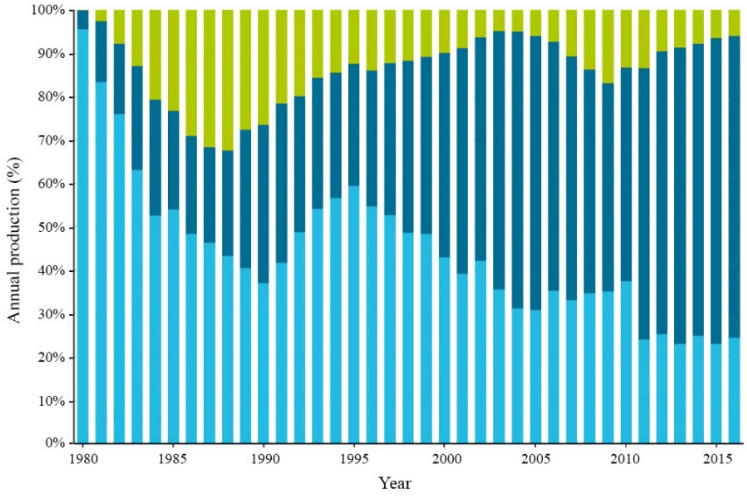

Figure 1.5. PV production per technology [14]

1.1.3. Solar cell I-V characteristic curve

The characteristic I-V curve of a solar cell (or panel) provides a detailed description of its energy conversion capability. The typical I-V curve of a silicon PV cell operating under normal conditions is shown in Figure 1.6 including its power production. The three characteristics points to define are [31][32]:

- **Short-circuit current, I_{SC}:** Maximum current value, occurs when the voltage is zero.
- **Open-circuit voltage, V_{OC}:** Maximum voltage value, appears when no load is connected, it is, when the current is zero.
- **Maximum power, P_{max}:** Corresponds to the (V_{mpp}, I_{mpp}) pair where the power reaches its maximum value. This point defines the ideal operation of a PV cell or module.

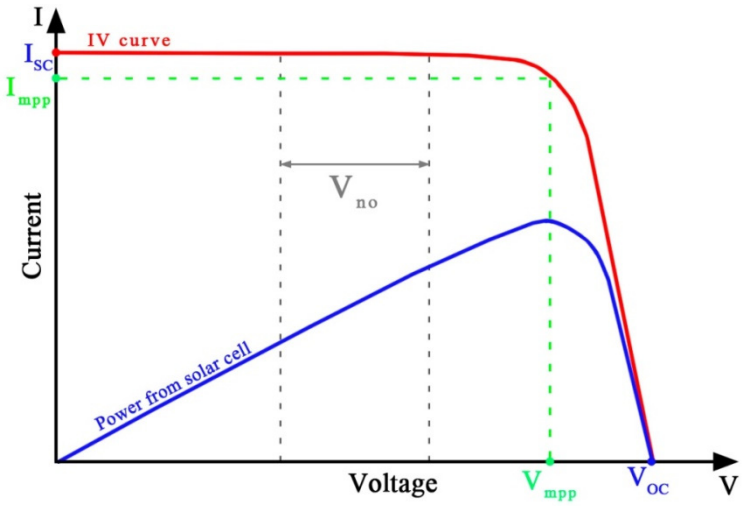

Figure 1.6. I-V curve of a solar cell with reference values

In addition to these values, the **nominal output voltage**, V_{no}, is used as a classification method and refers only to the operative range interval. Depending on the solar panel, this value might be 12 V or 24 V. The photovoltaic modules manufacturers provide these values at

Standard Test Conditions. STC. By definition, these conditions correspond to a solar irradiance of 1000 W/m^2, a cell temperature of 25ºC and an air mass of 1.5 (AM1.5) [33].

The energy production of a PV module, E_{DC}, depends on the solar radiation, G, the module tilt, β_T, and the module temperature, T_m. E_{DC} is defined with the Eq. 1.1, therefore, the two main operation parameters to define a PV module are the already defined short-circuit current (Eq. 1.2), I_{SC}, and open-circuit voltage, V_{OC} (Eq. 1.3) [34][35].

$$E_{DC} = I\,(G, \beta_T) \cdot V(T_m) \qquad \text{Eq. 1.1}$$

$$I = I_{STC} - \alpha\,(G - G_{STC}) \qquad \text{Eq. 1.2}$$

$$V = V_{STC} - \beta\,(T_m - T_{STC}) \qquad \text{Eq. 1.3}$$

The α and β parameters on Eq. 1.2 and Eq. 1.3 are known as **temperature coefficients**:

- The temperature coefficient of the short-circuit current, α, measures the variation of the I_{SC} values with the module temperature.
- The temperature coefficient of the open-circuit voltage, β, accounts the variation on the V_{OC} value with the temperature variation.

1.1.4. PV production variables

The PV arrays performance is measured with the **Performance Ratio**, PR [36]. This parameter is an unbiased indicator for PV systems evaluation [37][38]. The Performance Ratio is defined as the ratio of the **specific yield factor** and the **reference yield**, Eq. 1.4.

$$PR = \frac{Y_f}{Y_r} \qquad \text{Eq. 1.4}$$

The specific yield factor, Y_f (Eq. 1.5), is the ratio of the final energy output of the PV array, E_{DC}, and $P_{installed}$, the nominal PV installed power. The yield factor depends on the irradiation, the module temperature and the array tilt (via the E_{DC} value).

$$Y_f = \frac{E_{DC}}{P_{installed}} \left(\frac{kWh}{kWp}\right) \qquad \text{Eq. 1.5}$$

The reference yield Y_r (Eq. 1.6), is the ratio between the total irradiation measured in-plane of the array, G, and the G_{STC} value, the reference irradiance for PV modules under standard test conditions (1000 W/m^2, 25ºC). It measures the equivalent number of hours at the STC reference irradiance to provide the same solar energy.

$$Y_r = \frac{G}{G_{STC}} \left(\frac{kWh/m^2}{kW/m^2}\right) \qquad \text{Eq. 1.6}$$

The difference between the production variables Y_f and PR is that, while Y_f measures the PV system's production with respect to the installed power, the PR is an unbiased estimator of the capacity of the system to convert the solar incoming radiation into electric power. On the present work, both variables will be used depending on the analysis needs.

1.2. PHOTOVOLTAIC SYSTEMS

A photovoltaic system collects the sunlight and converts it into electricity. The main components of a PV system are shown in Figure 1.7.

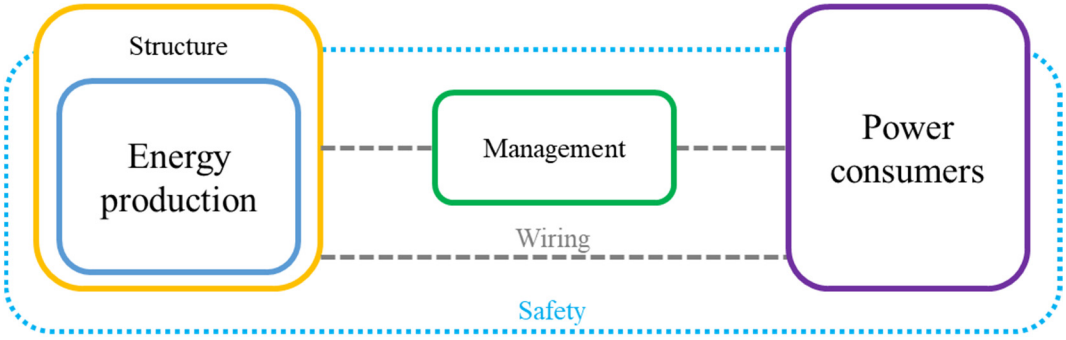

Figure 1.7. General scheme of a photovoltaic system

- **Energy production:** Includes the modules that constitute the PV array, the battery system for energy storage and the charge controller. These elements are deeply related and are the core of the installation.
- **Management system:** Allows the interconnection and communication between elements. These systems can be integrated into another device of the installation and/or include monitoring software.
- **Power consumers:** Include both the (optional) direct current (DC) power consumption and the DC/AC inverter, required for the connection of the usual alternate current (AC) devices.
- **Wiring:** All the electric connections between components and parts of the installation.
- **Structure:** Comprises the racking system for the physical support of the PV array and the wiring raceways.
- **Safety:** All the elements to include to ensure the installation and user's integrity. It is mainly related to the electric and clamping elements.

The PV modules collect the solar energy and send their power production to the charge controller. This device controls the state of charge of the batteries in such a way that the energy can be sent to the batteries (for a later use) or directly to the inverter. When the system's design does not require energy storage, the regulator is not required. The inverter is also not mandatory for the installation, it is only required when AC power consumers are present (the most common scenario). In addition, the electrical safety elements for protection of the devices and users must be installed.

This work focuses on the optimal design of the PV array. The design of a PV system (Figure 1.8) intersects different aspects:

- The **sizing** of the PV system, which relies on the energy demand and the available solar resource. This sizing determines the area of the PV array.
- The selection of the **technology** for the PV modules, mainly dependent on the installation's location climate. To a lesser extent, it can be conditioned by the elements availability or the economic restrictions, but this topic will not be considered for the study.

- The **design** of the PV system takes into account the expected uses of the installation, the potential restrictions and the racking system. It depends on the power consumption, the climate and the socioeconomic characteristics.

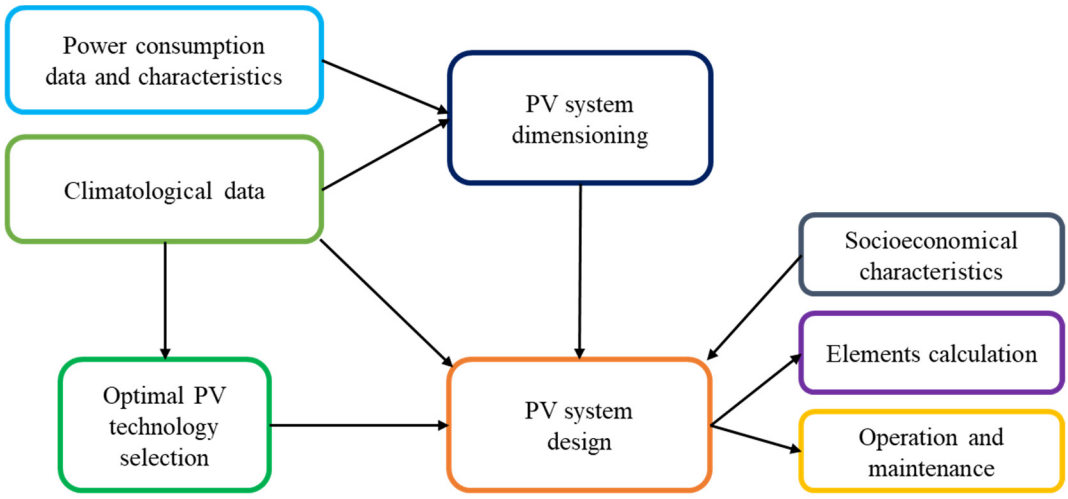

Figure 1.8. Photovoltaic system input data and system variables scheme

Once the PV system design is done, the additional elements can be dimensioned and the system's maintenance can be programmed. It can be seen that, as previously s explained, for a given location the climate plays a key role in the PV system's sizing, the optimal PV technology and the array design.

1.2.1. Types of PV systems

The solar PV energy was initially used in small-scale specific applications. However, its use has evolved and, currently, two types of PV systems are present; the stand-alone and the grid-connected photovoltaic systems.

- The **stand-alone PV systems**, or off-grid systems, operate as decentralized power production autonomous systems in small and medium-size scales. These self-managed schemes for local production, management and consumption have increased its versatility and reliability. This is possible due to the development of more efficient and affordable accumulation and control systems. For their implementation, is necessary to design tools to technically and economically optimize the installations, in addition to improve their deployment and accessibility.
- The **grid-connected PV systems** are a complementary energy source for local grids or national electric power systems. These systems are a power generation source used worldwide. Therefore, their optimization implies the use of devices to maximize their power production.

1.2.2. Design of an optimal PV system

The design of the photovoltaic system is a particularly relevant topic due to the challenge of finding the most suitable design. There is not a single optimal solution, but any selected design must be a compromise solution between costs and reliability. Also, the design must fulfil the user needs and be adequate for the climate characteristics of the installation's location.

Taking into consideration these dependencies, a photovoltaic installation can be defined as **optimal** if it accounts the characteristics of the location. Besides, the installation will be **suitable** when, in addition, it provides the required comfort levels and its accepted by the final user.

The design of a suitable installation is more complex but presents benefits compared to a standard design: its climate change mitigation potential increases, is more environmental-friendly and the lifecycle analysis is more positive. After this, a suitable PV system can be defined as the one with the lower multidimensional cost, which includes the energetic and economic associated costs.

- For a stand-alone PV system, the suitable sizing requires having a detailed description of the consumption and solar resource characteristics as basic inputs for the design. The selected design must be adapted to the needs and the user's economic capability. In addition, the potential future prospect of the installation and the user's expected comfort levels have to be included in the analysis.
- The suitable sizing of grid-connected PV systems focuses on the power production maximization. These connected systems appear both on rural electrification and in utility-grid connected systems. In these cases, solar trackers are often installed to maximize the radiation catchment. The multidimensional cost increase of these systems with respect to a fixed-tilt system imply that their installation must be carefully assessed.

With these inputs, the designed installation must be able to fulfil the final user comfort expectations. Therefore, prior to put into operation a PV system, the habits and customs of the final user must be reliably and in-depth known as well as the PV system's location climatic characteristics. The optimization of a PV system requires to first know the climate characteristics of the installation's location as they condition the optimal PV technology. Without considering these issues, the PV system will not be the optimal and most suitable option.

1.3. LIFECYCLE ANALYSIS

The evaluation of the environmental impacts associated with any product's life is essential to measure the potential impacts of its production, use and later disposal. This process, when considering a renewable energy, allows to environmentally evaluate its climate change mitigation potential. Therefore, the competitiveness of the PV technology does not only rely on the economic aspect, the environmental impacts of this energy source must be evaluated to determine its final benefit. The proper variable for this analysis is the Life Cycle Assessment, LCA [39].

Considering the PV technology hereafter, the LCA evaluates the environmental impacts of a PV system from the raw materials extraction, elements manufacturing, logistics and utilization until the end of life. The end of life includes the reuse, recycle or waste disposal. As it covers all the stages of the system's life, it is also known as cradle-to-grave analysis. The LCA can be expressed as shown in Eq. 1.7. The three terms, EPBT (Energy Payback Time), IRR (Internal Rate of Return) and IMP_{CC} (Input Mitigation Potential in terms of climate change) are explained in the following subsections.

$$LCA = EPBT + IRR + IMP_{CC} \quad \text{Eq. 1.7}$$

The International Energy Agency (IEA) recommendations include an exhaustive list of parameters to be considered for the full LCA analysis of a PV system [40].

1.3.1. Energy Payback Time

Considering the LCA model, the environmental impacts of a PV system are mainly quantified with the Energy Payback Time, EPBT [40][41][42]. The EPBT measures the required time, in years, to recover the energy used during the PV system lifespan [43][44].

$$EPBT = \frac{E_m}{E_p} = \frac{E_{Mat} + E_{Manuf} + E_{Trans} + E_{Inst} + E_{EOL}}{\eta_G \cdot E_{Agen} - E_{O\&M}} \left(\frac{kWh/m^2}{kWh/m^2 year}\right) \quad \text{Eq. 1.8}$$

In the EPBT expression (Eq. 1.8), E_m measures the energy required to extract and process the raw materials and manufacture the modules. This term is the sum of the primary energy demand for the PV system's materials extraction and manufacturing, E_{Mat} and E_{Manuf}, plus elements transportation and installation, E_{Trans} and E_{Inst}. It also includes the required energy for the system's dismantling at the End of Life, E_{EOL}. The annual energy generated by the PV system, E_p, depends on the grid efficiency, η_G, the annual energy generation, E_{Agen}, and the annual energy demand for operation and maintenance, $E_{O\&M}$.

Therefore, the EPBT for same technology PV modules depends on the array's location irradiation levels via the annual energy generation. Figure 1.9 shows the EPBT for polycrystalline silicon modules in Europe.

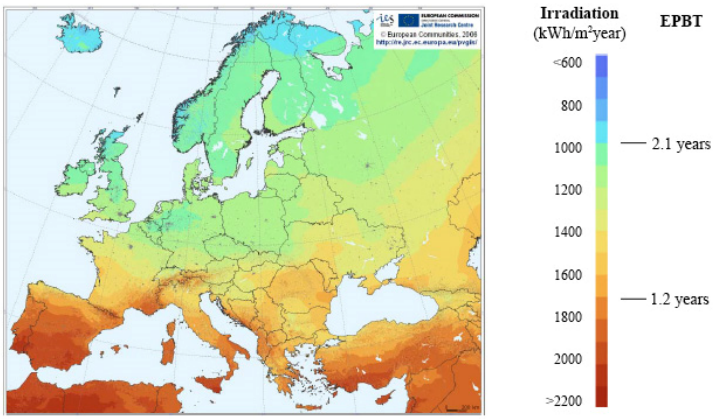

Figure 1.9. Energy Payback Time of polycrystalline silicon (rooftop install) [14]

1.3.2. Internal Rate of Return

The associated cost of a solar tracker with respect to a fixed-tilt system is evaluated by using the Internal Rate of Return, IRR. The IRR forecasts the expected return from a project or evaluates its profitability by comparing it to other potential investments.

The IRR is defined as the value which equals the Net Present Value, NPV, to zero. The NPV is a measurement of profit which calculates the difference between the costs (present cash outflows plus the initial investment) and the benefit (present cash inflows). Without considering taxes-associated values, the NPV can be defined as shown in Eq. 1.9, where *n* is the PV

installation lifespan and LCC, the Lifecycle Cost [45][46]. The LCC accounts all the costs for the installation, including the initial system cost and (C_i) the operation and maintenance (C_{OM}) annual costs (Eq. 1.10).

$$NPV = \frac{LCC}{(1 + IRR)^n} \quad \text{Eq. 1.9}$$

$$LCC = C_i + C_{OM} \quad \text{Eq. 1.10}$$

This value, like the EPBT, is measured in years. Thus, IRR and EPBT can be considered together.

1.3.3. Mitigation of potential environmental impacts

The environmental Input Mitigation Potential, IMP, can be defined to measure the availability of the selected energy source to mitigate the climate change effects or the associated-waste management [40][47]. This impact must be calculated following the national regulations on the installation's location. Due to this highly regional and legislative dependence, it will be not evaluated.

The Input Mitigation Potential in terms of climate change, IMP_{CC}, can be calculated with Eq. 1.11. The IMP_{CC} is measured in terms of the system's lifetime.

$$IMP_{CC} = \frac{CC_{Agen}}{\gamma_G - (CC_{Mat} + CC_{Manuf} + CC_{Trans} + CC_{Inst} + CC_{EOL} + CC_{O\&M})} \left(\frac{kg\ CO_2 eq}{kWh}\right) \quad \text{Eq. 1.11}$$

In Eq. 1.11, CC_{agen} represents the annual electricity generation (in kWh) and γ_G represents the difference on CO_2 emissions of using the national grid system minus the PV plant emissions (measured in kg of CO_2 equivalents per kWh, $kgCO_2eq/kWh$). The remaining impacts on climate change, measured in $kgCO_2eq$, are represented as CC_{mat}, for the impact of producing the materials of the PV system, CC_{manuf}, for the PV system manufacturing, CC_{trans}, for the materials transportation during the system's lifetime, CC_{inst}, for the impacts during the installation process, CC_{EOL}, for the end-of-life management and $CC_{O\&M}$, as the impact associated to the operation and maintenance processes.

Chapter 2 - PV tracker system net gain associated to the local climatic conditions

2.1. INTRODUCTION

The photovoltaic energy expansion is constant since the last century. Currently, the grid-connected centralized PV systems represent over 95% of the total photovoltaic systems in operation [24]. As these systems supply their power production to the utility grid, increase the generation will raise its advantages.

To improve the power production of PV arrays, solar trackers are frequently installed. These systems aim to maximize the power production by continuously following the sun's path. Market forecasts show an expected annual growth over 5% for solar tracker markets in the next years [48][49][50].

According to previous studies [51][52], the installation of a solar tracker system can increase the power production up to 25% for single-axis trackers [53][54][55] and up to 40%, or even higher depending on authors, for dual-axis trackers [56][57][58]. Even so, the analysis of existing tracker performance papers shows high variability in the gain percentages. Among the reasons, this discrepancy can be attributed to climate variations. However, the main problems are the use of simulations or the dependence of the results on the location, latitude or climate conditions on the data acquisition interval. Also, the benefit of the tracking systems is always assessed only in terms of its production increase.

This chapter will focus on evaluate the solar tracker suitability as function of climate conditions. The analysis is performed after experimental solar irradiation and power production data from a PV production field. The installation, located in a medium-irradiated area, has both tracker-equipped and fixed-tilt PV arrays. For the analysis, two same-manufacturer, same-technology, grid-connected arrays are considered. One of the arrays is equipped with a solar tracker system while the other is installed in a horizontal fixed-tilt position.

When starting to evaluate the net gain of the tracking system with respect to the fixed-tilt array, a high discrepancy was detected when comparing both array's performances on a fully sunny and an overcast day. The result comparison of both days showed a high difference in the tracker gain with the different climate conditions. For the fully sunny day, an almost 60% gain was calculated, while the overcast day showed a result compatible to zero. After this result, it was clear that the solar tracker gain deserved a more detailed analysis.

In addition to the climate-dependant production gain of a solar tracker, the study of the gain requires considering the economic and environmental associated costs as function of climate conditions. These costs cannot be ignored since the installation of a tracking system increases the economic investment and involves higher quantities of raw material and manufacturing processes than a fixed-tilt PV system. The economic costs, measured via the Internal Rate of Return, include the initial investment plus the operation and maintenance expenses. The environmental costs involve the energy costs, evaluated using the Energy

Payback Time, and the greenhouse gasses, GHG, emissions. The GHG emissions, besides being difficult to quantify, depend on manufacturing location and production processes. Thus, the GHG emissions will not be considered for the present study.

Therefore, to evaluate the net gain of a solar tracker, the production increase, as well as the economic costs, must be considered. But to assess the net gain dependence with climate conditions, a climatic variable must be found. Once defined, the solar tracker production increase and the associated costs can be characterised as a function of it. The difference between the tracker production increase and its associated costs will provide the tracker benefit limit as function of climate conditions.

The data analysis led to the publication of a research paper (full text in Manuscript I) [59]. The main result is the development of a method to determine the net gain of a solar tracker compared to a fixed-tilt system as function of climate conditions.

2.1.1. Solar photovoltaic racking systems

The design of a photovoltaic system requires to initially select the optimal PV technology for the location [60] but also to choose the design for the module's installation. The PV systems mainly use two main types of racking systems: fixed-tilt or tracker-equipped.

The amount of solar radiation received by a PV module is maximum when its position is perpendicular to the incoming sun rays. The sun's path variation along the day and the seasons, in addition to the latitude, makes the optimal angle a time-dependent value.

To maximize the received solar energy, the tracker systems modify the PV array tilt during the day. On the contrary, the fixed-tilt systems operate with the array installed on an angle which can be selected to maximizes the radiation catchment on the month with the maximum energy demand or fixed by physical constraints.

2.1.1.1. Fixed tilt systems design

The fixed-tilt racking systems represent the lower cost for the PV array installation but the performance is not optimal for all the year. When using this design, the PV modules are mounted into a structure. Depending on where the supporting structure is placed, the fixed-tilt systems are classified as:

- **Rooftop:** This option is only available when the roof is facing South (in the northern hemisphere) or North (for the southern hemisphere). For this racking system, the array tilt is restricted by the roof angle. Thus, the month for a maximum performance of the PV system is determined by the building's roof tilt.
- **Ground:** This option requires not-shaded terrain for the structure installation. When it is available, this is the most economical design. The optimal tilt for the location can be fixed when installing the structure.

The array optimal tilt must be calculated for the month with the maximum consumption-minimum radiation pair. Usually, this pair happens during the winter season (when the lower solar resource is available). For this cases, the optimal angle is usually calculated as function of the latitude, using a tilt equal to the latitude or with the Landau equation [61].

2.1.1.2. Solar trackers

Sola trackers enhance the solar radiation collection by following the path of the sun. This is done with mechanical systems able to minimize the angle of incidence between the sunlight and the PV modules. These devices are characterized by the tracker movement mechanism and the number or rotating axis. Regarding the working mechanism, the trackers can be defined as:

- **Passive trackers:** The movement is generated after solar heat generates a mass imbalance between upper and lower sides of the PV module [62][63]. These mechanisms can be used in PV arrays but are very uncommon. As main advantage, they do not require electronic systems and the price is low. The major disadvantage is that the non-precision orientation may decrease the performance. Also, as using thermal expansions, the tracking system does not work at low temperatures [64].
- **Active trackers:** The movement to control the alignment with the sun is generated by motors. The movement can be programmed according to the time and day (regardless of weather conditions) or controlled with a pyranometer which detects the maximum value of irradiation to face the array. Active trackers are widely used due to their precision and manageability. They also provide higher efficiency.

Figure 2.10 shows the different types of active trackers. Depending on the number of rotating axes, trackers are defined as single or dual-axis:

- **Single-axis trackers** rotate only on the zenithal or azimuthal axis. Single-axis horizontal trackers adjust the array tilt, while single-axis vertical trackers can rotate on the North-South axis or East-West, also known as single-axis azimuth trackers.
- **Dual-axis trackers** rotate on both axes to adjust the tilt for the solar elevation and the positioning on the sun's path. These devices are more precise, but also more complex and expensive due to the mechanism and the subsequent maintenance.

A general disadvantage of solar trackers is the energy consumption and maintenance requirements [63].

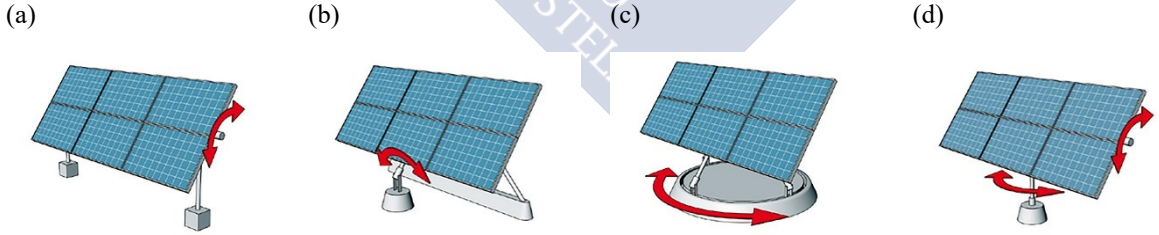

Figure 2.10. Types of solar tracker systems according to the rotating axis: Single-axis (a) horizontal, (b) vertical zenithal and (c) vertical azimuth trackers. (d) Dual-axis tracker [65]

2.1.2. Production variables

The data analysis on this chapter requires to define additional variables to the already defined Performance Ratio (Eq. 1.4) and yield factor (Eq. 1.5). The **variation** of the solar tracker system with respect to the fixed-tilt system is measured as function of different parameters. Eq. 2.12 shows the general expression for the variation, where X refers to the parameter's variation to be analysed on a defined basis.

$$\sigma(X) = 100 \cdot \frac{X_{Track} - X_{Fixed}}{X_{Fixed}} \ (\%) \qquad \text{Eq. 2.12}$$

For some analysis, the performance difference between the tracker-equipped and the fixed-tilt systems is considered. This value is calculated with the **Performance Ratio gain** (Eq. 2.13). This calculation is performed on a defined basis.

$$\Delta PR = PR_{Track} - PR_{Fixed} \qquad \text{Eq. 2.13}$$

2.2. EXPERIMENTAL SETUP

The production data from two photovoltaic arrays is considered. Both arrays are part of a grid-connected electric power plant owned by Norvento Enerxía and installed in 2008 [66]. The system, with a total 100 kWp of installed power, is distributed in 10 arrays. The installation is located in Vilalba (Spain) (coordinates 43.3146; -7.6650) (Figure 2.11). Selected arrays characteristics (hereafter, Fixed and Track) are shown in Table 2.1.

(a) (b)

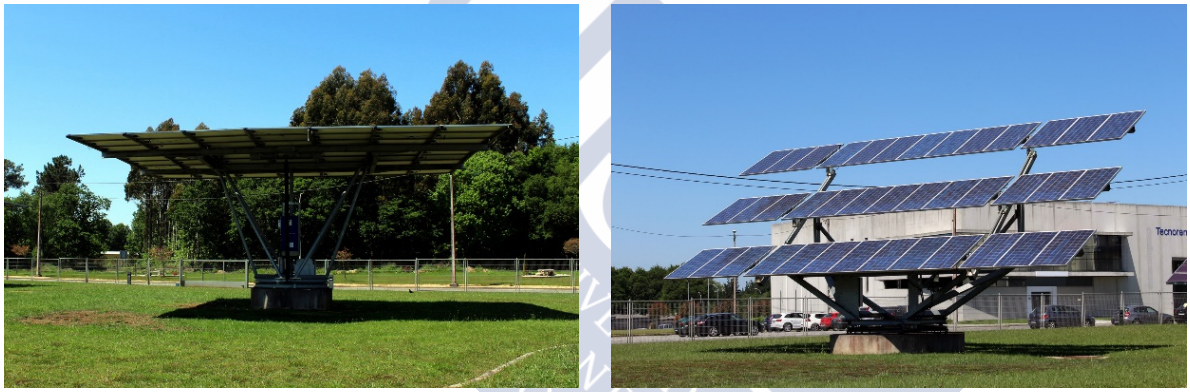

Figure 2.11. Considered PV arrays: (a) Fixed and (b) and Track

Table 2.1. Considered PV arrays characteristics

PV Panel technology	Brand and model	Unit power P_{rated} (W)	Array power P_{total} (W)	Inverter	Solar tracking
p-Si (Fixed)	Suntech STP260	260	14040	Ingeteam Ingecon Sun 12,5 [67]	No
p-Si (Track)	Suntech STP270	270	10530	Sunways NT10000 [68]	2-axis

The production values are measured at the inverter output with a 10-minute frequency. The inverter efficiencies are 94.9% for the fixed and 97.6% for the track system. Inverter-associated losses are neglected as the efficiency difference is less than 3%.

2.2.1. Solar radiation available databases

The main data source for the global horizontal radiation values is the pyranometer located on the Norvento Enerxía installations (LI-COR model LI-200SZ, 80μA per 1000 W/m^2 sensitivity [69]). The irradiation values are cross-checked with the Meteogalicia's Guitiriz-Mirador meteorological station [70], located 13 km far from the PV field. After the cross-check, datasets from both pyranometers are combined to complement the solar radiation database.

The daily global horizontal radiation values of both stations are compared for over 80 days. Results for the daily global irradiation from each source (G_{Norv} and G_{Guit}) are shown in Figure 2.12, with an average 6.3% difference measured between the datasets. The observed difference will be considered in the uncertainty calculation. The Guitiriz-Mirador global radiation data will be used when no on-location data are available.

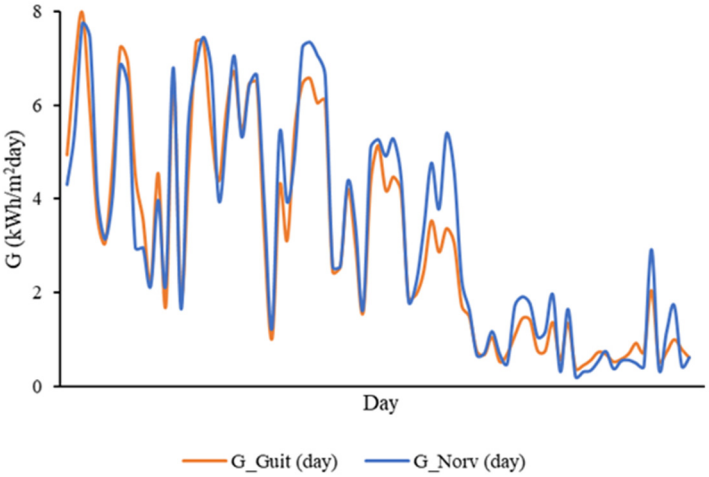

Figure 2.12. Meteorological station (G_{Guit}) and on-location (G_{Norv}) daily solar radiation values for a 5-month consecutive period

When analysing Figure 2.12, a systematic error is observed when comparing both global horizontal radiation values datasets. A calibration error on the on-location pyranometer affecting to irradiation values under 50 W/m^2 has been detected and corrected for the data analysis.

It must be noticed that neither the Norvento nor the Meteogalicia-Guitiriz meteorological stations are equipped with diffuse radiation pyranometers. The closest meteorological station with experimental diffuse horizontal radiation values is the Meteogalicia-EOAS meteorological station [70]. This station, located 84 km far from the PV field, experimentally measures both global and diffuse horizontal radiation values.

2.3. METHODOLOGY

Figure 2.13 shows the starting point of the research, the difference of the tracker gain for a fully sunny and an overcast day. After this plot, the climate dependence is clear and the first challenge for this analysis is to find a proper variable to assess the gain of a solar tracker with respect to the fixed-tilt array.

2.3.1. Solar radiation components

The solar tracker gain dependence cannot be considered as just function of the solar global horizontal radiation, as it is the sum of the direct (or beam) and diffuse horizontal radiation values [71][72].

$$GHI = B + DHI \qquad \text{Eq. 2.14}$$

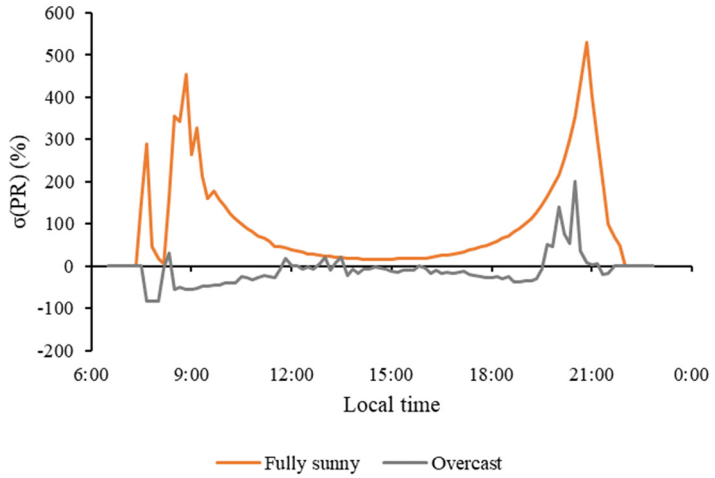

Figure 2.13. Performance Ratio variation comparison between a fully sunny and an overcast day

Eq. 2.14 is the general expression of the global horizontal radiation where:

- **Global horizontal irradiance**, GHI, is the total amount of solar radiation received per unit area on a horizontal surface on the surface of the earth.
- **Beam horizontal irradiance**, B, is the solar radiation directly received from the sun (not scattered) per unit area on a horizontal surface. This value is frequently measured in terms of direct normal irradiance, DNI. This topic will be discussed in the next chapter.
- **Diffuse horizontal irradiance**, DHI, measures the amount of solar radiation received per unit area on a horizontal surface with the direct solar radiation blocked.

It must be noticed that even for a fully sunny day, part of the incoming sun rays are scattered by the particles in the atmosphere. Therefore, during the daytime, the diffuse irradiance value is never zero. Considering an overcast day, all the sun rays can be dispersed by the atmosphere and diffuse horizontal can be equal to the global horizontal radiation.

2.3.2. Climate variable

Developing a method to relate the power production difference between a tracker-equipped and a fixed-tilt system requires defining the working variable. It is common to find microphysics model-based or simulations to assess the solar tracker net gain as function of the global radiation [56][58][73][74]. After the experimental results from Figure 2.13, these analyses have been proven as unreliable when considering overcast scenarios.

The Clearness Index, K_T, which measures the clearness of the atmosphere [75][76], somehow represents the desired variable. But it is also based on mathematical models. Due to the K_T model dependence, the use of the Diffuse Fraction, DF, is proposed. The DF is directly related to the Clearness Index, since it measures the cloudiness conditions, but defined with experimentally-measurable values. The DF (per-unit) over a horizontal surface is defined as the ratio between the diffuse, D, and the solar global radiation, G, values for a specific time interval (Eq. 2.15).

$$DF = \frac{DHI}{GHI} \qquad \text{Eq. 2.15}$$

Hence, the diffuse fraction might be considered as the variable for the net gain analysis by using experimental values. The difficulty is that no beam or diffuse experimental values are available on-location. As said, the closest diffuse radiation data source is the Meteogalicia-EOAS meteorological station [70].

Seeking to use experimental values, the possibility of utilize these diffuse radiation values is evaluated. Since its direct use is not possible as climate conditions probably differ between locations, a method to compare both locations in terms of climate conditions needs to be created. As the common variable between both locations is the global horizontal radiation, a criterion initially based on this variable is developed.

The criterion is proposed after analyzing fully sunny days, as solar radiation variations are easily visualized on clear sky days. After an initial comparison of 10-minute frequency global radiation values from both sources for different clear sky days, a pattern in terms of global radiation is detected. For similar days, the daily average global horizontal radiation value for both data source is comparable. In addition, the total daily global radiation values are also analogous.

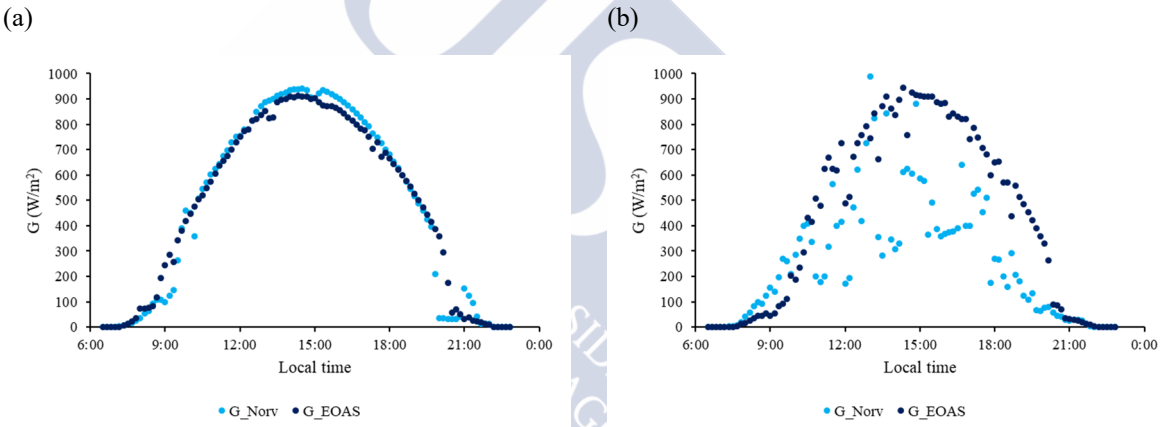

Figure 2.14. Example of solar radiation (a) comparable values and (b) non-comparable values

Figure 2.14 shows two examples of the global radiation values from Norvento (G_{Norv}) and Meteogalicia-EOAS (G_{EOAS}) pyranometers. While Figure 2.14a shows a day with similar radiation values for both locations, Figure 2.14b shows a non-comparable day in terms of irradiation.

2.3.3. Similarity criterion

After comparing the patterns and data, the similarity criterion is established as shown in Table 2.2. For the diffuse radiation values, shade ring effects are neglected [77][78].

For days verifying the three conditions, the solar radiation values similarity between both locations can be stated. Thus, an alternative source for diffuse solar radiation values is available for the PV system location and the DF can be used to evaluate the solar tracker gain compared to the fixed-tilt system.

Table 2.2. Similarity criterion conditions

Condition 1	The absolute difference between average global radiation values along the same day between both locations is less than or equal to 50 W/m^2 (Eq. 2.16). $$\Delta < G > = < G_{EOAS} > - < G_{Norv} > \leq \pm 50\ W/m^2$$ Eq. 2.16
Condition 2	The difference between the daily sum of global radiation between locations for the same day is less than or equal to 15% (Eq. 2.17). $$\Delta\left(\sum_n G\right) = 100 \cdot \frac{\sum_n G_{Norv} - \sum_n G_{EOAS}}{\sum_n G_{Norv}} \leq 15\%$$ Eq. 2.17
Condition 3	The global radiation spectra along the same day is similar for both locations.

Figure 2.15 shows two numerical examples of the criterion. The day on (a) is an adequate candidate as it verifies the Conditions 1, 2 and, mostly, Condition 3. Otherwise, the (b) example is a day not verifying Condition 1 and on the limit for Condition 2. This day cannot be selected as, also, the Condition 3 is not verified.

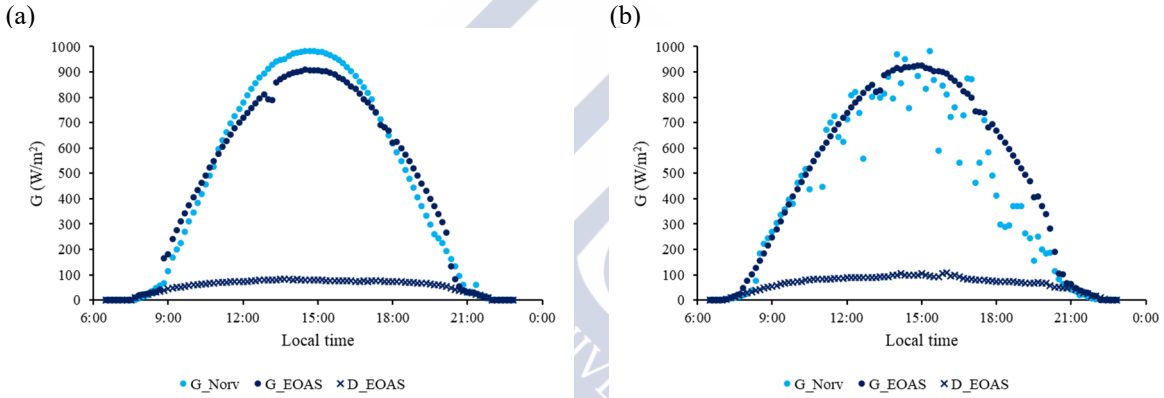

Figure 2.15. Example of (a) valid day and (b) non-valid day:
(a) Δ(∑G)=2% and Δ<G>=10 W/m^2, (b) Δ(∑G)=15% and Δ<G>=67 W/m^2

2.4. RESULTS

Once the similarity criterion is applied and the available data verifying the conditions are filtered, the tracker system net gain compared to a fixed-tilt system can be evaluated as function of the diffuse fraction. The DF is calculated for each day following Eq. 2.15 as the ratio between the average daily diffuse and global radiation values.

2.4.1. Data analysis

Figure 2.16 compares three days verifying the Condition 1 and 2: As reference, a fully sunny day verifying the linear tendency (a) is compared with a day above the linear tendency (b) and a day below (c). The global irradiation spectra of the PV field location (G_{Norv}) and the Meteogalicia-EOAS (G_{EOAS}) meteorological station are compared:

- For the reference day (a), both irradiation sources show the same behaviour pattern during the whole day.
- For the day (b), around the midday (local time from 12:00 to 16:00), global radiation values show a 9% difference. As this time interval is the maximum power production

time for the PV array, the diffuse radiation from the meteorological station cannot be considered as being underestimated.

- For the day (c), the morning period (until 12:00 local time) shows a 25% difference in the global radiation values from both data sources. Since sunrise and sunset intervals are when the solar tracker maximizes its gain compared to a fixed-tilt system, the use of the available diffuse radiation values does not reflect the real working conditions.

Regardless that the numerical conditions are verified, these differences for specific time intervals are the responsible that these days cannot be considered for the analysis.

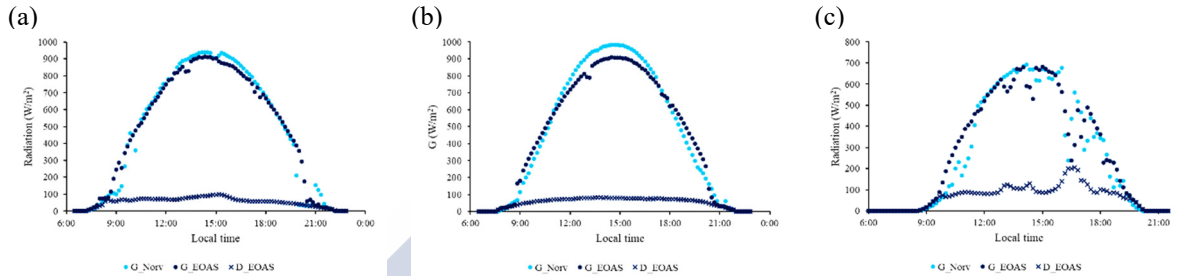

Figure 2.16. Comparison of (a) Day inside the linear tendency ($\Delta(\sum G)$=1%, $\Delta\langle G\rangle$=2 W/m^2) and days out the linear tendency (b) $\Delta(\sum G)$=2%, $\Delta\langle G\rangle$=10 W/m^2 and (c) $\Delta(\sum G)$=4%, $\Delta\langle G\rangle$=10 W/m^2

2.4.2. Diffuse fraction dependence with power production

After removing the non-representative points for the analysis, Figure 2.17a shows the relation between the Performance Ratio gain, ΔPR, and the diffuse fraction, DF. The linear correlation with the regression values is shown in Eq. 2.18.

$$\Delta PR = (-0.60 \pm 0.05)\, DF + (0.63 \pm 0.03) \qquad \text{Eq. 2.18}$$

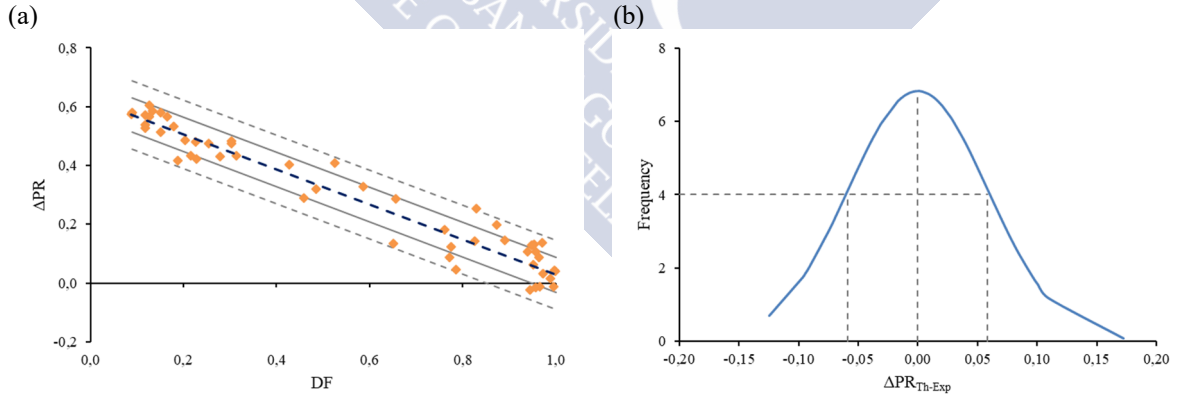

Figure 2.17. (a) Performance Ratio gain versus diffuse fraction (b) and frequency distribution

The linear fit is presented with the σ and 2σ standard deviation intervals, calculated with the standard deviation using the n-1 method [79]. These values are obtained after the frequency analysis of the difference between the linear fit calculated value and the experimental PR gain values (Figure 2.17b). The difference shows a mean value of μ=-0.001. Thus, the most probable result is to have no difference between the theoretically calculated (after the linear fit) and the experimental values. The standard deviation value is also calculated, with a value of σ=0.059. The 68.5% of the values lie inside the σ interval and 96.3% inside the 2σ interval, ensuring the statistical representativeness of the values. Analysing the frequency distribution of the

difference between theoretical and experimental values, a slight asymmetry appears on the positive range of $\Delta PR_{Th\text{-}Exp}$ (where *Th* stands for the value calculated using the linear fit). This means that regardless the mean value, the experimental values are slightly lower than expected [59].

2.4.3. Performance Ratio variation

Even if ΔPR measures the difference between the solar tracker and the fixed-tilt systems, the Performance Ratio variation, σ(PR), measures this difference as a percentage (Eq. 2.19).

$$\sigma(\mathrm{PR}) = 100 \cdot \frac{\mathrm{PR_{Track}} - \mathrm{PR_{Fixed}}}{\mathrm{PR_{Fixed}}} \ (\%) \qquad \text{Eq. 2.19}$$

Figure 2.18a plots the relation between the PR variation and the diffuse fraction. The σ and 2σ intervals are also included. The difference between the fit-calculated and the experimental values is analysed (Figure 2.18b), showing a mean value of μ=-0.0002, 72.2% values inside the σ interval and 94.4% inside the 2σ interval [59].

$$\sigma(\mathrm{PR}) = (-78.7 \pm 8.4)\ \mathrm{DF} + (79.7 \pm 5.6) \qquad \text{Eq. 2.20}$$

The linear fit for the PR variation dependence with the diffuse fraction is presented in Eq. 2.20. Analysing the results, a negative slope appears and an 11% error is measured. The negative slope is expected since solar tracker benefit decreases as diffuse fraction increases.

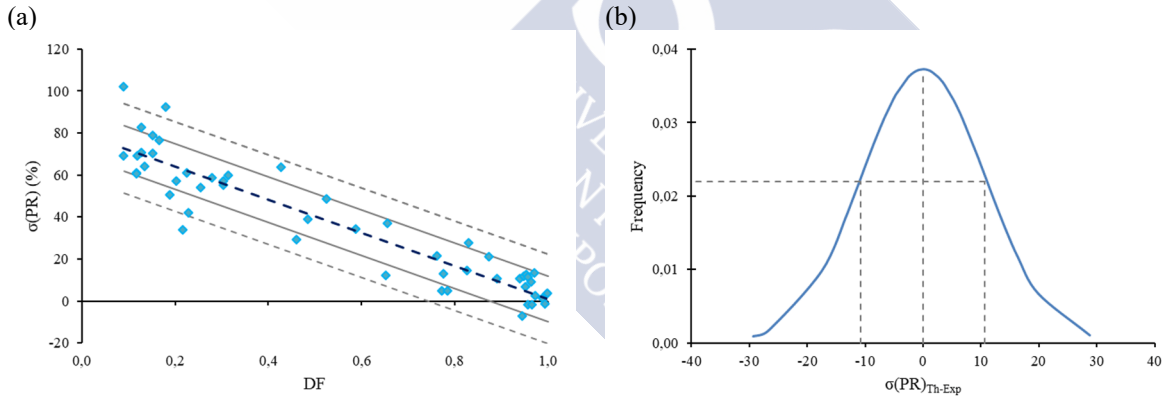

Figure 2.18. (a) Performance Ratio variation dependence with diffuse fraction and (b) frequency distribution of differences between theoretical and experimental σ(PR) values

The limit scenarios are evaluated:

- When DF tends to zero, the average PR gain is almost 80%. Considering the data uncertainty, the variation interval will vary from 69%-90% considering one σ deviation. For 2σ deviations, with 94% reliability, the σ(PR) moves from 58%-101% gain.
- For DF values tending to 1, the average σ(PR) is almost null since only 1% positive variation is measured for overcast conditions. The PR variation for one σ deviation goes from -10% to 12%. Considering the 2σ standard deviation interval, the σ(PR) values interval, [-20, 22]. Therefore, the gain in overcast conditions is compatible to zero.

2.4.4. Energy Payback Time variation

The energetic analysis of the PV system is performed with the Energy Payback Time variation (Eq. 2.21). The EPBT for each system is measured with Eq. 1.8, where the energy generated, E_p, is measured with the yield factor, Y_f (Eq. 1.5). Since this analysis focus on the tracker versus fixed-tilt PV systems, comparing both gains requires to consider the higher EPBT of the solar tracker system for an unbiased analysis of the performance increase. For the evaluation, only both system's PR needs to be used for the LCA.

As in the previous section, for the tracking system the yield factor is calculated after deducting the tracker power consumption from the power production (with the tracker consumption estimated in 50 Wh for a 1 kW array [80]). The inclusion of this term produces a slight redundancy in the final result as it introduces, on average, an error of 0.5%.

$$\sigma(\mathrm{EPBT}) = 100 \cdot \frac{\mathrm{EPBT_{Track}} - \mathrm{EPBT_{Fixed}}}{\mathrm{EPBT_{Fixed}}}\ (\%) \qquad \text{Eq. 2.21}$$

The EPBT for a system equipped with a solar tracker system doubles the EPBT for a fixed-tilt [52][57][81][21]. By using the EPBT definition (Eq. 1.8) into Eq. 2.21, and considering the relation between fixed-tilt and tracker systems EPBT, the relation in Eq. 2.22 is obtained.

$$\sigma(\mathrm{EPBT}) = 100 \cdot \frac{\frac{E_m^{\mathrm{Track}}}{Y_f^{\mathrm{Track}}} - \frac{E_m^{\mathrm{Fixed}}}{Y_f^{\mathrm{Fixed}}}}{\frac{E_m^{\mathrm{Fixed}}}{Y_f^{\mathrm{Fixed}}}} = 100 \cdot \frac{2\,Y_f^{\mathrm{Fixed}} - Y_f^{\mathrm{Track}}}{Y_f^{\mathrm{Track}}}\ (\%) \qquad \text{Eq. 2.22}$$

The EPBT variation for each day versus DF is plotted in Figure 2.19a, including the σ and 2σ intervals. The statistical analysis of the difference between the linear fit calculated value and experimental values (Figure 2.19b) shows a mean value of μ=0.003, 68.5% values inside the σ interval and 94.4% inside the 2σ interval [59].

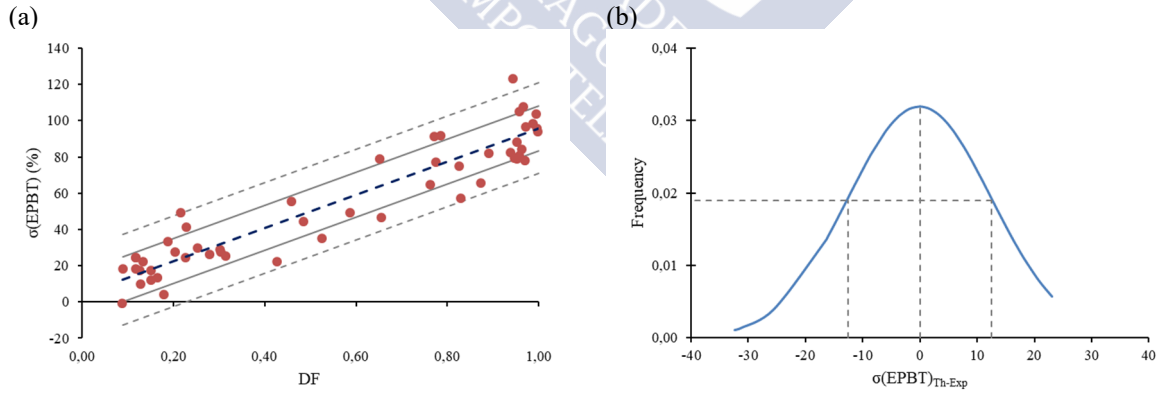

Figure 2.19. (a) Energy Payback Time variation dependence with diffuse fraction and (b) frequency distribution of differences between theoretical and experimental σ(EPBT) values

The linear fit equation for the EPBT variation shows a slope of 91.6 with an error of 11%. The intercept is compatible to zero. The positive slope shows the increasing number of years to compensate the energy increase for the tracker manufacturing as the diffuse fraction increases. Taking into consideration the standard deviation intervals, DF values below 0.09 (for the σ

interval) or under 0.23 (for the 2σ interval) will make the required number of years for the tracker system lower than for the fixed-tilt system.

2.4.5. Internal Rate of Return variation

For the proper comparison of solar tracker and fixed-tilt systems, the economic investment has to be considered since the Lifecycle Cost for a tracker-equipped system exceeds the fixed-tilt costs. For this analysis, the Internal Rate of Return variation (Eq. 2.23) is assessed as shown in Eq. 2.24, where LCC is the Lifecycle Cost (see Eq. 1.10) and Y_f is the yield factor (Eq. 1.5). The tracking system Y_f value is calculated once the solar tracker power consumption is deducted from the array's production. The solar tracker consumption is estimated at 50 Wh for a 1 kW array [80]. As for the EPBT, this term produces an error of 0.5% on the final result.

$$\sigma(\mathrm{IRR}) = 100 \cdot \frac{\mathrm{IRR_{Track}} - \mathrm{IRR_{Fixed}}}{\mathrm{IRR_{Fixed}}}\ (\%) \qquad \text{Eq. 2.23}$$

The IRR for each system is assessed as the ratio between economic cost and energy production (Eq. 2.24). According to NREL [82], the required time to achieve the same return for the tracker system with respect to the fixed-tilt system is a 50-60% higher. Assuming 1.5 times higher time to reach the same Net Present Value for a solar tracker compared with a fixed-tilt system [83][81][84], the σ(IRR) equation can be written as Eq. 2.25. This cost includes the initial economic investment for the tracker purchase plus installation. It also accounts the maintenance and the system failures.

$$\mathrm{IRR} = \frac{\mathrm{LCC}}{Y_f} \qquad \text{Eq. 2.24}$$

$$\sigma(\mathrm{IRR}) = 100 \cdot \frac{\frac{\mathrm{LCC_{Track}}}{Y_f^{\mathrm{Track}}} - \frac{\mathrm{LCC_{Fixed}}}{Y_f^{\mathrm{Fixed}}}}{\frac{\mathrm{LCC_{Fixed}}}{Y_f^{\mathrm{Fixed}}}} = 100 \cdot \frac{1.5 Y_f^{\mathrm{Fixed}} - Y_f^{\mathrm{Track}}}{Y_f^{\mathrm{Track}}}\ (\%) \qquad \text{Eq. 2.25}$$

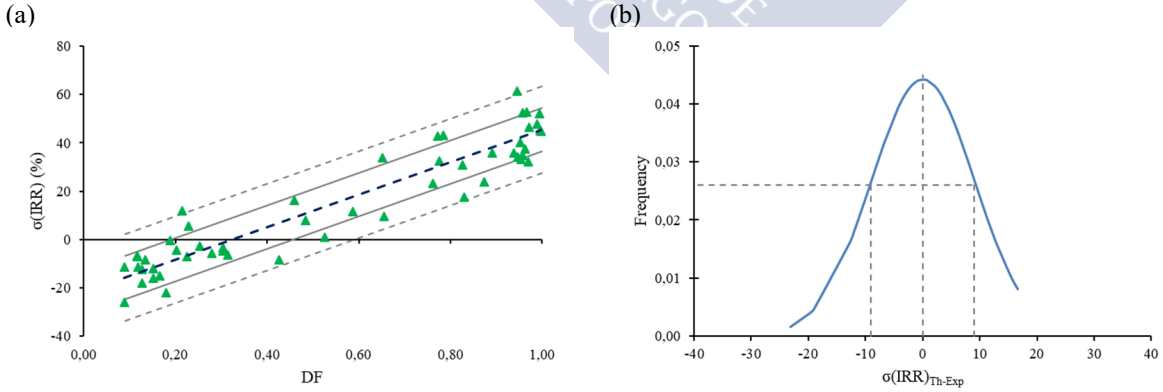

Figure 2.20. (a) Internal Rate of Return variation dependence with diffuse fraction and (b) frequency distribution of differences between theoretical and experimental σ(IRR) values

The IRR variation as function of the DF is presented in Figure 2.20a including the σ and 2σ intervals. Figure 2.20b shows the frequency distribution for the difference between the linear fit calculated and experimental σ(IRR) values. The statistical analysis shows a mean value of μ=0.002, 66.7% of values inside the σ and 94.4% inside the 2σ intervals. The linear fit for the

σ(IRR) and DF relation slope is 67.1 with an error of 11%. The intercept has a negative value of -21.6 with an error of 22%.

The analysis of the dependence of IRR with DF shows a positive slope. With an average DF intercept of 0.32, this intercept moves between 0.19-0.46 for one standard deviation and 0.05-0.59 for two standard deviations (94% reliability).

2.4.6. Cost variation

To evaluate the overall associated costs with a solar tracker compared to a fixed-tilt system, the convolution of the costs will be done with the addition of the EPBT and the IRR. By considering the equations for σ(EPBT) and σ(IRR) (Eq. 2.21, Eq. 2.22 and Eq. 2.23 to Eq. 2.25 respectively) the Eq. 2.26 for the Cost variation, σ(CV), can be derived.

$$\sigma(CV) = \sigma(EPBT) \otimes \sigma(IRR) = 100 \cdot \left[\left(\frac{E_M^{Track}}{E_M^{Fixed}} \frac{LCC_{Track}}{LCC_{Fixed}}\right)\frac{Y_f^{Fixed}}{Y_f^{Track}} - 2\right] = 100 \cdot \left(\frac{3.5\, Y_f^{Fixed}}{Y_f^{Track}} - 2\right) \quad \text{Eq. 2.26}$$

The Cost variation sums the economic and energetic costs variations and can be plotted versus the diffuse fraction to evaluate its dependence on the climate conditions. Figure 2.21a shows the linear relation including the σ and 2σ intervals. The frequency distribution for the difference between fit-calculated and experimental σ(CV) values (Figure 2.21b), has a mean value of μ=0.007, 68.52% of the values inside the σ interval and 94.44% inside the 2σ.

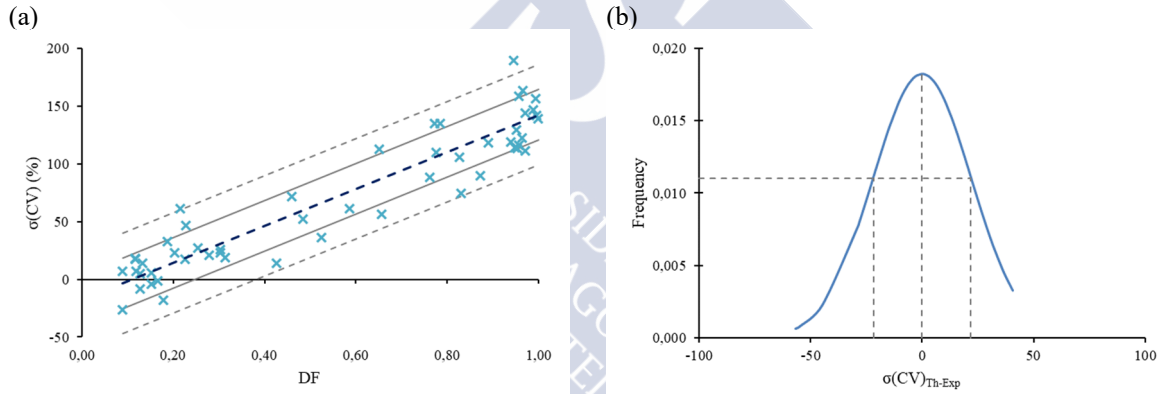

Figure 2.21. (a) Cost variation dependence with diffuse fraction and (b) frequency distribution of differences between theoretical and experimental σ(CV) values

The linear fit for the σ(CV) dependence with DF has a slope of 160.4 with an error of 11%. The intercept value is -17.7% with an error of 65%. Considering the average value, DF values below 0.11 will compensate the costs faster than established with the power production increase. Analysing the standard deviation intervals, for σ interval, this DF value would be 0.25 and, for 2 σ, the value would be 0.38.

2.4.7. Solar tracker net gain

After the experimental data analysis, the Performance Ratio variation and the Cost variation are characterized as function of climate conditions. The net gain of a solar tracker with respect to a fixed-tilt system is calculated after subtracting the overall associated costs, σ(CV), to the PR variation, σ(PR).

Plotted together in Figure 2.22, the region on the left to the intersection between production and costs restricts the climate conditions to have a net gain for installing a solar tracker system. By using the intersection for each linear fit, the average DF limit value for net gain is 0.41±0.06. But this numerical value only stands as the most probable, the standard deviation intervals must be considered. Table 2.3 shows the intercept value for the ±σ, ±2σ intervals.

Table 2.3. DF intercept value for σ, 2σ standard deviation intervals

		σ(PR)			
		-2σ	-σ	+σ	+2σ
σ(CV)	-2σ	0,50	0,55	0,64	0,68
	-σ	0,41	0,45	0,54	0,59
	+σ	0,23	**0,27**	0,36	0,41
	+2σ	**0,14**	0,18	0,27	0,31

For the σ deviation, the DF interval to have net gain for installing a tracker system is [0.27, 0.54] with 49.5% reliability. For the 2σ deviation, the gain moves on the [0.14, 0.68] DF interval with 89.2% reliability.

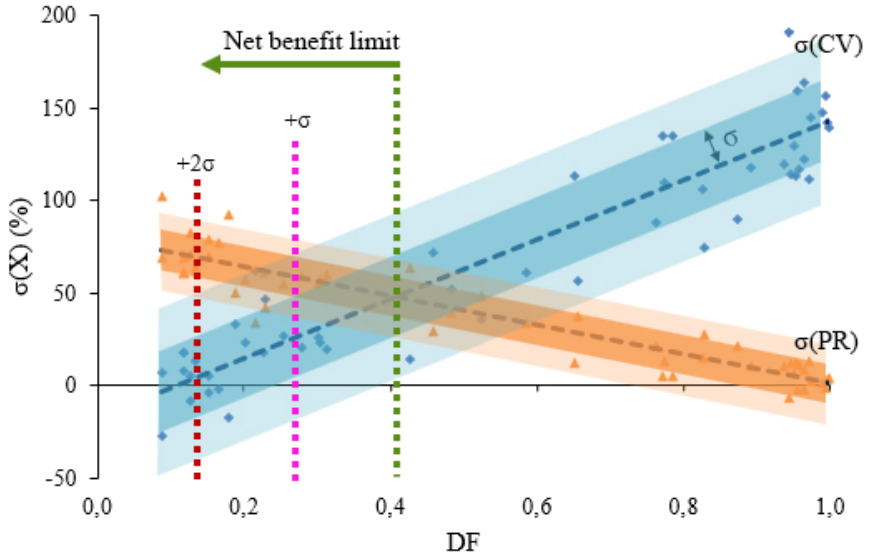

Figure 2.22. Performance Ratio variation and cost variation versus Diffuse Fraction

Therefore, once the relevance of the diffuse fraction as the parameter to measure the benefit of installing a solar tracker is verified, this method allows assessing the net gain for installing a solar tracker as function of climate conditions.

It must be noticed that the Performance Ratio variation is calculated for a solar tracker system compared to a horizontally-tilted array on a 42º latitude location. Optimal fixed-tilt system positioning facing south will affect the fixed tilt values.

Chapter 3 – Net benefit evaluation method for solar tracker connected PV systems

3.1. INTRODUCTION

As discussed in the previous chapter, the benefit of a solar tracker compared to a fixed-tilt PV system can be evaluated in terms of the climate conditions. For the analysis, the benefit is calculated after subtracting the tracker associated costs to its production increase. The climatic dependence is assessed with the diffuse fraction, which measures the cloudiness conditions. Thus, the benefit is related to a variable which defines the climate characteristics.

This chapter focuses on how to extend the developed method so it allows to evaluate the tracker suitability for any location or region. After the experimental results, obtained for a wide range of DF values from 0.10 to 1.00, the promising idea of extending the procedure worldwide is presented. The main obstacle is the absence of experimental solar diffuse radiation databases. Therefore, the main challenge is to characterize the world in terms of diffuse fraction. Currently, several online resources offer solar global irradiation maps [85] but diffuse radiation is usually computed after microphysics models [75][76] and not as easy to retrieve as solar global irradiation values.

To solve the lack of historical data required to characterize any world location in terms of diffuse fraction values, the NASA-SSE database [86], currently integrated into NASA-POWER [87], is considered. This database, with a resolution of 100 by 100 km, provides monthly average solar global and diffuse horizontal values for any given location. Only the latitude and longitude are required as input values. To ensure the data reliability, the database is validated with experimental values obtained from the AEMET Spanish meteorological service [88].

To create a statistically-representative database, almost 700 cities are characterized in terms of diffuse fraction. As a simplification, and since the annual basis is adequate for the solar tracker gain calculation, the annual average diffuse fraction is considered. For cataloguing each location and easily visualize results, the Köppen-Geiger climate classification is used [89]. This classification is selected due to its simplicity. Since it only considers temperature and precipitation values for the climate cataloguing, is one of the most used classifications. A relation between the monthly diffuse fraction and the different Köppen-Geiger climates is found. With the data, 29 categories for the existing climate types allow visualizing the results.

After the data selection, the solar tracker net benefit interval is calculated for each Köppen-Geiger climate type: A table with the Net Performance Ratio gain intervals for each climate is created and, additionally, a world map as general results tendency visualization is presented.

The results show a correspondence with the previously published gain intervals and, at the same time, prove the location dependence of the solar tracker gain percentage. This analysis led to the publication of a research paper [90]. The full paper is presented in Manuscript II.

3.2. METHODOLOGY

In the previous chapter, linear relations for the Performance Ratio (PR), Internal Rate of Return (IRR) and Energy Payback Time (EPBT) variations for a tracker-equipped compared to a fixed-tilt PV array were obtained as function of the diffuse fraction. The tracker production increase is represented with the PR variation, σ(PR). The tracker-associated costs are expressed with the Cost variation, σ(CV), as the convolution of the IRR and the EPBT variations.

These results are determined with experimental data from two PV arrays part of a grid-connected photovoltaic array owned by Norvento Enerxía [91]. Details of the experimental setup can be consulted in Chapter 2, Section 2.2. This method can be extended to any planet location as the study is developed for a solar global radiation range from 0 to over 1000 W/m^2, wide enough to ensure the representativeness of the equation. After this, and assuming the results validity, the method will be extrapolated to an annual basis as a first approximation.

This method depends on the diffuse fraction, DF, defined as the ratio between the diffuse and global radiation (Eq. 2.15). The main challenge for this procedure is to obtain a reliable data source for diffuse radiation values. Solar global horizontal radiation values are available from several sources, but diffuse horizontal radiation values are not generally available. Because of this difficulty, part of this chapter is dedicated to this purpose. Figure 3.23 sums the followed procedure. The work hypotheses are:

- The climate of a selected location can be characterized by the annual average diffuse fraction. The main purpose of this hypothesis is characterizing each location using only one value. However, this procedure can be repeated on a daily or monthly basis if a more dedicated study for a single location is required.
- The experimental results, obtained on a medium-irradiated area on a daily basis, can be extrapolated to an annual basis in terms of statistical intervals. The validity of this hypothesis is validated with experimental results.
- The Köppen-Geiger climate classification fully characterizes the diffuse fraction for a given location. This is probably the hardest hypothesis, as once a location is classified with the Köppen system, the DF value for the location is assigned. The DF values are obtained as the mean value of the dataset for the climate type.

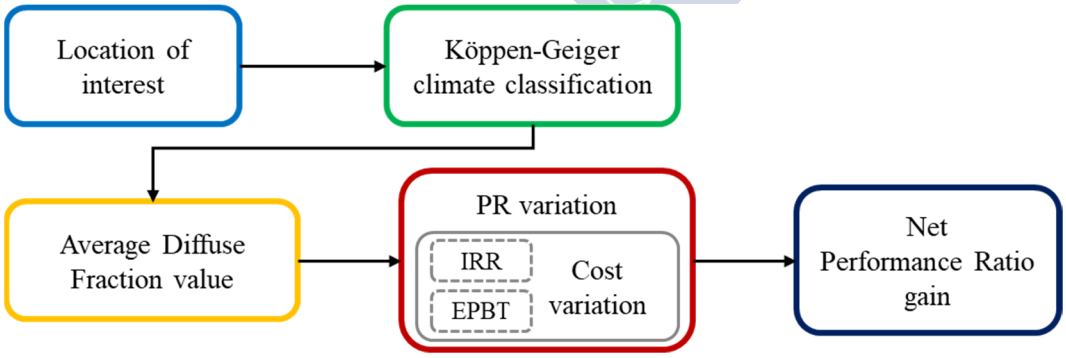

Figure 3.23. Applied methodology for the case of study

The experimental linear fit for the Performance Ratio variation, σ(PR), and Cost variation, σ(CV), are required for the calculation of the Net Performance Ratio gain, σ(PRN). The linear fit for the σ(PR) shows a negative slope of -78.7 with an 11% error and an intercept of 79.8 with a 7% error. The σ(CV) dependence with the diffuse fraction shows a slope of 160.4 with

an 11% error and an intercept compatible with zero (see Chapter 2, section 2.4.6 for additional information).

The **Net Performance Ratio gain**, σ(PRN), of a tracker-equipped compared to a fixed-tilt system evaluates the production increase after simultaneously taking into account the associated costs, σ(CV), and the PR variation, σ(PR). This evaluation can be done using different levels of restriction.

The most conservative criterion considers the intersection between σ(PR) and σ(CV) as the pair ($DF_{Maximum}$, $\sigma(PR)_{Minimum}$) to have benefit for installing a tracker compared with a fixed-tilt system for a given location. The obtained average values are (0.41±0.06, 53.3±8.1) (see Chapter 2, section 2.4.7 for further details and reliability discussion). Considering the standard deviation intervals, this criterion ignores DF values over 0.41 and PR variation values under 53.3%. The σ(PRN) calculated linear fit with this method shows a negative slope of -78.7 with an 11% error and an intercept of 32.1 with a 31% error. This method is the used in the published paper [90] and its results will be compared with the alternative analysis.

A more adequate and less restrictive criterion is applied on this chapter. The equations for σ(PR) and σ(CV) as function of the diffuse fraction allow to calculate their values including the standard associated errors. Using this method, the Net Performance Ratio gain, σ(PRN), is calculated as the difference between the PR variation and the Cost variation (Eq. 3.27).

$$\sigma(\mathrm{PRN}) = \sigma(\mathrm{PR}) - \sigma(\mathrm{CV}) \qquad \text{Eq. 3.27}$$

Therefore, a dedicated database with diffuse fraction values for the different Köppen-Geiger climate types has to be created. After, the average DF values for each climate can be used to calculate the Net Performance Ratio gain of a tracker-equipped PV array compared to a fixed-tilt system for the different existing climates.

3.3. CLIMATE CLASSIFICATION

Extending the Net Performance Ratio gain result to any location requires finding a suitable database for solar radiation and a data grouping criterion to manage and visualize the solar radiation information. Therefore, characterize the σ(PRN) of a solar tracker with respect to a fixed-tilt system requires to collect and catalogue the data with a climatic criterion. For it, and prior to select a solar radiation data source, a climatic classification has to be selected. Once defined, this classification will be used to group the diffuse fraction data.

3.3.1. Climate classification systems

There are several methods to classify climates based on different measurable values. The lack of a unique classification criterion shows the interest of this analysis. Any climatic classification must be based upon simple and easy to acquire data. After the data, the result must provide a general overview of the climate but, at the same time, offer details to distinguish climates alike. Modern climate classifications depend on, at least, two values. Usually, these values are precipitation and temperature.

- **Astronomical climates** [92]: The most ancient classification system defines the climates in terms of the latitude. The astronomical systems measure the temperature

decrease and the seasonal variations with the increasing latitude. These systems are not empirical methods based on measurable parameters.

- **De Martonne classification** [93]: This system is based on a geographical criterion. This classification identifies nine climatological regions after temperatures thresholds plus annual average temperature and precipitations. Each of the nine regions is constituted by similar climates. This system is not numerically defined.
- **Köppen-Geiger classification** [89]: This semi-empirical climate classification is the most popular. Initially defined in terms of vegetation, the climates are numerically defined in terms of temperature and precipitation. The climates are defined after the limits of zones with different vegetation distributions. The Trewartha classification [94] is a modification of the Köppen-Geiger system.
- **C.W. Thornthwaite classification** [95]: This is an empirical climate classification based on the precipitation effectiveness (water balance) and the thermal efficiency. It also uses the potential evapotranspiration, relevant for the vegetation growth. This system divides the regions in climates from mostly humid to mostly dry. The required values for the classification (thermal efficiency and water balance) are not easily available for any location.

After considering the availability of precipitation and temperature values, the Köppen-Geiger climate classification will be considered as the data grouping system. Genetic approaches, like the Heinrich Walter classification [96], are not considered for this analysis.

3.3.2. Köppen-Geiger climate classification

This classification was created by the German climatologist Wladimir Köppen in 1884 and subsequently revised by himself and Rudolf Geiger. The final classification is able to describe each climate type with a series of letters to describe its characteristics [89][97].

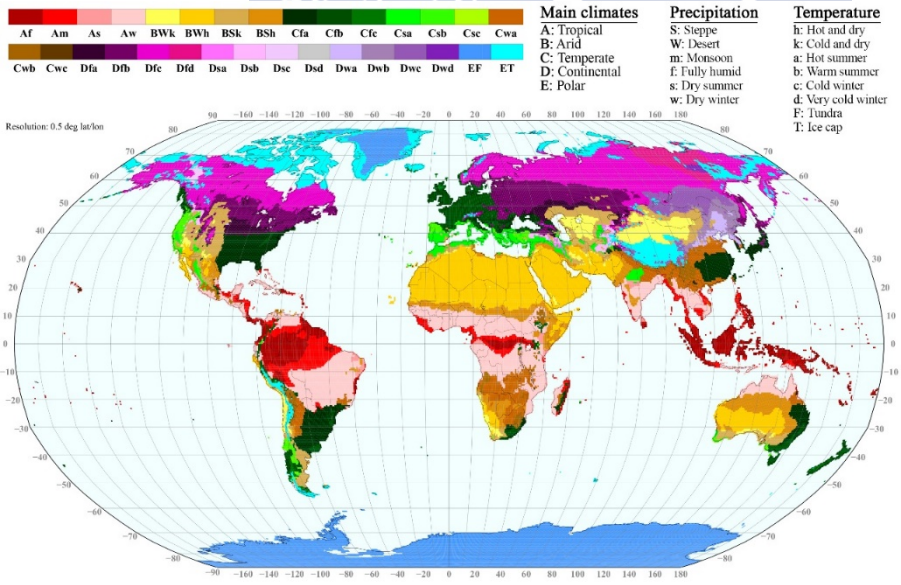

Figure 3.24. World map of Köppen-Geiger climate classification [89]

This classification divides the climates into five major types represented with a capital letter, which defines the temperature general regime. The five main climates are subdivided into various subtypes, represented with additional letters. While the second letter represents the seasonal precipitation type, the third letter indicates the heat level. From Table 3.4 to Table 3.6

the main types and subtypes criteria are shown. Figure 3.24 shows the Köppen-Geiger climate distribution worldwide.

Table 3.4. Köppen-Geiger main groups classification and criteria

1st letter	Description	Criteria
A	Tropical	No month with average temperature under 18ºC
B	Arid	Evaporation surpasses the average year precipitation
C	Temperate	Coldest month with average temperature over -3ºC and below 18ºC
D	Continental	Coldest month with average temperature over -3º and hottest month above 10ºC
E	Polar	No month with average temperature above 10ºC

Table 3.5. Köppen-Geiger precipitation classification criteria

2nd letter	Applies to climates	Description	Precipitation
S	B	Steppe	Annual precipitation over 50% of the potential evaporation
W	B	Desert	Annual precipitation lower than 50% of the potential evaporation
m	A	Monsoon	Driest month with less than 60 mm but more than 4% of the total annual precipitations
f	A, C, D	Fully humid	Precipitation over 60 mm all year
s	A, C, D	Dry summer	Precipitation less than 60 mm in summer
w	A, C, D	Dry winter	Precipitation less than 60 mm in winter

Table 3.6.Köppen-Geiger temperature classification criteria

3rd letter	Applies to climates	Description	Temperature
h	B	Hot and dry	Average annual temperature over 18ºC
k	B	Cold and dry	Average annual temperature under 18ºC
a	C, D	Hot summer	Maximum temperatures over 22ºC
b	C, D	Warm summer	Maximum temperatures under 22ºC and at least four months over 10ºC
c	C, D	Cold summer	Less than four months over 10ºC and minimum temperature over -38ºC
d	C, D	Very cold winter	Less than four months over 10ºC and minimum temperature under -38ºC
F	E	Tundra	Warmest month with average temperature between 0ºC and 10 °C
T	E	Ice cap	Average annual temperature under 0ºC

When calculating the climate for a location, it can happen that a climate fulfils the conditions of more than one climate subtype. If this happens, a hierarchical system is applied to determine the climate [97]. This hierarchical system is presented in Table 3.7. For example, a climate satisfying *BS* and *Ds* criteria is classified as *BS*. Also, a climate verifying *As* and *Aw* conditions will be classified as *As*.

Table 3.7. Hierarchical order criteria for Köppen-Geiger climate classification in case of climate fulfilling multiple subtypes

	Main type	Subtypes hierarchical order
1st	E	ET → EF
2nd	B	BSh → BSk → BWh → BWk
3rd	A	Af → Am → As → Aw
4th	C	Csa → Csb → Csc → Cwa → Cwb → Cwc → Cfa → Cfb → Cfc
5th	D	Dsa → Dsb → Dsc → Dsd → Dwa → Dwb → Dwc → Dwd → Dfa → Dfb → Dfc → Dfd

3.4. SOLAR RADIATION

The solar radiation reaching the Earth surface can be experimentally determined or estimated with the use of micro-physics models. The values can be directly measured with ground-based instrumentation, or remotely with satellites.

Models for solar radiation are required since the number of solar radiation measuring stations is not sufficient to characterize any location. The first theoretical model for the global solar radiation estimation was proposed by Ångström and Prescott [98]. Since then, new models and improvements to increase their reliability were developed.

3.4.1. Solar radiation variables

The solar radiation available databases offer different variables. Prior to analysing the available solar radiation datasets, the basic definitions to be taken into consideration are presented [71][72]. In Chapter 2, Section 3.1 the basic solar radiation variables were defined. The diffuse fraction is defined in Section 3.2 of the same chapter.

In addition to these variables, the direct normal irradiance (DNI) can be defined as the amount of solar radiation received per unit area on a flat surface always placed perpendicular to the Sun's beam. Eq. 3.28 shows the relation between global horizontal, diffuse horizontal and direct normal irradiation, where θ is the solar zenith angle [71][72].

$$\mathrm{GHI} = \mathrm{DHI} + \mathrm{DNI}\ \cos\theta \qquad \text{Eq. 3.28}$$

The presence of the solar zenith angle on Eq. 3.28 makes no possible to consider the DNI values for an unbiased net gain analysis as it depends on the latitude and time. Thus, a database including the DNI as an alternative for calculating the DHI value will not be suitable for this analysis. Only databases including GHI and DHI values for the direct calculation of the Diffuse Fraction (Eq. 2.15) can be considered.

3.4.2. Global solar radiation databases

To extend the results to a worldwide scale, a database must be created to characterize any globe location in terms of the diffuse fraction. Thus, a solar radiation database must be found to collect monthly solar global and diffuse horizontal data after a latitude-longitude pair. For this purpose, the following databases were initially considered:

- **NREL - National Solar Radiation Data Base** [99]: The database uses PSM and SUNY models (Table 3.8). This site provides GHI and DNI values for the United States, Central America, part of South America and India. This database cannot be considered due to the lack of DHI values and the limited regional data availability.
- **PVgis - Photovoltaic Geographical Information System** [100]: Uses the ECMWF and COSMO-REA models (Table 3.8).Provides GHI and DNI and covers Europe, Africa and South Asia. Cannot be considered due to the limited regional data availability and the absence of DHI data.
- **World Bank Group - Global Solar Atlas** [101]: Uses the SolarGIS models (Table 3.8). Provides free worldwide GHI and DHI but on annual basis.
- **NASA-SSE - Surface meteorology and Solar Energy** [86][87]: Uses the Pinker and Laszlo algorithm (Table 3.8). Provides GHI, DHI and additional climate values (temperature, precipitation, wind, …) for a given latitude-longitude pair.

Table 3.8. Satellite model resolution

Model	PSM [102]	SUNY [103]	ECMWF [104]	COSMO-REA [105]	SolarGIS [85]	NASA-SSE [106]
Temporal resolution (h)	0.5	1	3	1	< 1	3
Spatial resolution (km^2)	4x4	10x10	30x30	6x6	0.25x0.25	100x100

After this analysis, the NASA-SSE database will be selected since it provides all the required values for the analysis. In addition to the availability of solar global and diffuse horizontal radiation values, it offers the required climatic data to determine the Köppen-Geiger climate for the location.

3.5. DATABASE VALIDATION

Until now, the meteorological data and solar radiation data sources are defined. Also, the data cataloguing system is selected. Before starting to create the database for the diffuse fraction values, the solar radiation values must be validated. After the solar radiation data source validation, the database can be constructed.

3.5.1. NASA-SSE data validation after AEMET/CM-SAF databases

Several authors state the low reliability of the NASA-SSE data source, analysing its high associated error comparing with other data sources [107]. However, it is considered one of the most complete database worldwide as it provides multiple meteorological variables. In order to validate the NASA-SSE solar radiation values, the AEMET experimental radiation values for 47 Spanish cities in the Iberian Peninsula. The AEMET's solar global and diffuse radiation values are collected from the "*Atlas de Radiación Solar en España*" (Solar Radiation Atlas for Spain) [90][108].

The AEMET solar radiation values are validated with the Climate Monitoring Satellite Application Facilities (CM-SAF) [109]. This solar radiation data source has a high resolution (3x3 km) and high accuracy (0.19 kWh/m^2day maximum deviation with respect to data from 12 meteorological stations around the world). The data comparison of the CM-SAF and 29 AEMET meteorological stations located in Spain shows a 6.7% difference between both databases. Thus, the AEMET radiation atlas can be considered as a reliable source for radiation values comparison.

The monthly global, GHI, and diffuse, DHI, radiation values are collected for each location from the NASA-SSE and the AEMET data sources. To easily compare the results, the annual average global, <G>, and diffuse, <D>, horizontal values for each location is calculated. The results are shown in Figure 3.25. It can be seen that for mainly all locations the experimental values both for GHI and DHI are higher than the satellite-based.

Table 3.9 shows the difference between the NASA and the AEMET's data sources for the global and diffuse radiation annual average values, as well as the diffuse fraction. The low difference between both datasets allows considering the NASA-SSE solar radiation data source as valid for the intended analysis [90]. It must be remarked that the diffuse fraction value shows a small discrepancy as the ratio compensates the variations.

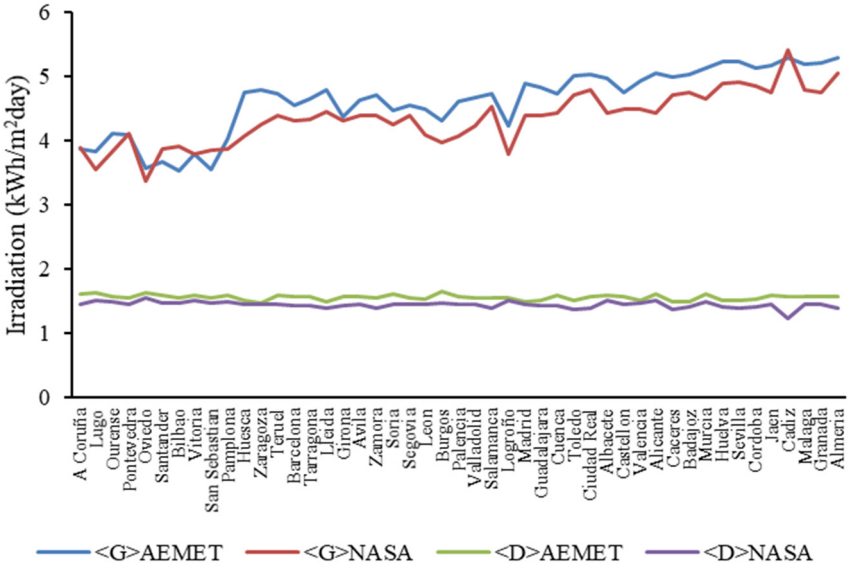

Figure 3.25. Solar global and diffuse annual average values from AEMET and NASA-SSE for the 47 cities considered for the data validation

Table 3.9. Difference of annual average NASA radiation values with the AEMET data source for validation

Global radiation	Diffuse radiation	Diffuse Fraction
-8.01%	-6.2%	-2.87%

However, this validation is not enough to ensure the data validity. As any world location will be experimentally characterized as function of the DF value or its equivalent Köppen-Geiger climate type, a monthly data validation per climate is required. Since there are no experimental solar radiation values to validate the 80% of the world, this validation will be done with the Spain's AEMET database.

For that end, cities of the six Köppen-Geiger climates types existing in the Iberian Peninsula are used. For the analysis, the climate type is calculated for each considered city. After, the monthly difference between AEMET and NASA-SSE can be assessed for the different climate types. As an example, one city for the 6 main climate types in Spain is shown in Figure 3.26. For all the considered cities, a good accordance between both datasets is observed.

Regarding the differences of both datasets for the monthly global radiation, it is detected that the *Cfb* climate, unlike the others, has a negative difference between G_{AEMET} and G_{NASA} for the winter to the summer season in mostly all the 10 analysed cities. It must be noticed that this climate type is the cloudiest of the existing in the Iberian Peninsula. For the rest of the climates, the difference between both datasets varies from 2% (March, *BSh*) to 14% (October, *Cfa*).

Considering the differences for the monthly diffuse radiation datasets, a similar behaviour for all the climates appears for the autumn to spring interval while the summer season shows high discrepancies between both data sources.

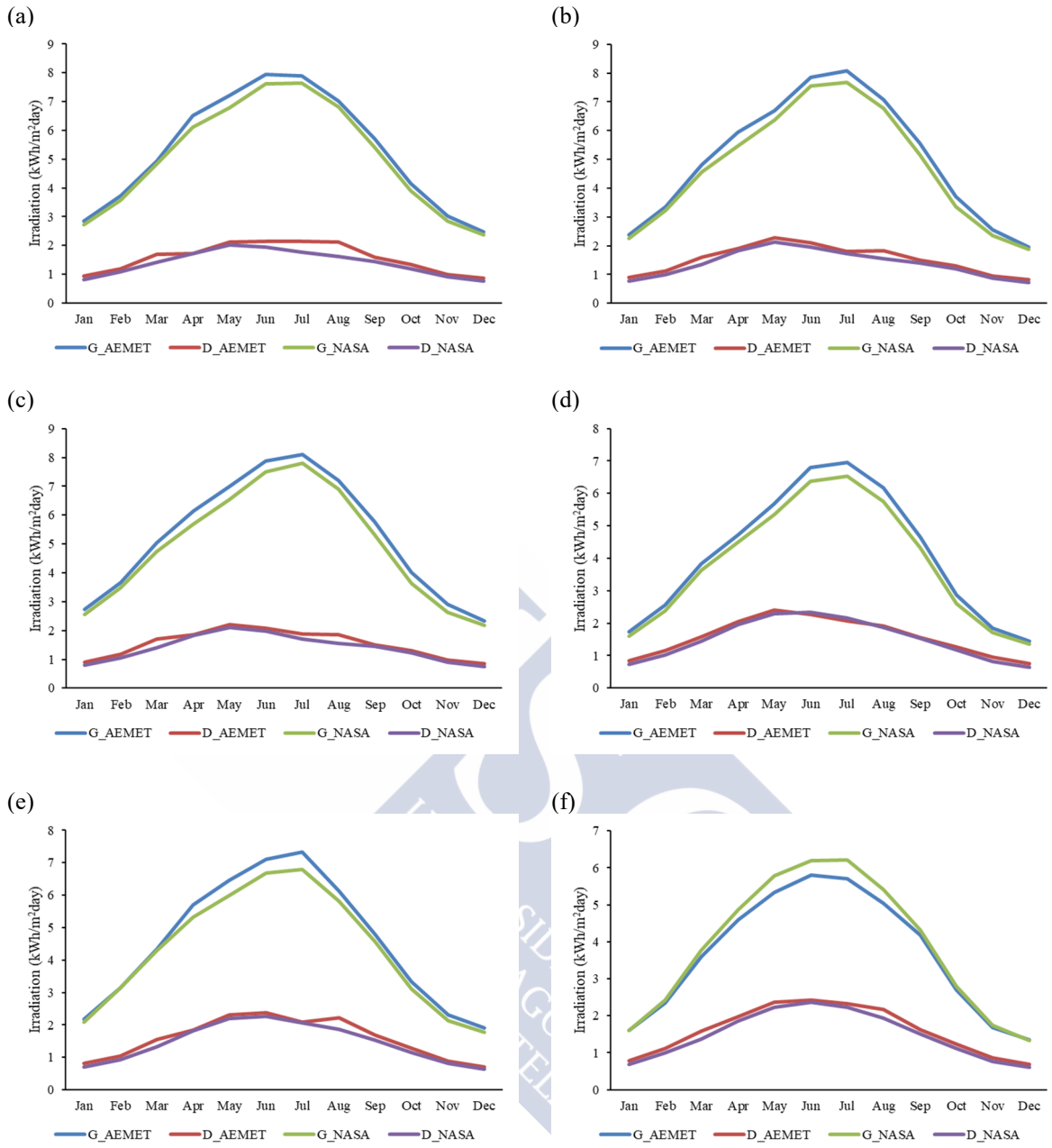

Figure 3.26. Monthly average global and diffuse radiation values for experimental (AEMET) and satellite (NASA-SSE) data bases: (a) Almería, *BSh* climate; (b) Toledo, *BSk* climate; (c) Málaga, *Csa* climate; (d) Ourense, *Csb* climate; (e) Zaragoza, *Cfa* climate; (f) Santander, *Cfb* climate

3.5.2. Data selection and filtering

As explained before, the NASA-SSE allows gathering at once solar radiation data plus meteorological data for a given location. As input value, only the location's latitude and longitude are required.

Figure 3.27 shows the procedure for the data selection. Using the Köppen-Geiger climate classification as a cataloguing system, the data for the cities to create the database are collected. The primarily cities cataloguing is done using the *Weatherbase* website [110]. This website provides meteorological information for any city worldwide. For each of the cities, the geographical coordinates and the elevation are additionally collected using the *Geobase* website

[111]. The geographical coordinates are required as input data for the NASA-SSE data retrieve. The elevation is required for later climate type data filtering.

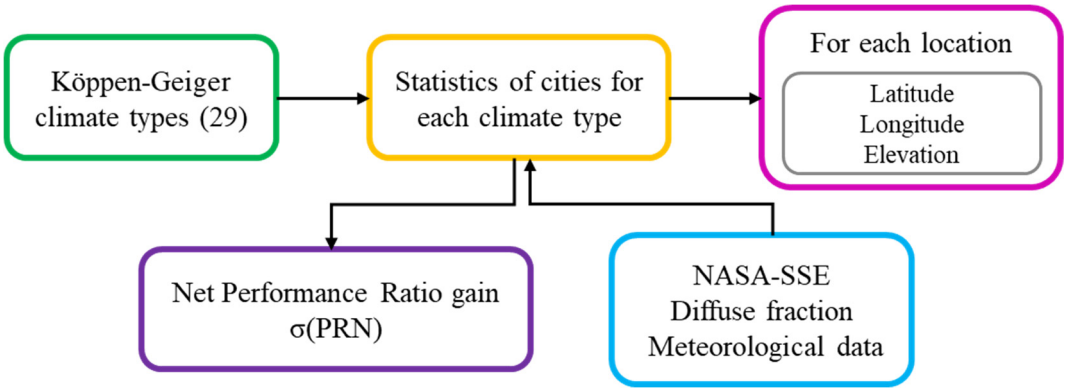

Figure 3.27. Applied methodology for the database data selection

With the input data for each city, the solar radiation and meteorological data are retrieved from the NASA-SSE data source for the locations. These values allow to calculate the monthly diffuse fraction and the Köppen-Geiger climate type for each city.

All the southern hemisphere gathered data are translated to the northern hemisphere to avoid the seasonal differences in the statistical analysis. After these values, the Köppen-Geiger climate classification can be calculated for each location. The different climate types are grouped into subsets, with the monthly diffuse fraction for each city.

Aiming to create an unbiased database for each climate subset, the following filters were applied to each subsample:

- To avoid the elevation effect, locations over 1500 m above mean sea level are removed from the database for the Köppen-Geiger *A*, *B*, *Cf* and *Cs*. This criterion does not apply to the *Cw*, *Ds* and *Dwc* climates as they appear at high altitudes.
- The minimum accepted distance between locations, in latitude and longitude, is 0.5º inside each subsample.

After the data filtering, the database has 689 cities belonging to the 29 Köppen-Geiger climates [90]. The database, with over 35000 values, is considered hereafter for the whole analysis.

3.5.3. Diffuse fraction pattern of behaviour for Köppen-Geiger climate types

Once created the database and prior to calculating the Net Performance Ratio gain, σ(PRN), of a tracker compared with a fixed tilt system, the relation between climate and diffuse fraction must be assessed. Only if the DF is a descriptor of the different Köppen-Geiger climates, the data cataloguing will be feasible.

The behaviour of the monthly diffuse fraction is assessed on this section for each climate subtype. For this analysis, the monthly average value for each data subset is calculated. The results are shown in Figure 3.28, where the average DF value along the year for the Köppen-Geiger climates is plotted. Different patterns appear for each climate type. Analysing each plot, it can be seen that *Cw* climates show quite similar behaviour (Figure 3.28e), but *Cwa* and *Cwb*

climates appear at different height above the sea level, around 1000 m for *Cwa* and 2000 m for the *Cwb* climate subtypes. Therefore, the DF is a descriptor of the climate types and one of the initial hypotheses is confirmed.

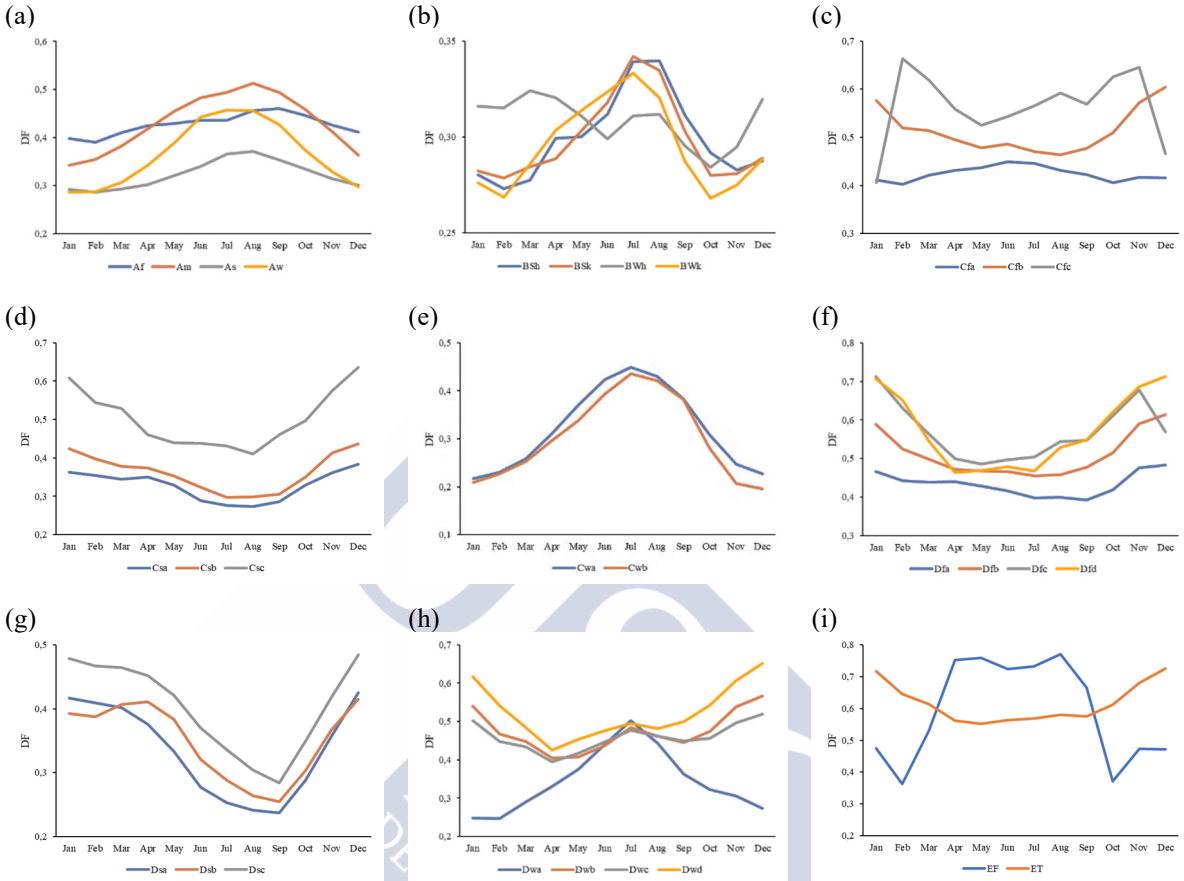

Figure 3.28. Monthly average diffuse fraction values for the different Köppen-Geiger climate types: (a) *A*, (b) *B*, (c) *Cf*, (d) *Cs*, (e) *Cw*, (f) *Df*, (g) *Ds*, (h) *Dw* and (i) *E*

Table 3.10. Available statistic and data analysis results for each Köppen-Geiger climate subtype

Köppen climate	Sample statistic	Data inside the interval	
		σ	2σ
Af	26	66,35	97,12
Am	26	67,95	94,87
As	21	69,05	96,03
Aw	58	64,66	96,84
BSh	32	67,45	96,09
BSk	35	70,00	96,67
BWh	32	75,00	94,27
BWk	15	60,56	98,89
Cfa	42	65,08	97,62
Cfb	69	66,91	97,22
Cfc	21	69,05	97,22
Csa	39	71,37	94,87
Csb	19	63,16	100,00
Csc	2	100,00	100,00
Cwa	15	67,22	97,78
Cwb	20	72,50	96,25

Köppen climate	Sample statistic	Data inside the interval	
		σ	2σ
Dfa	21	65,87	98,02
Dfb	46	65,40	96,92
Dfc	41	70,33	95,33
Dfd	4	64,58	100,00
Dsa	8	70,83	97,92
Dsb	18	82,41	94,91
Dsc	4	85,42	100,00
Dwa	20	78,33	93,33
Dwb	3	66,67	100,00
Dwc	18	75,93	92,59
Dwd	1	100,00	100,00
EF	11	66,67	98,48
ET	22	67,42	96,59

For ensuring the average values reliability, the corresponding statistical analysis must be done. For this, the standard deviation and frequency distribution of the difference between the monthly average DF and the DF value for each location are calculated. The percentage of values lying inside the σ and 2σ are also calculated to ensure the strength of the analysis. The normal distribution of the values shows the statistical representativeness of the datasets for each sample.

The number of samples for each climate type plus the percentage of values inside the σ, 2σ intervals is shown in Table 3.10. The low data sample for some climate types is a consequence of the lack of retrieving inhabited locations where the climate appears.

As examples of the frequency distribution, Figure 3.29 shows the frequency distribution for the average DF values of four different climate types on different seasons (January for winter, April for spring, July for summer and October for autumn).

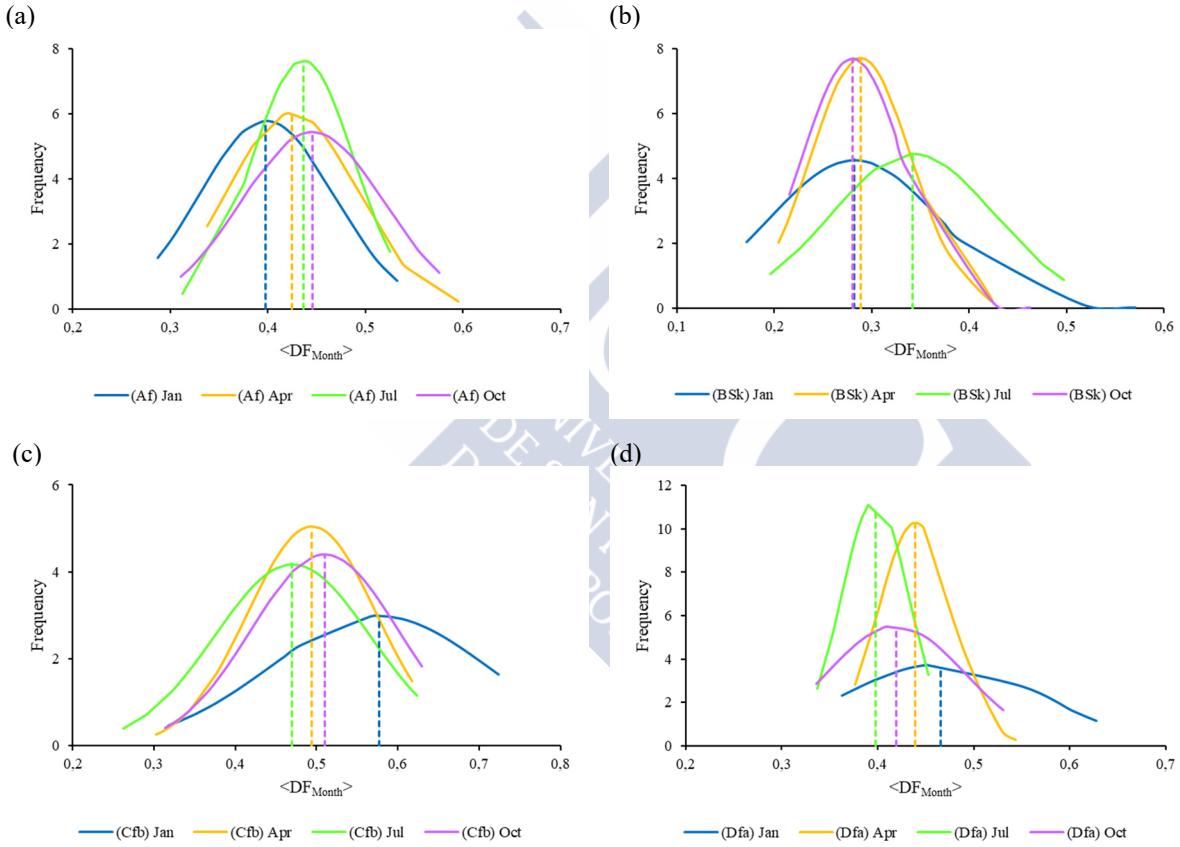

Figure 3.29. Average monthly DF frequency distribution on different seasons for climate types (a) *Af*, (b) *BSk*, (c) *Cfb*, (d) *Dfa*

Analysing the monthly variation of the mean values and the normal distribution for each selected climate, the DF values range can be visualized. Also, the climatic seasonality can be visualized with the DF mean value shift with the different seasons. Also, the data cut shows the minimum and/or maximum DF values found for each climate with the collected data. The analysis of each subset shows the differences between climates:

- The frequency distribution for the *Af* climate type (tropical rainforest) is shown in Figure 3.29a. It can be seen that the minimum calculated DF value is lower than 0.30 and

appears in January. The maximum DF value appears on April. Also, the variation between standard deviation values and the low DF seasonality can be seen. For this climate, the diffuse fraction values are inside the [0.39, 0.46] interval.

- For the *BSk* climate (cold semi-arid, Figure 3.29b), a low seasonality with only one rainy season appears. Low DF values appear during all the year, with monthly DF mean values inside the [0.28, 0.34] interval, showing values under 0.20 in January and July. Also, the similar behaviour appears in April and October.
- The *Cfb* climate (temperate oceanic, Figure 3.29c) shows a high seasonal variability in the DF values, lying between the [0.46, 0.60] interval. Even if the distribution width is higher than in the previous cases, January shows a particularly high standard deviation: the mean value of 0.58 refers a standard deviation of 0.13. The extremely high range in terms of this season DF values would require further analysis.
- The winter variability appears also on the *Dfa* climate (humid continental with hot summer, Figure 3.29d). For January, the mean DF value, 0.47, refers a 0.11 standard deviation value. The monthly DF values lie inside the [0.39, 0.48].

3.6. RESULTS

The monthly diffuse fraction frequency accurately characterizes the different Köppen-Geiger climates. This monthly characterization provides useful information for sizing or analysing PV systems. But when considering the advantages of installing a solar tracker as racking design on a PV system, its gain integrated along the year is the value of interest. Therefore, the annual average DF value can be considered as representative for the analysis.

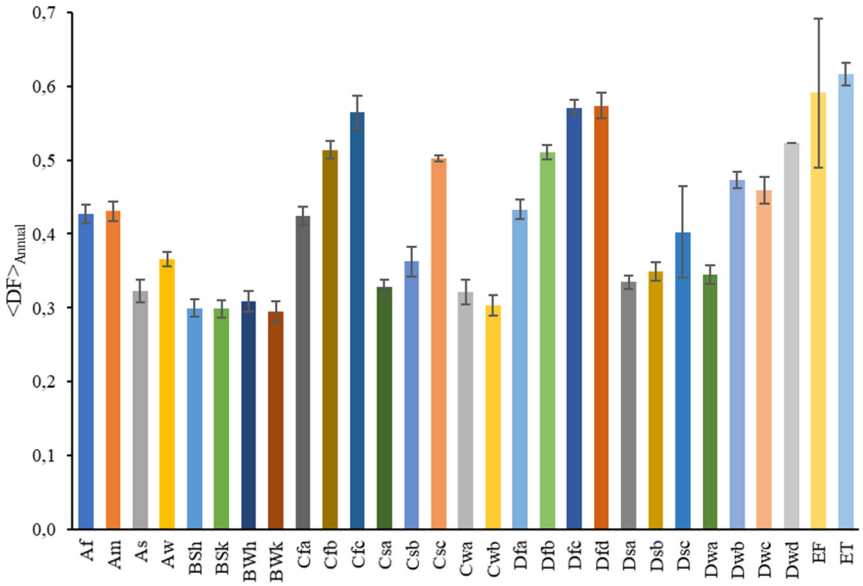

Figure 3.30. Average annual diffuse fraction value for the Köppen-Geiger climate types

Thus, the annual average diffuse fraction value for each climate will be considered hereafter for the tracker gain calculations. Figure 3.30 shows the average annual diffuse fraction value for each climate including the standard error bars. The average associated error to the annual average diffuse fraction value is 4.1%. However, *Dsc* (subarctic) and *EF* (polar) climates show a 15% and 17% standard error respectively. This high error values are related to the difficulty of gathering enough statistics in these extreme climates. Despite these two climates,

the low standard error ensures the validity of the annual average values for the solar tracker Performance Ratio variation calculation.

3.6.1. Performance Ratio variation for the Köppen-Geiger climate types

As said, the monthly DF values allow to individually calculate the Performance Ratio variation, σ(PR). But the production increase of installing a tracker compared to a fixed-tilt system should be measured on an annual basis. For this, the average annual σ(PR) for each climate is calculated. The results, including the standard error bars, are plotted in Figure 3.31.

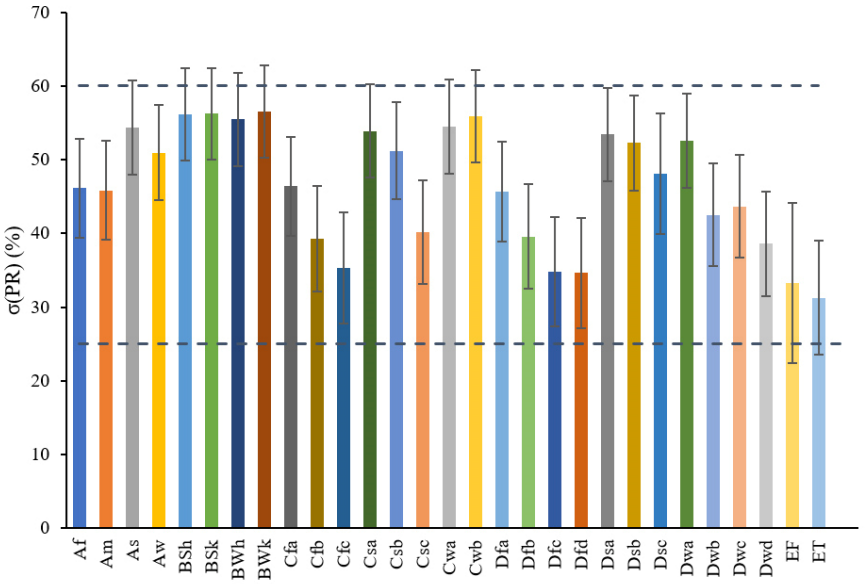

Figure 3.31. Annual average Performance Ratio variation for the Köppen-Geiger climate types

After this plot, it can be seen that the published results from different authors stating the solar tracker production increase, defined with the σ(PR), up to a 40% is valid for just some specific climates. Also, a σ(PR) over 25% is observed for all the climates.

Therefore, the usually-stated solar tracker gain range of 25-40% is verified. But the gain is function of the climate type and can be univocally defined for any location once the climate conditions are known. In fact, the detailed knowledge of climate conditions plays a key role in determining the Performance Ratio variation prior to the racking design selection.

3.6.2. Net Performance Ratio gain dependence with Köppen-Geiger climate types

The calculated annual average σ(PR) value does not take into consideration the tracker associated multidimensional costs. The net benefit of a solar tracker compared with a fixed-tilt system requires considering both the Performance Ratio variation and the Cost variation, σ(CV). As seen in Section 3.2, two different levels of restriction are considered for this dependence analysis.

The application of the most conservative criterion leads to the published results [90]. In this section, these results will be compared with the less restrictive criterion. For both methods, the annual average diffuse fraction values for each climate type (Figure 3.30) are considered. Figure 3.32 shows the annual average Net Performance Ratio gain for each climate including the associated standard errors for both methodologies.

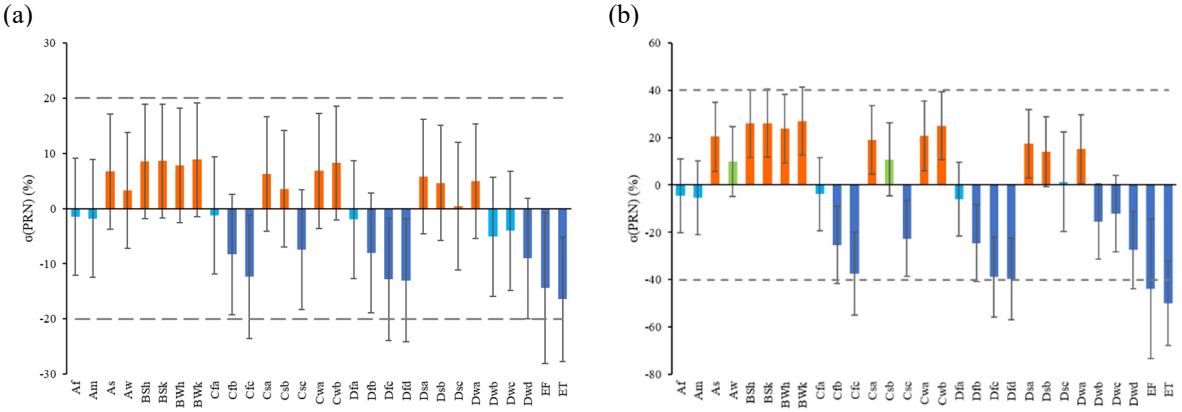

Figure 3.32. Net Performance Ratio gain for the Köppen-Geiger climate types (a) conservative (b) less restrictive method

Considering the most conservative criterion, the σ(PRN) interval has over a 25% variation between climates: The maximum value appears for the *BSk* (cold desert) climate with a 9% gain, while the minimum σ(PRN) of -16% appears on the *ET* (polar ice cap) climate.

The application of the less restrictive method increases the σ(PRN) interval to a 77% variation between the maximum 27% average gain for the *BSk* climate to the minimum -50% for the *ET* climate. The main difference of this method compared with the conservative criterion is that this method allows to find advised climates even considering the associated standard errors.

For both methods, the calculation of the standard error for the Net Performance Ratio gain shows a high associated error, mainly related to the high error of the intercept value (see Section 3.2). Therefore, tendencies must be considered instead of results. For the analysis, four categories are considered:

- **Advised climates:** For these climates, the σ(PRN) values interval is fully included in the positive range. Installing a solar tracker is the optimal racking design solution as the production increase is ensured.
- **Positive tendency climates:** For these climates, the σ(PRN) is mainly in the positive range, even if the negative range is included. Due to this associated uncertainty, the positive tendency is adequate instead of referring to totally positive climates. For this climate, the solar tracker is as a recommendable design solution as the production net improvement is expected.
- **Negative tendency climates:** The σ(PRN) values, including its error bars, move along a positive to negative data range. The resolution of this method does not allow to make a decision in terms of system racking design. Higher data statistic or on-location experimental data are required to choose the optimal design.
- **Totally not advised climates:** The full σ(PRN) data interval moves in the negative range. Also, the associated errors are mainly in the negative range. For these climates, a fixed-tilt PV system is particularly suggested as the optimal design.

Table 3.11 shows the number of climates inside each defined the categories. The main difference between both methods is the decrease of no conclusive climates when considering the less restrictive method. Hence, the conservative criterion seems inadequate for determining the suitable climates for solar tracker installation.

Table 3.11. Number of climates inside defined categories for the two considered methods

	Advised climates	Positive tendency climates	No conclusive climates	Totally not advised climates
Conservative criterion	-	14	10	5
Less restrictive method	11	2	5	11

Table 3.12. General results of Diffuse Fraction and Net Performance Ratio gain for the Köppen-Geiger climate types

Köppen-Geiger climate type		<DF_{Annual}>	Average σ(PRN)	σ(PRN) interval	Result
Af	Tropical rainforest	0.43±0.06	-4,6	[-20.1, 10.8]	Negative tendency
Am	Tropical monsoon	0.43±0.07	-5,5	[-21.0, 10.1]	Negative tendency
As	Savannah	0.32±0.07	20,3	[5.6, 35.0]	Advised
Aw	Tropical wet	0.37±0.07	9,9	[-4.8, 24.7]	Positive tendency
BSh	Hot semi-arid	0.30±0.07	25,9	[11.6, 40.1]	Advised
BSk	Cold semi-arid	0.30±0.07	26,1	[11.8, 40.4]	Advised
BWh	Hot desert	0.31±0.08	23,7	[9.3, 38.2]	Advised
BWk	Cold desert	0.30±0.05	26,9	[12.5, 41.2]	Advised
Cfa	Humid subtropical	0.42±0.08	-3,9	[-19.3, 11.5]	Negative tendency
Cfb	Temperate oceanic	0.51±0.10	-25,3	[-41.7, -9.0]	Totally not advised
Cfc	Subpolar	0.56±0.10	-37,6	[-55.1, -20.0]	Totally not advised
Csa	Hot-summer Mediterranean	0.33±0.06	19,0	[4.6, 33.4]	Advised
Csb	Warm-summer Mediterranean	0.36±0.09	10,8	[-4.5, 26.1]	Positive tendency
Csc	Cool-summer Mediterranean	0.50±0.01	-22,6	[-38.6, -6.6]	Totally not advised
Cwa	Monsoon-influenced humid subtropical	0.32±0.06	20,7	[6.0, 35.4]	Advised
Cwb	Subtropical highland	0.30±0.06	25,0	[10.6, 39.4]	Advised
Dfa	Hot-summer humid continental	0.43±0.06	-6,1	[-21.6, 9.5]	Negative tendency
Dfb	Warm-summer humid continental	0.51±0.06	-24,6	[-40.8, -8.3]	Totally not advised
Dfc	Subarctic	0.57±0.07	-38,9	[-55.9, -21.9]	Totally not advised
Dfd	Extremely cold subarctic	0.57±0.03	-39,6	[-56.9, -22.3]	Totally not advised
Dsa	Hot, dry-summer continental	0.33±0.03	17,5	[3.0, 32.0]	Advised
Dsb	Warm, dry-summer continental	0.349±0.05	14,0	[-0.8, 28.7]	Advised
Dsc	Dry-summer subarctic	0.40±0.12	1,3	[-19.7, 22.3]	Negative tendency
Dwa	Monsoon-influenced hot-summer humid	0.35±0.06	15,0	[0.3, 29.7]	Advised
Dwb	Monsoon-influenced warm-summer humid continental	0.47±0.02	-15,6	[-31.4, 0.3]	Totally not advised
Dwc	Monsoon-influenced subarctic	0.46±0.08	-12,2	[-28.3, 3.9]	Totally not advised
Dwd	Monsoon-influenced extremely cold subarctic-continental	0.52±0.00	-27,5	[-43.7, -11.3]	Totally not advised
EF	Tundra	0.59±0.33	-43,8	[-73.2, -14.3]	Totally not advised
ET	Ice cap	0.62±0.07	-49,9	[-67.6, -32.1]	Totally not advised

These Net Performance Ratio gain intervals constitute a promising method to primarily assess the suitability of installing a solar tracker system. The results, resumed on Table 3.12 for the less restrictive method, ease the estimation of the σ(PRN) of a solar tracker system versus a fixed tilt design worldwide. Despite being non-representative as a result due to the associated errors, the average Net Performance Ratio gain is included. The σ(PRN) intervals for the conservative criterion can be consulted on the published paper (see Manuscript II) [90].

The results in Table 3.12 constitute the reference values for the Net Performance Ratio gain of a tracker compared to a fixed-tilt system for a given location knowing the climate classification. The values, considering the σ(PRN) intervals, are compatible with the research paper results but as, previously, the gain is limited to specific climates.

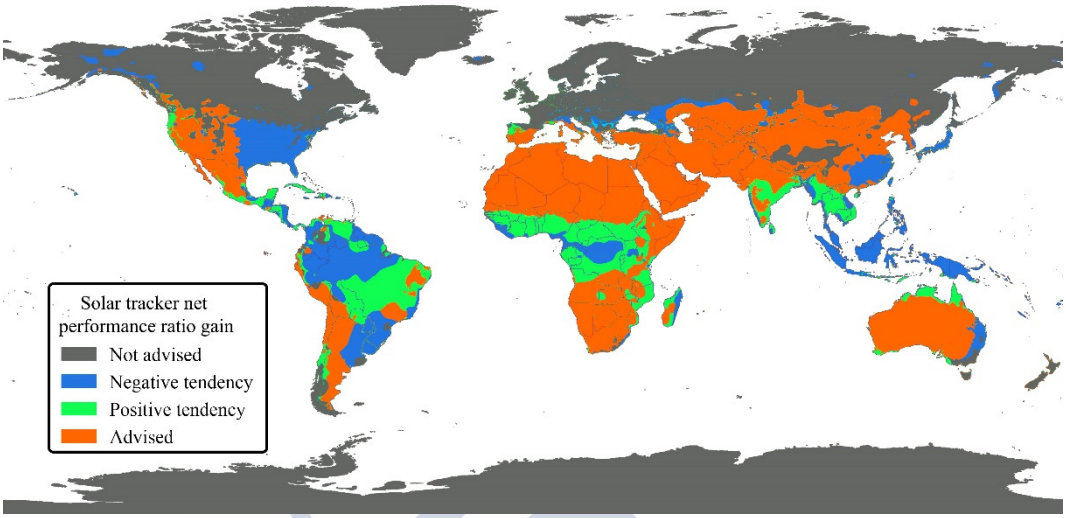

Figure 3.33. Solar tracker Net Performance Ratio gain

In order to offer a visualization of the tracker suitability, a world map is presented in Figure 3.33. This general estimation does not consider the microclimate variations within regions. Thus, to ensure the reliability of the result, the climate of the PV system location must be analysed prior to decide the optimal racking design. After this general map, it can be seen that latitudes over 40ºN appear as the less suitable for solar tracker installing (regardless the local microclimates). The world map considering the conservative criterion [90] shows a similar tendency. However, the less restrictive method seems more accurate to describe the adequateness of installing a solar tracker.

3.6.3. Performance Ratio gain dependence in economic terms

In addition to the developed analysis, an alternative evaluation only based on the economic profitability can be done. For this section, only the Performance Ratio variation, σ(PR) and the Internal Rate of Return variation, σ(IRR) are used.

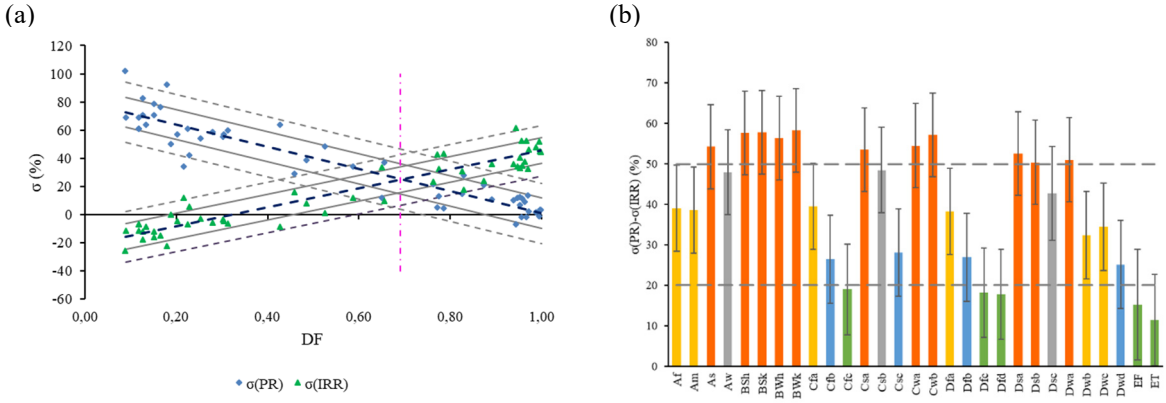

Figure 3.34. (a) Intersection of σ(PR) and σ(IRR) and (b) tracker gain per climate

The PR variation presented in Chapter 2, Section 2.4.3 measures the difference between a tracker-equipped system compared to a fixed-tilt array. The IRR variation, presented in the Section 2.4.5 of the same chapter, measures the expected income increase of a tracker system compared to a fixed-tilt system in terms of economic investment. Further discussion on the IRR can be found in Chapter 1, Section 1.3.2.

For this analysis, a similar procedure to the developed to obtain the Figure 2.22 is followed. For this case, the intercept between the linear fit of σ(PR) (Figure 2.18a) and σ(IRR) (Figure 2.20a) is calculated. Considering associated errors, this DF limit value for economic profitability is 0.69±0.04. Therefore, not considering the energy associated costs, it is, the environmental costs, makes almost any climate profitable. Only the polar climates, *EF* and *ET*, are nearly zero gain considering the associated error.

Chapter 4 - Optimal PV technology selection depending on climatic conditions

4.1. INTRODUCTION

The photovoltaic technology presents a high potential worldwide, but the system's efficiency depends on the selected PV technology, the installation's location irradiation levels and the module temperature [17]. The inadequate selection of modules can lead to low system yields and/or fast degradation processes [18][19].

As seen in Chapter 1, the solar photovoltaic market has shown a sharp growth over recent years mainly because of its increasing competitiveness. The main contributor to this raise is the silicon price drop during the last years [13], crucial since the commercial PV panels prevalent technologies are silicon-based, but other commercial technologies are available [14][112]. The PV market is dominated by polycrystalline (p-Si) and monocrystalline (m-Si) modules, followed by thin-layers technologies [113]. Thin-layer includes the amorphous silicon (a-Si), CdTe and CIS commercial modules.

When designing a PV system, the most common practice is to select the PV module technology considering its price, market availability and expected lifespan. Several studies about the PV technologies performance on real sun conditions have been developed, but the results are limited to temperate climate conditions [18][114][115] or based on simulations [116][117][118].

To optimize the design of a photovoltaic system, it is established that the commercial PV modules must be characterized as function of global solar radiation and temperature. For this purpose, two experimental set-ups are considered to assess the power production dependence of different commercial modules under real sun conditions. While one of the setups is measured under controlled solar radiation and temperature conditions, the other operates under standard working conditions. The comparison of the results of both systems allows to determine the behaviour of each commercial technology.

After the analysis, the adequate PV commercial module for a location can be selected as function of climate conditions. The results also allow creating a decision table to ease the selection of the optimal technology just by knowing the installation's location climate characteristics (solar radiation and temperature ranges). As an additional visualization of the results, a world map is presented (full text is presented in Manuscript III) [60].

Besides this study, the standard operation experimental setup allowed to obtain additional results. The performance of same-technology PV modules from different manufacturers has been assessed and also a thermal analysis of the arrays has been carried out to evaluate the degradation processes for the different PV technologies.

4.2. EXPERIMENTAL SETUP

For the analysis of the response of the different commercially-available PV technologies, the production data of different PV modules under controlled conditions and on standard operation conditions are used. The analysis of both setups is done under real sun conditions; therefore, it allows to separately evaluate the response of the two setups and cross-check the results. With this, the evaluation of the PV technologies validity and its climatic response can be done. Thus, the optimal PV technology as function of the climate conditions can be obtained.

The controlled environment mainly characterizes the PV panels response under, separately, fixed temperature or fixed irradiation conditions. This analysis, besides of being impossible on standard operation conditions, allows to independently evaluate the technologies response with temperature and irradiation. The grid-connected production data measure the regular response from a PV array under non-controlled conditions. The comparison of the results from the two setups allows to extract conclusions on the PV technologies response under different real sun conditions.

4.2.1. Laboratory setup

Four brand-new different commercial PV panel technologies are considered for this setup (Table 4.13). Even if the UMG (Upgraded Metallurgical Grade) module is a polycrystalline panel, it is considered as a different technology as its purification processes is metallurgical instead of chemical [112][119]. This purification process involves a lower use of energy and raw materials than the regular p-Si panels. The silicon price drop has decreased its deployment but its environmental advantages make the UMG a competitive technology.

Table 4.13. Laboratory setup - Photovoltaic panels characteristics

PV technology	Brand and model	P_{rated} (W)	V_{mpp} (V)	I_{mpp} (A)	V_{oc} (V)	I_{sc} (A)
CIS	Wurth Solar WSK0001	5.5	12.00	16.50	22.00	0.35
m-Si	Isofoton I-53	53	17.40	3.05	21.60	3.27
p-Si	Suntech STP-280	280	35.20	7.95	44.80	8.33
UMG	Ferrosolar SFS-270	270	35.86	7.53	44.50	8.10

Figure 4.35. Laboratory - Location of the solar PV panels

An HT IV-400 curve tracer is used (Table 4.14) for measurements [120]. This device provides the panel I-V curves as well as the main parameters (current, voltage and output power). It also measures the irradiance and the module temperature when I-V data are retrieved.

Table 4.14. Laboratory data acquisition device characteristics

	Range	Resolution	Accuracy
Voltage (V)	5.0 - 999.9	0.1	±(1.0%rdg+2dgt)
Current (A)	0.10 - 15.00	0.01	±(1.0%rdg+2dgt)
Maximum power (W)	50 - 9999	1	±(1.0%rdg+6dgt)
Irradiance (with reference cell) (mV)	1.0 - 100.0	0.1	±(1.0%rdg+5dgt)
Temperature of module (ºC)	-20.0 - 100.0	0.1	±(1.0%rdg+1°C)

On this setup, the modules dependencies with the irradiance and the temperature are separately measured. Two dedicated data samples are collected. The first sample measures the power output for different fixed module irradiation values and varying module temperature from 34ºC to 55ºC. The second sample measures the production for different fixed temperatures of the PV modules within a range of global irradiation from 100 to 1000 W/m^2. Measurements are made in Santiago de Compostela (Spain) (42.8735, -8.5575) with solar PV panels facing South (Figure 4.35). Data are retrieved for four non-consecutive fully sunny days.

4.2.2. Grid-connected measurements

The experimental setup is the Grid-connected solar PV field presented in Chapter 2, Section 2.2. This PV installation has a selection of different silicon-based PV technologies. Almost all the arrays are equipped with solar tracking systems, while two of the arrays are placed with a fixed tilt. PV arrays main characteristics are shown in Table 4.15. The ID is the identificatory name of each array. Systems without tracker are horizontally-positioned.

Table 4.15. Experimental setup - Photovoltaic panels characteristics

PV technology	Brand and model	ID	Unit power P_{rated} (Wp)	Array power (Wp)	Inverter	Solar tracking
a-Si	Mitsubishi MA100	a-Si MI	100	3000	Ingeteam Ingecon Sun 2,5	Yes
m-Si	Trina TSM-170	m-Si TR1	170	10710	SMA Sunnyboy SWR3300	
p-Si	Suntech STP270	p-Si SU2	270	10530	Sunways NT10000	
p-Si	Suntech STP270	p-Si SU3	270	10530		
p-Si	Trina TSM-220	p-Si TR1	220	11880	SMA Sunnyboy SWR3300	
p-Si	Tenesol TE2000-210	p-Si TE	210	13230	Ingeteam Ingecon Sun 12,5	No
p-Si	Suntech STP260	p-Si SU1	260	14040		

The power production of each array and the global irradiance are simultaneously measured with 10-minute frequency on the installation's location [60] (Vilalba, Spain, coordinates 43.3146; -7.6650). According to the AEMET climatic atlas [88][121], the location has a *Csb* Köppen-Geiger climate type (see Chapter 3, Section 3.3.2 for more details).

The production data acquisition is done by the inverter monitoring systems of each PV array. Inverter associated losses are neglected and will not be subject of study in this chapter. The pyranometer characteristics (LI-COR LI-200SZ) can be consulted in Chapter 2, Section 2.2.1. For the thermal analysis of the PV arrays, a thermal camera is used (Flir E-50, with a measurement range from -20ºC to 650ºC and a precision of ±2ºC [122]).

The analysed period is selected to avoid the ageing effects in the PV modules. It includes only the most irradiated months to have higher control over the diffuse fraction (additional information on this topic is available in Chapter 2, Section 2.3.2).

4.3. METHODOLOGY

The relevance of this analysis stands on the fact that no systematic studies of PV panels degradation in high-irradiation real sun conditions have been made. The power production and the long-term natural degradation studies are mainly carried out in medium irradiation regions [123]. Moreover, the long-term extreme irradiation degradation in real sun conditions is not considered for the PV modules certification [124].

For this analysis, the power production of the PV modules on controlled (hereafter, Laboratory setup, noted with the "Lab" subscript) and non-controlled (hereafter, Grid-connected setup, noted with the "Grid" subscript) conditions data will be analysed.

The results comparison from both setups will allow selecting the optimal commercial PV technology according to the climate conditions with a simple decision table to visualize the results. To decrease the statistical uncertainties, the temperature and radiation values have been divided into four radiation intervals shown in Table 4.16.

Table 4.16. Global radiation and temperature interval values

Radiation interval	Low	Medium	High	Very high
G value (W/m^2)	>300	300-600	600-800	<800

Temperature interval	Intermediate	High	Very high
T value (ºC)	30-40	40-50	50-60

4.4. RESULTS

The analysis of the production data from the Laboratory and the Grid-connected experimental setups allowed to characterize the different solar PV technologies. The main conclusions and the result discussion are presented in the published paper (Manuscript III) [60].

But the analysis of the experimental data allows to obtain additional results. The Laboratory data make possible the calculation of the temperature coefficients of the controlled-conditions tested PV modules. This is relevant as these coefficients measure the dependence on production of the technologies with the cell temperature and the irradiation levels.

The Grid-connected data permits the comparison of the production data from same-technology PV modules from different manufacturers. Also, the response of the technologies for low and high global radiation values is analysed to determine the response on the low and high radiation extreme values. In addition, a climatic analysis of the optimal PV technology results is also presented.

4.4.1. Laboratory setup: I-V curves

The plot on Figure 4.36 shows an example of the characteristic I-V curve [34] for the analysed monocrystalline PV module (Table 4.13) under real sun conditions for a fixed

radiation value. Further discussion on PV modules characteristic I-V curves can be found in Chapter 1, Section 1.1.3.

As defined in Chapter 1, the two main operation parameters to define a PV module are the open-circuit voltage (Eq. 1.3) and the short-circuit current (Eq. 1.2). As said, for these equations, the G_{STC} value is equal to 1000 W/m^2 and the T_{STC} corresponds to a module temperature of 25ºC and the V and I equations can be rewritten as Eq. 4.29 and Eq. 4.30.

$$V = V_{STC} - \beta\,(T_m - 25) \qquad \text{Eq. 4.29}$$

$$I = I_{STC} - \alpha\,(G - 1000) \qquad \text{Eq. 4.30}$$

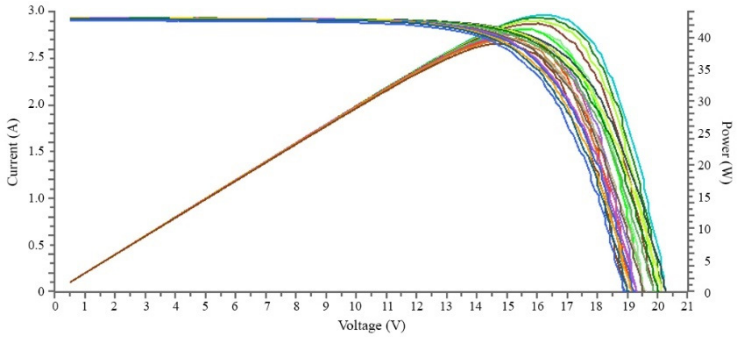

Figure 4.36. IV curve for m-Si PV module for a constant irradiation (825±5 W/m^2) and a temperature range from 38ºC to 56ºC (lines from right to left respectively)

The Figure 4.36 shows the I-V curves for a PV module for different temperatures. After the plot, it can be seen that the temperature increase has almost no effect on the I_{SC} value. However, the effect of the increasing temperature on the V_{OC} value is remarkable. Anyway, the voltage decrease with the temperature compensates the current increase [34]. The variation of the operating temperature of a PV module affects the current and voltage values.

The Laboratory experimental measurements allow to separately measure the production values for a fixed module temperature or a fixed irradiation value. Therefore, these values will allow to calculate the α and β coefficients for the tested solar modules (see Chapter 1, Section 1.1.3 for additional information on this topic). This analysis is not directly possible in the Grid-connected system as the module temperature is not measured. But the analysis of the sunset production data allows to obtain an approximation to the response of the technologies behaviour with the temperature.

4.4.2. Temperature dependence

This section focuses on the analysis of the temperature response of the analysed modules. This evaluation can be only done in the Laboratory setup since fixing the irradiation value is not possible on the Grid-connected setup. The controlled-conditions experimental setup allows to evaluate the module's voltage with increasing temperature for a fixed global radiation value and calculate the temperature coefficient of the open-circuit voltage, β.

4.4.2.1. β coefficient for Laboratory experimental setup

Applying the Eq. 4.29 to the experimental data in Figure 4.36, the dependence of I_{SC} and V_{OC} with the temperature can be plotted (Figure 4.37). From this example, it can be seen that a temperature variation of 18ºC on the module generates almost no variation in the current value,

showing a variation of only 1%. For the voltage, this module temperature variation leads to a 6% difference in its value.

The Eq. 4.29 allows to experimentally obtain the β value for the Laboratory data of the four selected technologies with the use of the slope of the linear fit. The intercept will provide the V_{STC} voltage under this fixed irradiation conditions. This value must be close to the module's V_{OC} value provided by the manufacturer.

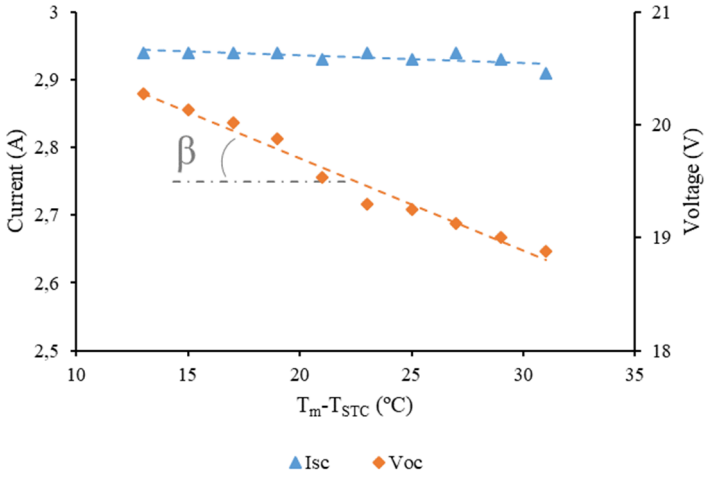

Figure 4.37. Current and voltage variation for m-Si PV module at fixed radiation

The results of the relative β coefficient for the four considered technologies under similar global radiation values are presented in Table 4.17. After the V_{STC} and comparing the values with the available V_{OC} values provided by the manufacturers for each technology (Table 4.13), the V_{diff} represents how far the intercept value is from the manufacturer's V_{OC} value (Eq. 4.31).

$$V_{diff} = 100 \cdot \frac{V_{OC} - V_{STC}}{V_{OC}} (\%) \qquad \text{Eq. 4.31}$$

Table 4.17. Temperature coefficient β and intercept value for the Laboratory tested modules

PV technology	**β** (%/ºC)	**β_{manuf}** (%/ºC)	**V_{STC}** (V)	**V_{diff}** (%)
CIS	-0.23±0.01	-0.29	20.4	9.7
m-Si	-0.40±0.02	-0.42	21.2	2.0
p-Si	-0.35±0.02	-0.33	43.8	2.3
UMG	-0.39±0.01	-	44.1	0.8

After the data, a better performance for the p-Si is observed among the silicon-based modules as its voltage loss with the increasing temperature is lower than the other selected technologies. This result is complementary to the published results [60].

Comparing the experimental relative β values Table 4.17 with the β values provided by manufacturers, β_{manuf}, for the CIS, m-Si and p-Si tested modules [125][126][127], a great accordance appears for the m-Si and p-Si modules. The CIS value has a higher difference with the experimentally measured β value.

In addition to the β coefficient, some manufacturers provide the value of the temperature coefficient with the current, often noted as α_{SC} (please notice this is not the α coefficient to be

discussed in next section). This value represents the slope of the variation of I_{SC} with the temperature (see Figure 4.37). The manufacturer values of α_{SC} are available for the m-Si and the p-Si tested modules. The m-Si module has a manufacturer-provided α_{SC} value of 1.748 mV/ºC while the experimentally calculated is 2.857 mV/ºC. For the p-Si, the manufacturer value of 0.055%/ºC is experimentally calculated as 0.065%/ºC. A high accordance appears for the p-Si. The m-Si, unlike, shows a higher difference.

4.4.3. Radiation dependence

The analysis of the radiation dependence of the tested commercial PV technologies shows special interest when considering the low and high radiation intervals. The low radiation intervals allow characterizing the optimal PV technology on cloudy conditions. The high radiation intervals are deeply related with the loss of performance with high temperatures; thus, these results are associated with the temperature dependence. In addition to the published results on the solar radiation performance dependence [60], additional analyses are presented in this section.

For this analysis, a similar procedure to the developed for the β coefficient is used for calculating the α coefficient at a fixed module temperature. This analysis will be also done with the yield factor (Eq. 1.5) to somehow compare the response of the PV technologies from both setups with the solar radiation. Therefore, the Laboratory and Grid-connected results can be compared. Further information on the PV production variables can be consulted on Chapter 1, Section 1.1.3.

4.4.3.1. α coefficient for Laboratory experimental setup

The Laboratory setup allows measuring the current and voltage of the PV technologies for a fixed module temperature. For this section, the relative α coefficient will be calculated using Eq. 4.30. Figure 4.38 shows the current and voltage variation for the monocrystalline silicon module as an example. The relative α coefficient values for the four analysed technologies are presented in Table 4.18. The difference between the linear fit intercept, I_{STC}, and the I_{SC} value provided by the manufacturer (Table 4.13) is measured with I_{diff}, defined on Eq. 4.32.

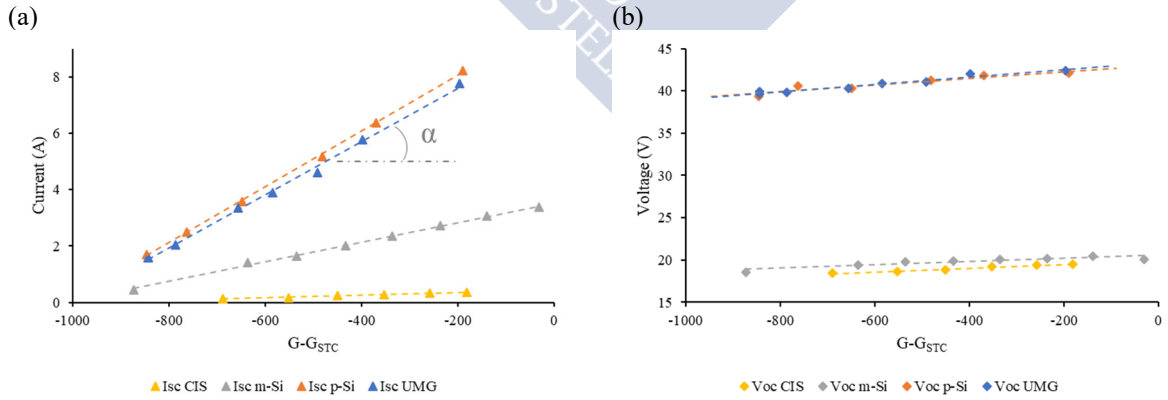

Figure 4.38. (a) Current and (b) voltage variation for m-Si PV module at fixed temperature

The absolute or relative α coefficients are not provided by manufacturers. Therefore, no comparison with expected values can be done. The comparison of the α values for each technology on Table 4.18 shows a similar dependence of the p-Si and UMG panels with the radiation, while the m-Si and the CIS modules show a lower current increase with the increasing

irradiation. Comparing the relative α, a similar variation in terms of percentage is measured for the four technologies.

Table 4.18. α coefficient and intercept value for the Laboratory tested modules

PV technology	α (mA/Wm^{-2})	α (%/Wm^{-2})	I_{STC} (A)	I_{diff} (%)
CIS	-0.0005±0.0001	-0.1008±0.0001	0.44	-26
m-Si	-0.0035±0.0001	-0.0962±0.0002	21.2	-8
p-Si	-0.0099±0.0002	-0.0963±0.0003	43.8	-20
UMG	-0.0095±0.0004	-0.0971±0.0006	44.1	-17

$$I_{diff} = 100 \cdot \frac{I_{SC} - I_{STC}}{I_{SC}} \ (\%) \qquad \text{Eq. 4.32}$$

In addition to the formal analysis of the α coefficient, an alternative analysis can be done to compare the Laboratory and the Grid-connected setups in some way. The Figure 4.39, already presented on the published paper [60], shows the Y_f as function of the global radiation for the tested panels for a fixed module temperature (38ºC) plus the physical meaning of the coefficient to be used on this case, α_f (Eq. 4.30).

The relative α_f coefficient can be calculated with the variation of the slope of each linear fit. Unlike the previous formal α coefficient, this analysis is not directly done using the current values and the irradiation correction ($G-G_{STC}$) is not applied. For this reason, the temperature coefficient will be noted as α_f since the yield factor is used for the slope analysis.

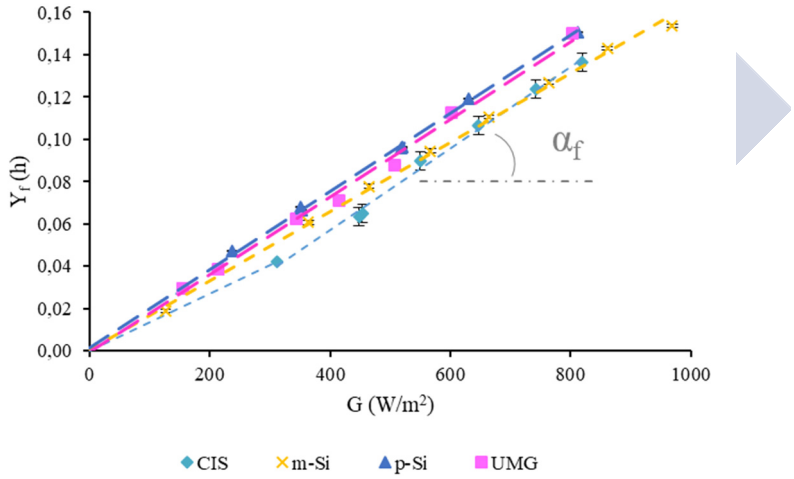

Figure 4.39. Yield factor dependence with global radiation for a fixed module temperature

After the power production data analysis, the relative α_f temperature coefficient for the tested technologies is presented in Table 4.19. The increase stays around 1% per W/m^2 for the silicon-based technologies, while the CIS, despite showing a higher increase, shows lower production for low radiation values.

4.4.3.2. Coefficient for the Grid-connected setup

As previously said, the Grid-connected setup has no control over the modules temperature nor current values. But the analysis of the technologies production at sunset allows to evaluate the thermal effects. For a fully sunny day, the module's temperature during the sunrise period

is cool, while during the sunset the full day thermal effects are accumulated. Therefore, the temperature effect on the solar panels production can be assessed.

For the analysis of the temperature dependence, the power production values of the three tested technologies on the experimental setup are used; a-Si MI, m-Si TR1 and p-Si SU3 (Table 4.15). For this section, the corrected yield factor, Y_{fc} [60], is separately measured during the sunrise and sunset of a fully sunny day for global radiation values under 200 W/m^2 (see Manuscript III for details on the arrays selection and the yield factor correction procedure).

The results are plotted in Figure 4.40. The numerical results, presented in Table 4.19, show the similar dependence for the three tested technologies during the sunset period when the thermal effects are accumulated. For this period, the p-Si shows the lower loss of yield, becoming the most robust PV technology. The a-Si shows the worst response to the thermal effects.

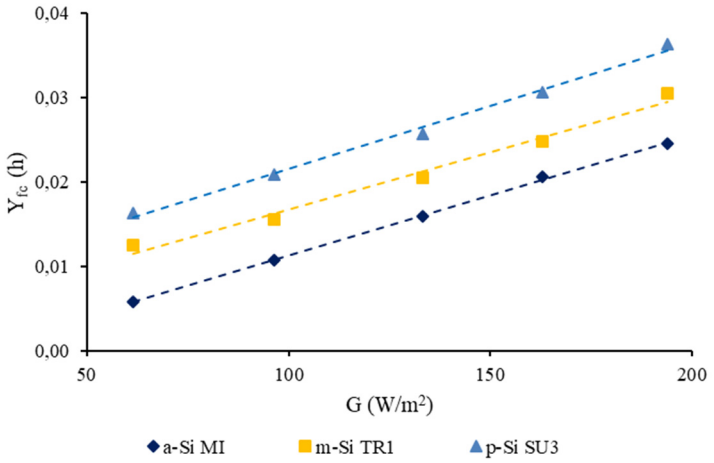

Figure 4.40. Corrected yield factor for the Grid-connected tested technologies during sunset for global radiation values under 200 W/m^2

Table 4.19. Temperature coefficient for the tested PV technologies: Laboratory setup with fixed temperature and Grid-connected setup with thermal accumulation of a fully sunny day

PV technology	**Laboratory setup** α_f (%/Wm^{-2})	**Grid-connected setup** α_f (%/Wm^{-2})
a-Si	-	1,25
CIS	1.68	-
m-Si	0.97	0,81
p-Si	0.92	0,69
UMG	1.05	-

The comparison of the relative temperature coefficients, α_f, of both setups shows compatible results for the two comparable technologies (m-Si, p-Si) when considering the Laboratory data and the Grid-connected values. It must be noticed that the comparability appears despite the fact that the Grid-connected setup has no ensured a constant temperature in the modules and, also, these modules are affected by ageing processes, which affects to their performance.

The monocrystalline and polycrystalline modules show compatible results when comparing the Laboratory and Grid-connected results. The thin-film modules, a-Si and CIS, show also values on the same range, with a 26% difference. In addition, it must be noticed that the p-Si show the lower losses with the increasing global radiation for both setups.

4.4.3.3. Grid-connected working limits on radiation

When considering the PV panels performance, it is relevant to consider the low and high to very high radiation values behaviour as these extreme climate conditions are frequent in several climates. In previous sections, the losses with increasing temperature and radiation were evaluated. But the yield factor (Eq. 1.5) on the low and high radiation intervals must be also assessed to find the adequate PV technology. The optimal technology will be the one that, for a given climate, provides the higher performance with the lower temperature and radiation losses.

For the response analysis, a fully sunny day with an average global radiation of 632 W/m^2 for the day and a maximum value of 983 W/m^2 is used. In addition to the thermal analysis done in the previous section, the corrected yield factor values in the low and high to very high radiation intervals (Table 4.16) for the same day are analysed. This analysis will allow to see the response of the tested technologies on the different radiation intervals.

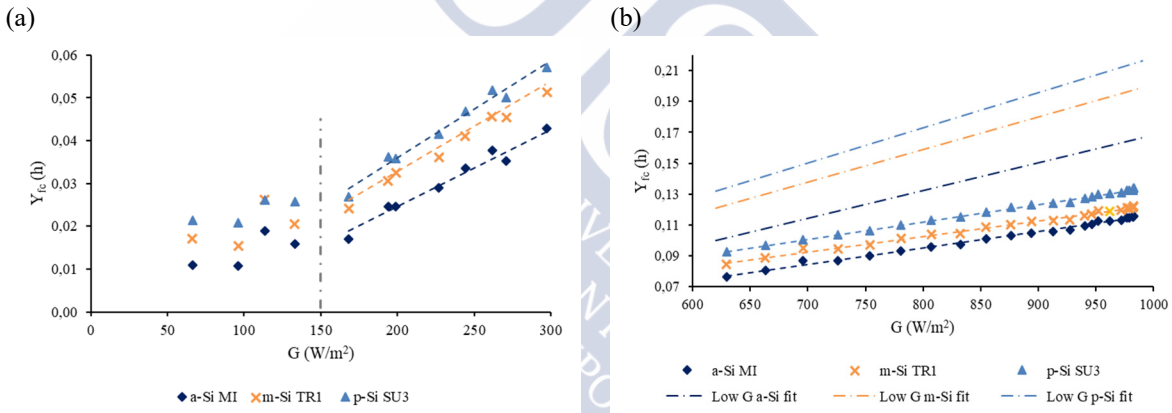

Figure 4.41. Corrected yield factor for the Grid-connected selected technologies (a-Si, m-Si and p-Si) for global radiations values (a) under 300 W/m^2 and (b) Over 600 W/m^2

Figure 4.41a shows the Y_{fc} for global radiation values under 300 W/m^2. A lack of linearity is observed for the three tested technologies for global radiation values below 150 W/m^2. For values over this limit, the response of the three technologies is linear with radiation. Regarding the yield of each technology, the a-Si shows a lower response than the monocrystalline and polycrystalline modules.

The Figure 4.41b shows the PV modules response for the high to very high solar radiation intervals. In addition to the experimental yield values, three additional lines are included on the plot. These lines correspond to the expected theoretical response of the modules if the linear fit from Figure 4.41a continued until the high radiation interval. A clear loss in yield is measured for the three technologies comparing the experimental results with the expected after the low G linear fit. The higher slope decrease is for the m-Si and the p-Si (with a 52% and 50% decrease respectively), while the a-Si reduction is 40%. Besides that, and as expected from the previous

results, a better performance for the p-Si appears with respect to the other considered technologies.

4.4.4. Optimal PV technology selection

Comparing the results from the evaluated commercial technologies will allow determining the optimal technology for different climatic conditions as the temperature and radiation dependences are assessed.

On this section, the main results of the full analysis are presented [60]. These results required to avoid the systematic effects of considering two different experimental setups. In addition to the solar tracker data correction, the unbiased value of the Performance Ratio variation, $\sigma(PR_i)$, is defined using the procedure presented on Eq. 2.12 to compare the results from both setups. $\sigma(PR_i)$ measures the variation of each technology with respect to its average value (Eq. 4.33), where PR_i is the PR value in the *i* radiation interval for a given technology and <PR> is the mean value of the PR along the radiation interval for that technology.

$$\sigma(PR_i) = 100 \cdot \frac{PR_i - < PR >}{< PR >} \ (\%) \qquad \text{Eq. 4.33}$$

Figure 4.42a shows the PR variation for the different radiation intervals for the comparable technologies of the Laboratory and Grid-connected setups. The p-Si shows stability along the full radiation spectrum while the m-Si is more efficient for medium to high radiation levels. The Figure 4.42b shows the results of the not comparable technologies. The thin-films, a-Si and CIS, show the more unstable behaviour. The UMG appears as the most stable candidate of these, showing a good performance on the full radiation range.

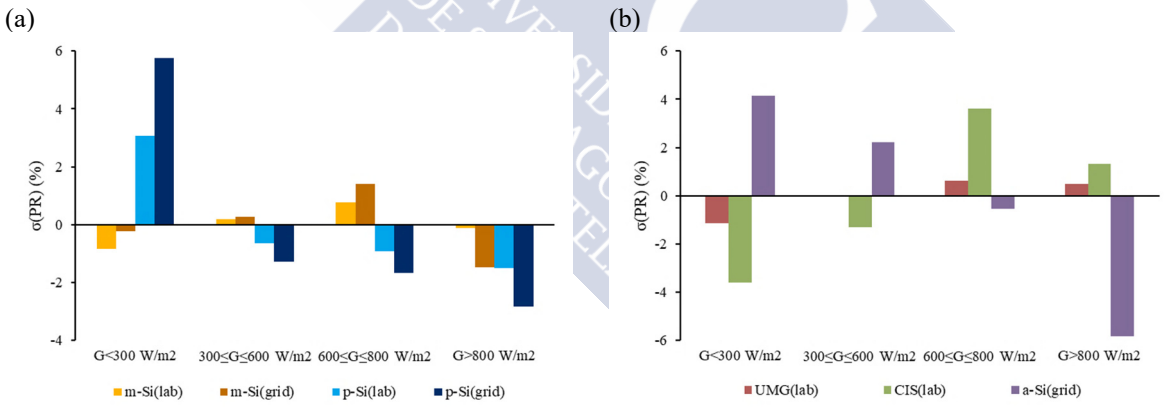

Figure 4.42. PR variation from average PR value for (a) m-Si and p-Si and (b) for UMG, CIS and a-Si technologies

From the experimental results [60], it can be seen that the temperature effect has almost equal influence in the tested technologies. However, the p-Si presents a more stable behaviour. Therefore, the main variable for the technologies suitability analysis is the global radiation. For this study, additional parameters such as economic analysis or technology availability on the installation's location are not considered.

With the available data, a guide for the optimal PV technology selection worldwide is created after the identification of the tested technologies behaviour with the solar global radiation intervals. A general decision table, proposed after the defined temperature and

radiation intervals (Table 4.16) for this analysis, is presented in the published paper [60]. For the table interpretation, it must be noticed that the level of appropriateness for each technology is defined from 1 (less suitable) to 4 (optimal technology) but the value does not represent the suitability percentage. The extra suitability point for the p-Si technology comes after its stability and lower performance loss with the increasing temperature.

Once analysed the response of each technology, the procedure can be extended by simply cataloguing each world region in terms of solar radiation and temperature. With the climatic database created for the Chapter 3 analysis, an alternative suitability analysis is proposed here using the Köppen-Geiger climate classification [17]. Additional information about this climate classification can be consulted on Chapter 3, Section 2.3.2. The optimal technology, in terms of this Köppen-Geiger climate classification, is presented in Table 4.20.

Table 4.20. Optimal PV technology for each Köppen-Geiger climate type

Optimal PV technology	**p-Si**		**p-Si UMG**	**p-Si UMG m-Si**	**p-Si UMG m-Si a-Si**
Köppen-Geiger climate type	As BSh BSk BWh BWk Csa	Cwa Cwb Dsa Dsb Dwa	Af Am Aw Cfa Csb Dfa Dsc	Cfb Csc Dfb Dwb Dwc Dwd	Cfc Dfc Dfd EF ET

As a brief description of the climates, the p-Si is the optimal technology for the desert and semi-arid climates and temperate/cold climates with dry hot summers. The UMG and p-Si are optimal for humid climates, including the rainforest, monsoon and temperate. For the temperate and continental climates with warm to cold summers, the m-Si, p-Si and UMG PV technologies are adequate. The polar and highland climates allow installing any of the silicon-based PV technologies.

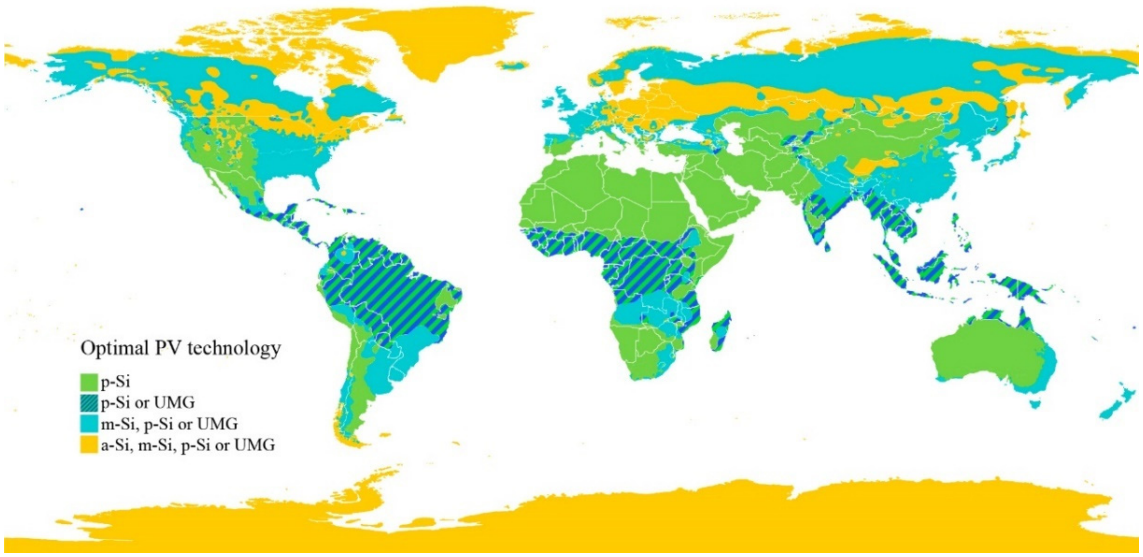

Figure 4.43. Optimal photovoltaic technology worldwide attending to the Köppen climatic classification

This decision table constitutes an adequate tool to select the optimal PV technology for any location in terms of performance according to the climate. As a visualization, Figure 4.43 shows a worldwide general PV technology selection based on the Köppen-Geiger climate classification [17]. The existence of microclimates should be analysed for a more accurate technology selection.

4.5. GRID-CONNECTED EXPERIMENTAL SETUP ADDITIONAL RESULTS

During the Grid-connected available data evaluation, some additional results were obtained. These results include the response of same technology PV modules from different manufacturers. But also, the effect of the maintenance and fault control over the system's performance is assessed.

4.5.1. Manufacturer effect

The Grid-connected system includes same-technology PV modules from different manufacturers. The comparison of the Performance Ratio (Eq. 1.4) of these arrays for a fully sunny day will allows to verify if the manufacturer effect appears. This effect makes same-technology PV modules from different manufacturers to have different production values under the same circumstances.

On the Grid-connected setup, two systems initially allow this analysis; the p-Si TR1 and p-Si SU3 would be comparable. But to avoid potential tracker effects, the fixed-tilt polycrystalline arrays p-Si TE and p-Si SU1 performances are analysed (Table 4.15).

Figure 4.44a shows the Performance Ratio for the different-manufacturer arrays without tracking system. The PR for the arrays shows an 8.8% difference between the PR of both arrays.

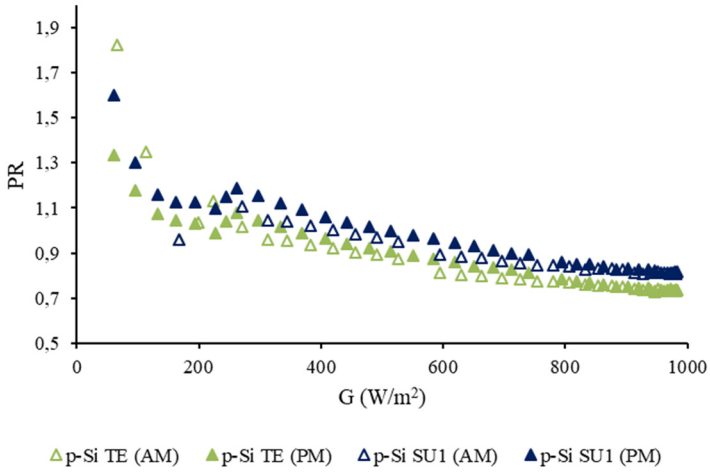

Figure 4.44. Performance ratio for same technology (p-Si), different manufacturers arrays

But for a proper analysis of the results from Figure 4.44, this 8.8% difference must be compared with the other tested PV technologies to ensure if the deviation is due to the manufacturer effect or is the result of measurement associated errors.

The difference between the analysed a-Si MI, m-Si SU1 and p-Si SU3 (Table 4.15), showed the higher performance of the p-Si in all the global radiation intervals [60]. The performance of

the m-Si is an 11.8% lower than the p-Si, and this difference increases to a 28.1% when compared with the a-Si.

Therefore, the manufacturer's effect exists. But assuming the 8.8% as the associated error for the p-Si technology, the m-Si will show just a 3% lower performance. The difference in terms of PR for the a-Si is 25%, still high even considering this error.

As the comparison is done with same technology and same age arrays, the PR difference of the fixed-tilt arrays can be only due to variations in the production processes (including the PV modules encapsulants).

4.5.2. Effect of maintenance and fault control

Regardless the climatic and technological considerations, a proper design, maintenance and fault control are essential to ensure the proper operation of a PV system. In addition to the inevitable ageing of the PV modules and the auxiliary systems, the lack of maintenance, the accumulation of dust and dirt on the surface of the PV modules and other failures associated with an inadequate maintenance decrease the installation's performance.

Regular quality checks of the installations are essential: visual inspections, thermographic controls and production values analysis will help to detect eventual problems and minimise the malfunctioning or failures on PV systems. Also, problems related to inadequate design decisions or bad interventions in the surroundings can lead to faults. Placing structures close to an array can shade a solar panel, leading to production decreases. The basic control procedures and the problems which allow to detect are presented in Figure 4.45.

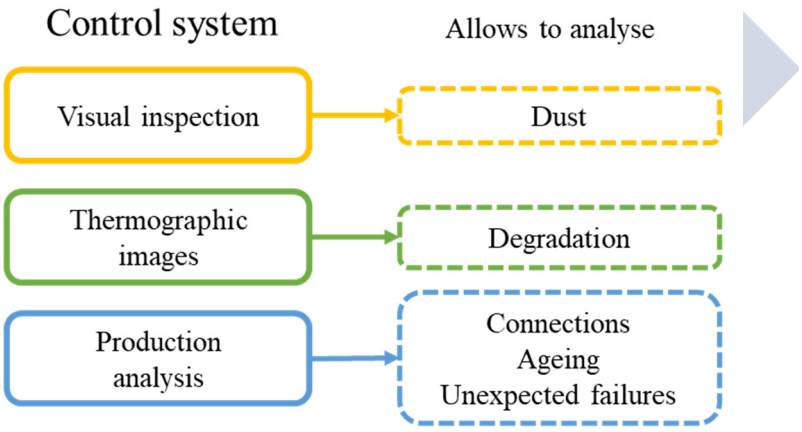

Figure 4.45. Maintenance procedures for early fault control

4.5.2.1. Degradation

The degradation and ageing of the PV systems are unavoidable. Anyway, a correct maintenance protocol and/or the prompt repair or replacement of damaged parts can mitigate its consequences.

Studies have demonstrated that the degradation mechanisms of the PV modules are location-dependent [18][123]. This dependence is mainly related to climatic factors. For example, in regions with great seasonal temperature variations, the thermomechanical fatigue on the system interconnections is the main degradation mechanism.

The potential damages on PV modules are classified after the patterns appearing on the panel's surface [128][129]:

- **Filiform anomalies or spiders:** Lines or cracks appearing on the surface of the solar cells. Depending on the colouration and dispersion, these anomalies can be defined as Type I or Type II. Type I have dispersions with blade shape and silver colouration. Type II presents a complex and large shape with a more transparent colouration. These anomalies are common in monocrystalline panels.
- **Lava-like malformations:** Shadows on PV arrays or a short-circuit on a module (or an array) may cause reverse voltages on the solar cells. The reverse current may result in cell short-circuit failure, melting the contact material and the silicon in localized areas with lava-like flow patterns [130].
- **Colour changes:** These changes are caused by an increased absorption of light in the violet-blue range. The brownish appearance is caused by the encapsulants of the modules, even if is not a problem itself. The yellowish (or bluish) type is usually due to a cell operating temperature increase. The Figure 4.46 shows one PV array of the analysed field, the p-Si CO (see Table 4.15), with colour change defects which affect to the module operating temperature, as can be seen in the thermographic image.

(a) (b)

Figure 4.46. (a) PV array (p-Si CO) with colour change defects and (b) thermography of the alteration on the module's operating temperature

(a) (b)

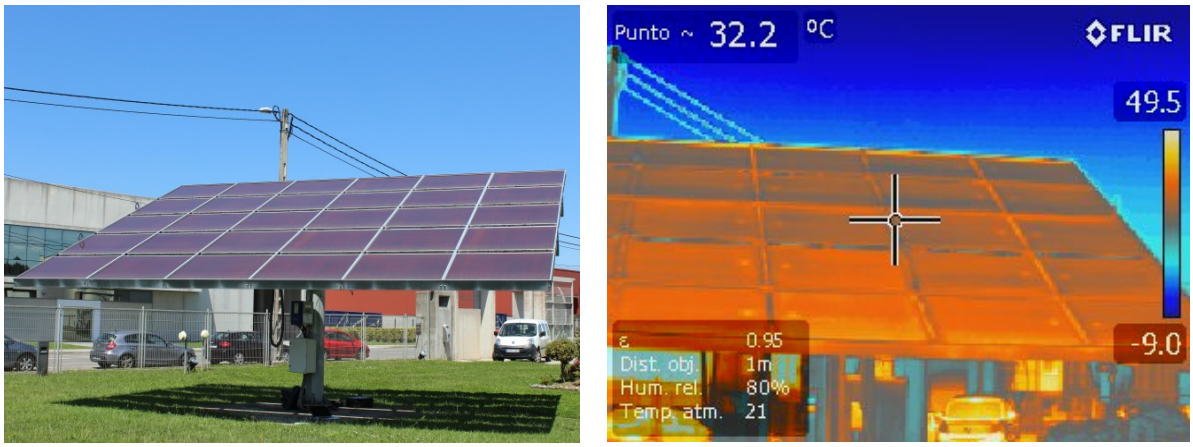

Figure 4.47. (a) Amorphous PV array (a-Si MI) and (b) thermographic image

These damages appear in the monocrystalline and polycrystalline technologies. Their structure and manufacturing processes make them more susceptible to these failures. The amorphous technology shows a much more uniform thermal response. Figure 4.47 shows the a-Si array on the PV field and the temperature stability on its surface.

4.5.2.2. Effect of dust accumulation

The PV system's location and its climatic characteristics can increase the dust depositions such as sand or other particles. The presence of dust or dirt in the modules prevents the sunrays from reaching the panel, which is equivalent to the reduction of the PV system's effective surface area. This effect can be controlled with measurements of the panel operating temperature. Anyhow, this parameter is not usually measured in standard installations [131]. The most common system's monitoring is focused on power production and, with these data, only the slow and continuous decrease in the production over time can account this effect.

The loss of performance of a PV system due to the accumulation of depositions is difficult to quantify. However, researchers indicate that this performance can be reduced up to 20% per month by dust depositions on the surface of PV arrays. This is especially relevant in low-latitude desert and steppe regions [132]. These climates present sand and dust storms which deeply affect the PV systems performance [133].

(a) (b)

Figure 4.48. (a) Presence of bird's faeces and (b) thermographic image

(a) (b)

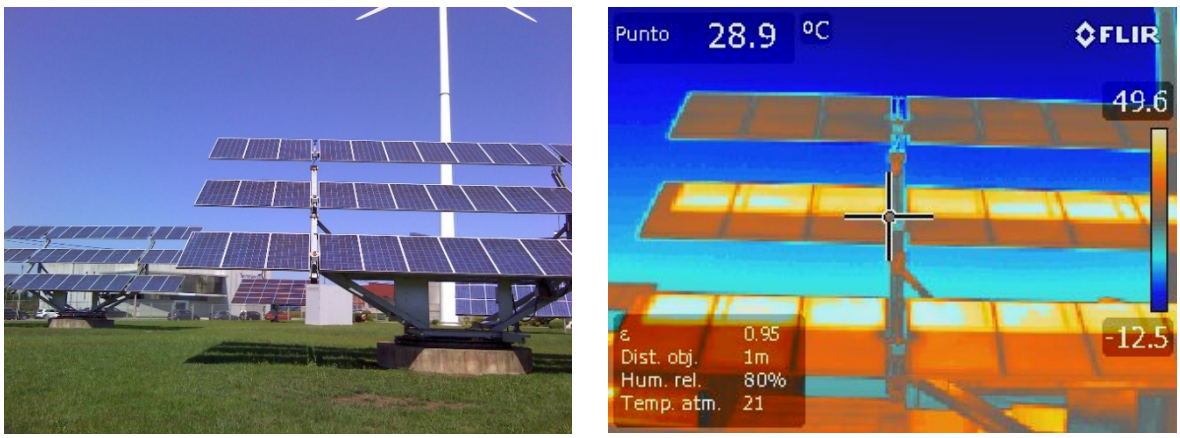

Figure 4.49. (a) Tracker-equipped PV array (p-Si SU2) and (b) thermographic image

The effect of dust and dirt cause the module's temperature increasement on the affected areas. The Figure 4.48 shows the thermal variation on the PV module due to the module's contact box as well as the effect of bird's faeces. The influence of the depositions into the module's operating temperature can be seen.

In addition to these defined damages, structural design failures may appear as consequence of industrial design decisions. An example of these potential failures can be seen in Figure 4.49, where a tracker-equipped array presents different temperature on the modules due to the reflection on the upper line of modules. Even if this design may have potential advantages in terms of air circulation for the system's cooling, presents a remarkable disadvantage as it affects the uniformity of the system's temperature.

4.5.2.3. Unexpected failures

The analysis of the production allows detecting unexpected system failures. On this section, two examples of failures detected after the production analysis of the PV arrays are presented. One failure is related with a shadowing on one array and the other with a mechanical failure on a solar tracker.

As previously said, the maintenance of a PV system is fundamental to ensure its adequate operation. But when a PV field includes solar tracker systems, the maintenance is crucial since they have electronically-controlled moving parts. As the movement intends to maximize the power production, a fault in the solar tracker control system can lead to remarkable production decreases.

During the analysis of the power production of the arrays of the PV field, a production anomaly was detected in the m-Si SN array (Table 4.15). Its power production for the fully sunny day shows a nearly zero production during certain hours. After a visual inspection of the PV array, it was settled that the failure was due to the solar tracker malfunction.

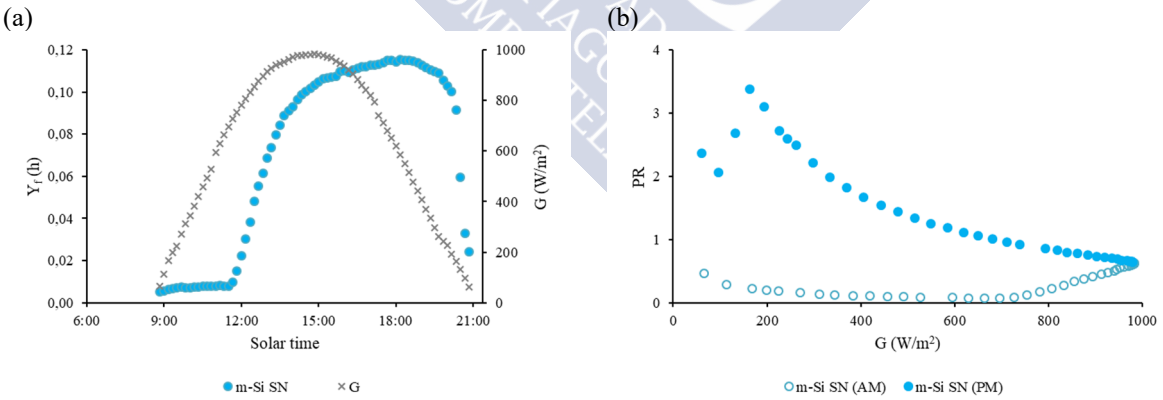

Figure 4.50. Solar tracker malfunctioning: (a) Yield factor misalignment with global radiation and (b) Performance Ratio during morning and afternoon periods

Figure 4.50a shows the yield factor along the fully sunny day plus the global radiation. A total desynchronization between the radiation and the production can be seen. Also, it can be seen that the maximum production does not happen at solar noon. This indicates a failure on the solar tracker azimuth and tilt positioning during morning time. Figure 4.50b shows the performance ratio for the array during the morning and afternoon.

Comparing this array PR with the reference monocrystalline array (m-Si TR1) for the full period of analysis, a 53% less production is measured. Even if little percent of the loss could be attributed to the manufacturer's effect, the PR decrease is mainly related to the tracker malfunctioning.

Also, and after the analysis of the power production, a discrepancy between the production of the p-Si SU2 and p-Si SU3 (same-technology, same-manufacturer, tracker-equipped) arrays was detected. Figure 4.51a shows the yield factor from both arrays and the corresponding solar global radiation along the fully sunny day. It can be seen the difference between both arrays during the morning time and, after noon, both arrays perform exactly equal (as expected). A decrease of 17% in Performance Ratio is measured for the p-Si SU2 with respect to the p-Si SU3.

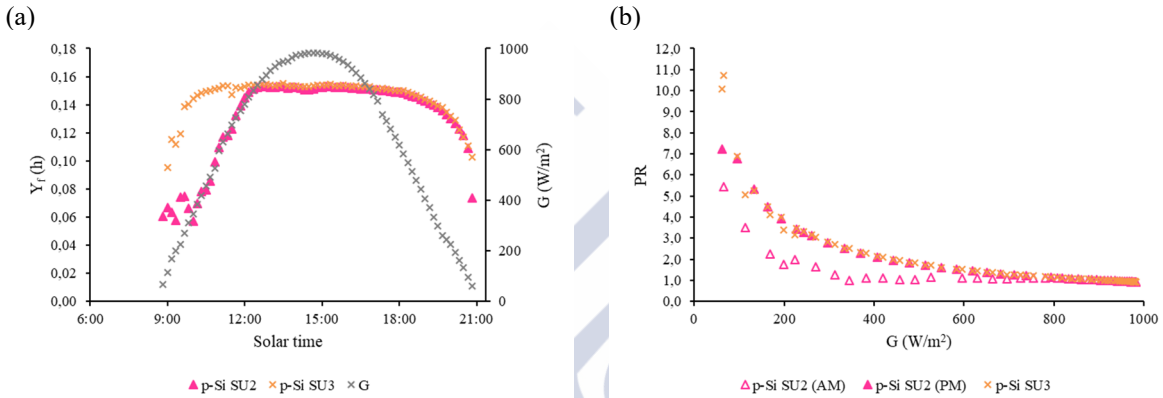

Figure 4.51. Shadowing effect production loss effect (a) Yield factor difference between equal arrays during morning time (b) Performance ratio during morning and afternoon periods

After a visual inspection of the PV field, it was confirmed that the installation of a meteorological turret close to the array of study is the responsible for this abnormal performance during morning time.

Chapter 5 - Stand-alone PV systems sizing as function of consumption types and climatic conditions

5.1. INTRODUCTION

In previous chapters, the challenges related to the design of grid-connected PV systems have been discussed. In this chapter, the stand-alone PV systems are analysed as its share in the total PV systems in operation is increasing. Besides of offering a wide range of applications, the stand-alone PV systems provide energetic independence on any location; from urban locations to remote regions worldwide.

The main difference between the grid-connected and the stand-alone PV systems is the sizing procedure. For the grid-connected PV systems the sizing is limited to the available area for the modules racking once the regional legal constraints are met. But the stand-alone PV systems require an energetic accumulation system to ensure the power supply when solar resource is not available. As this energy storage is usually done with batteries, the analysis of the environmental impacts of stand-alone PV systems require to include the batteries.

The sizing of a stand-alone PV system requires to size both the PV array and the battery system capacities. The array capacity can be defined as the required number of modules to fulfil the system's daily energy demand. The battery system capacity is determined after fixing the number of days that the system can operate without incoming solar radiation. The remaining components of the PV system (see Chapter 1, Section 1.2) are not subject of study.

Upon this basic sizing definition, the procedure may seem trivial. The main goal of a stand-alone PV system is that the designed installation can fulfil the user's consumption requirements even in overcast conditions. The PV array capacity is sized so that its power production fulfils the energy demand for a given time interval, usually a day. To that end, the solar radiation values along the year on the PV system's location and the user's power demand values for the given time interval are required. For the battery system capacity sizing, the daily power demand and the desired days of autonomy must be determined. So, increasing the battery system or the PV array capacity might appear as the sizing solution.

The suitable sizing of a stand-alone PV system requires to ensure its technical, economic and environmental feasibility. Thus, in addition to fulfil the user's expected comfort levels and being economically affordable, the environmental impacts must be the minimum possible. Hence, undersizing a PV system to reduce the economic or environmental costs is not advised as it endangers the capacity to provide the required energy. Moreover, oversizing the system can make the PV system unaffordable in economic and/or environmental terms.

Therefore, in addition to the already discussed optimal modules technology and PV racking systems, also the batteries must also be evaluated to obtain the most sustainable solution for the PV systems sizing.

Currently, the PV modules are less expensive in economic and environmental terms than the battery systems. This tendency, deeply related with the raw material costs, may change due to market fluctuations or emerging new technologies. Despite this market trend, an adequately-sized battery system can be economically affordable [134][135]. The lifecycle assessment, LCA, of the batteries strongly depends on the selected battery technology and its end-of-life process. Depending on the selected batteries and its recycling, these environmental impacts may become up to over 5 times lower [136] (see Chapter 1, Section 1.3 for discussion about the LCA).

This chapter analyses the stand-alone PV systems sizing considering the economic and environmental costs. After reviewing two of the most employed sizing procedures and analysing their limitations, a sizing method for stand-alone PV systems based on reliability is proposed.

The developed method, like previous sizing methods, allows to select the optimal battery-array configuration for a fixed system's reliability value [13][137][138]. But unlike previous methods, it allows to analyse different power consumption types and the climates seasonality.

The analysis of an existing stand-alone PV system with the developed sizing method led to the publication of a paper to establish the LLP method applicability limits as function of the climate conditions and of the power consumption types (full text in Manuscript IV) [139].

5.2. PV SIZING METHODS

There are multiple proposed methods for sizing PV systems. On this section, only two of the most commonly used are presented. The Worst Month method is the mostly used despite not considering the economic or the environmental aspects. The Loss of Load Probability method, as currently defined, does not consider the environmental impacts nor the economic aspects.

5.2.1. Worst Month method

The Worst Month method, WMM, is the most conservative sizing method. Even if it induces a high oversizing, is used by professionals and is the most referenced in the bibliography due to its simplicity [35][140][141]. Some designers use this sizing method considering the three worst months, reducing the oversizing but also the system's reliability.

The WMM sizing procedure is based on the use of monthly average daily values for the higher power demand and the lower beam radiation value (Eq. 2.14). Thus, the basic requirement for sizing the PV system (Eq. 5.34), becomes Eq. 5.35.

$$E_{DC} \geq E_{Demand}\ (Wh/day) \qquad \text{Eq. 5.34}$$

$$E_{DC,min} \geq L\ (Wh/day) \qquad \text{Eq. 5.35}$$

where E_{DC} is the energy production of a PV module (Eq. 1.1), and $E_{DC,min}$ is the energy production of the PV modules in the month with the lower beam radiation value. The average

daily energy demand, *L*, is the daily average power consumption, E_{Demand}, in the month with the higher energy demand. These values must be evaluated prior to the system's sizing.

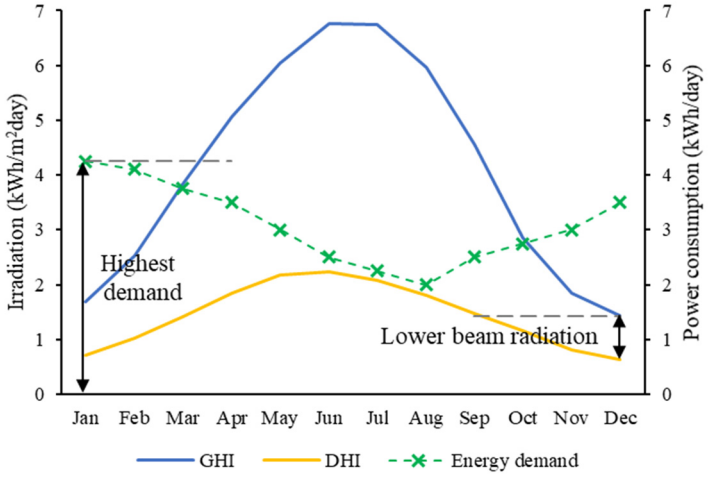

Figure 5.52. Solar irradiation and power consumption variability along the year

Figure 5.52 shows an example of average available solar radiation and variable power consumption. In the plot, the monthly average daily global and diffuse horizontal radiation values, GHI and DHI, are plotted to visualize the available beam radiation together with the monthly average daily power consumption. Additional information of the solar radiation components can be consulted in Chapter 2, Section 2.3.1.

The solar radiation values are basic for the system sizing. When available, experimental data sources must be considered. When no local or regional meteorological stations are available, model-based solar radiation databases can be used (see Chapter 3, Section 3.4.2 for further information on this topic).

For the Figure 5.52 example, and considering the principles of the WMM, December would be selected to calculate the monthly energy production as it is the month with the lower beam solar radiation availability. For the energy demand, the January power consumption would be selected for the system sizing.

For the WMM sizing, the process is developed in two consecutive and independent steps; first, the PV array is sized and after, the battery system.

5.2.1.1. PV array sizing

Once the daily average energy demand is known, the WMM allows to determine the minimum number of PV modules to fulfil the energy demand in the month with the lower beam radiation, B. This irradiation value, also known as direct radiation, can be calculated as the difference between the global, GHI, and diffuse, DHI, monthly average daily irradiation values (Eq. 2.14).

The expression on Eq. 5.36 allows to calculate the required number of modules for the array, *A*, using the average daily power demand, *L*, the power production of the selected modules to install, P_{max}, and the monthly average daily lower beam radiation value, B_{min}.

$$A = \frac{L\ (Wh/day)}{P_{max}(Wp/module)\ \frac{B_{min}(Wh/m^2 day)}{1000\ W/m^2}} \quad \text{Eq. 5.36}$$

Additional information on the P_{max} value can be consulted in Chapter 1, Section 1.1.3.

5.2.1.2. Battery system sizing

The sizing of the battery system only relies on the daily energy demand and the expected autonomy. The required battery system capacity to ensure the daily power demand, $E_{Demand,day}$, can be defined as in Eq. 5.37. The denominator in the equation accounts battery-related parameters. These parameters are characteristic for each battery technology [142]; V_{bb} is the manufacturer-provided battery voltage and the DoD is the battery depth of discharge, which depends on the selected battery technology. The global installation performance factor, R, accounts the battery system losses [143].

$$C = \frac{L}{V_{bb} \cdot DoD \cdot R} \left(\frac{Ah}{day}\right) \quad \text{Eq. 5.37}$$

Once the daily battery capacity, C, is calculated, the total battery system, C_N, can be calculated with Eq. 5.38 after fixing the desired days of autonomy for the system. For it, the emergency charge, QE, is defined. The QE value accounts the days that the system can work without incoming solar radiation, it is, only using the stored energy in the battery system. This number is related with the climate seasonality, as it is measured with the consecutive overcast days. However, the QE value is mostly fixed after the system's designer experience.

$$C_N = C \cdot QE\ (Ah) \quad \text{Eq. 5.38}$$

Therefore, in the Worst Month method, the reliability is based on the QE value. Depending on the climate seasonality, this method may increase the battery system to a non-feasible limit in economic and environmental terms [136][144][145][146].

The main limitations of the WMM arise from the basic sizing hypothesis. The power consumption seasonality is not taken into consideration as only the minimum solar radiation and maximum energy demand values are considered. This may induce an even higher system's oversizing. Besides, the oversizing, especially relevant in high-seasonality climates, increases the final cost, as well as the energetic and environmental costs. It also must be noticed that oversizing generates an energy excess which is not used for consumption or battery charge, is discarded.

5.2.2. Loss of load probability sizing method

An alternative to the Worst Month method sizing system is the Load Probability method, LLP, proposed by several authors [147][148][149][150] to offer a solution to the WMM limitations. The LLP method define the PV systems in terms of reliability as the ratio between the energy deficit and the energy demand considered in terms of charge and for a determined PV system operation time (Eq. 5.39).

$$LLP = \frac{\int_t \text{Energy deficit}}{\int_t \text{Energy demand}} > 0 \quad \text{Eq. 5.39}$$

To allow a simple comparison of the LLP method with the WMM, the array capacity (C_A, Eq. 5.40) and the battery system capacity (C_S, Eq. 5.41) for a given time interval (usually, from daily to annual basis), are defined in a similar form than previously. After, and to apply the LLP method, the sizing procedure is as follows:

1. The maximum simultaneous consumption, *L*, of the projected installation is calculated. This consumption will be equal to a C_s=1, it is, the energy for a QE=1.
2. The array capacity, calculated with the WMM, is equivalent to C_A=1, it is, the number of modules enough to provide energy for one day.

$$C_A = \frac{\eta\, A\, S\, G_d}{L} \qquad \text{Eq. 5.40}$$

$$C_s = \frac{C}{L} \qquad \text{Eq. 5.41}$$

In the C_A and C_S equations, Eq. 5.40 and Eq. 5.41, η is the array efficiency, A is the required number for modules (Eq. 5.36), S is the surface of each module, G_d is the average daily irradiation, C is the daily battery capacity (Eq. 5.37) and L is the average daily energy demand.

From these definitions it can be seen that increasing the PV system size will improve the system's reliability and, thus, decrease the LLP value. But, at the same time, this system's oversizing increases the associated costs.

Table 5.21. Most common LLP values [34]

Energy application	LLP value	System reliability
Domestic illumination	10^{-1}	90 %
Home appliances	10^{-2}	99 %
Telecommunication systems	10^{-4}	99,99 %

Therefore, the basic hypothesis of the LLP method is that the PV system reliability can be fixed. The most commonly used LLP values are presented in Table 5.21.

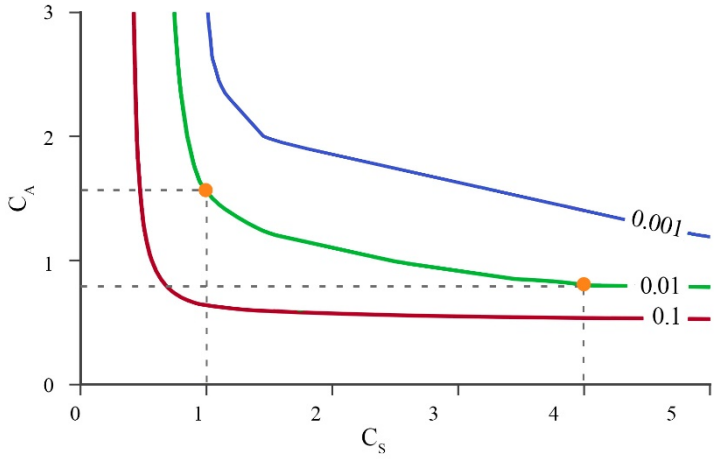

Figure 5.53. Isoreliability curves for different LLP values

For a fixed reliability value, the (C_S, C_A) pairs represent an **isoreliability curve.** Figure 5.53 shows an example of typical isoreliability curves for different LLP values. As an example, for the LLP=0.01 isoreliability curve, the same reliability would be obtained with the (4, 0.8) pair than with the (1, 1.6). For a PV system, this result implies that the 99% reliability can be obtained with 4 units of battery capacity, C_S, and 0.8 units of PV array, C_A, with 1 unit of C_S and 1.6 units of C_A, or with any (C_S, C_A) pair along the curve. This flexibility in terms of system configuration allows selecting the optimal (C_S, C_A) pair along the isoreliability line.

There are different approaches to the LLP method [149][150][151], but the most common are based on numerical methods [147][152] defined with the battery system state of charge after a given day *j*. The main assumptions of the method, regardless the authors, are:

- The energy demand, *L*, is constant and provided by the battery system.
- For the solar radiation values, the average value on the selected time basis is considered.

When considering the energy deficit for a given time interval, the LLP can be defined as in Eq. 5.42, where the numerator represents the total energy deficit on the considered time interval, N.

$$LLP = \frac{\sum_{j=1}^{N} E_D(j)}{N} \qquad \text{Eq. 5.42}$$

Several authors provide a solution type as Eq. 5.43 by using model-based solar radiation values and fixed energy demands [147][149]. The *a* and *b* coefficients are function of the LLP value and depend on the climate and location. For a fixed LLP value and with the production-consumption values, these parameters can be determined for a given location on the desired time basis.

$$C_A = a\, C_S^{\,-b} \qquad \text{Eq. 5.43}$$

A simplification of this method, provided by Zanesco et al.[153], uses a simple system to calculate the *a* and *b* coefficients with the location's latitude and the clearness index, K_T, limited to 0.1 and 0.01 LLP values.

Therefore, and according with the economic and environmental constraints for the installation's location in the design moment, this method allows to choose the optimal solution by varying the array or battery system size. This flexibility permits the designer to adapt the sizing in economic terms. It must be noticed that the optimal configuration depends on market variations or other external parameters such as legislation. Despite this advantage with respect to the Worst Month method, the environmental analysis is not considered.

5.3. METHODOLOGY

One of the main limitations of the LLP sizing studies is the use of the hypothesis that energy production and demand are constant values. These hypotheses are also used over daily values. Thus, the production and demand along the day are ignored, but this variability may affect to the battery system capacity requirements.

Most authors consider a constant energy demand through 24 hours a day [148][154][155], while others only consider the day-time [156] or nigh-time [157] power demands. The study of different energy demand profiles is limited to simple profile variations [158][159]. No real energy demand or seasonal climate variation have been used for the LLP evaluation.

The sizing of a PV system allows using different time intervals for the radiation and energy demand values, from daily to an annual basis. But improving the sizing method requires to define the optimal (C_S, C_A) pair after analysing the solar irradiation resource and the energy demand in detail.

On this section, the different energy demands types and the empirical approach which led to a method proposal is presented. After, the developed program is presented, as well as the experimental power consumption and solar radiation data sources used for the analysis. With these values, the validity limits of some LLP methods are assessed and the proposed method is analysed. Also, additional applications of the methods are presented.

5.3.1. Power consumption types effect on the system sizing

The assumption of a constant energy demand on the LLP method does not reflect the real power consumption scenarios. Different energy demand profiles can appear on a PV system depending on the energy demand type, mode or frequency of use. The energy consumption can be classified according to its type, mode or frequency (Table 5.22), but also with the reliability:

- **Mode:** Depending on the energy demand value along the day, consumption modes can be classified as **constant** or **variable**.
- **Frequency of use:** Relies on the energy demand time interval. Thus, the frequency can be considered as **diurnal**, **nocturnal** or **continuous** if the consumption appears the 24 hours of the day.
- **Reliability:** Is defined as the system's failure probability and depends on potential restrictions derived from the installation's use. For the LLP method, this value is fixed by the system's designer as function of the acceptable failure rate of the installation (see Table 5.21).

Table 5.22. Decision table for optimal (C_S, C_A) pair selection as function of the consumption

Consumption type	Consumption mode	Consumption frequency
Constant type [CT] $C_S \approx 1$; $C_A \approx 1$	Constant mode [CM] $C_S \approx 1$; $C_A \approx 1$	Nocturnal or seasonal frequency [NF] [SF] $C_S >> 1$; $C_A > 1$
Variable type [VT] $C_S > 1$; $C_A > 1$	Peak mode [PM] C_S or $C_A \geq 1$ + %peak	Diurnal frequency [DF] $C_S < 1$; $C_A \approx 1$
Variable predictable type [VPT] C_S or $C_A \geq 1$ + %peak	Adaptable mode [AM] $C_S < 1$; $C_A \lesssim 1$	Continuous (daily) frequency [CF] $C_S \approx 1$; $C_A \approx 1$

Including the power demand variability in the system's sizing increases its difficulty. But the average energy demand is an extremely biased estimator as it does not allow to distinguish mainly diurnal or mostly nocturnal profiles.

Starting with the simplest demand profile, the constant continuous consumption where the optimal (C_S, C_A) pair is (1, 1), additional detailed information about the energy demand allows to predict the region of the optimal (C_S, C_A) pair. Meanwhile the diurnal profile allows to reduce the battery system, the nocturnal requires its increase.

But this analysis is also relevant since the most frequent stand-alone PV systems, the rural electrification installations and housing systems, show variable power demands. On these systems, uncontrolled energy demands or new appliances generate a variability. For them, the C_S and C_A values should be defined with the peaks of maximum energy demand. This evaluation is usually done after a historical data record.

Table 5.22 sums the different consumption types, modes and frequencies together with the tendency values of C_S and C_A. It is also included the abbreviation of each consumption. These profiles are presented over an LLP=0.1 typical isoreliability curve in Figure 5.54.

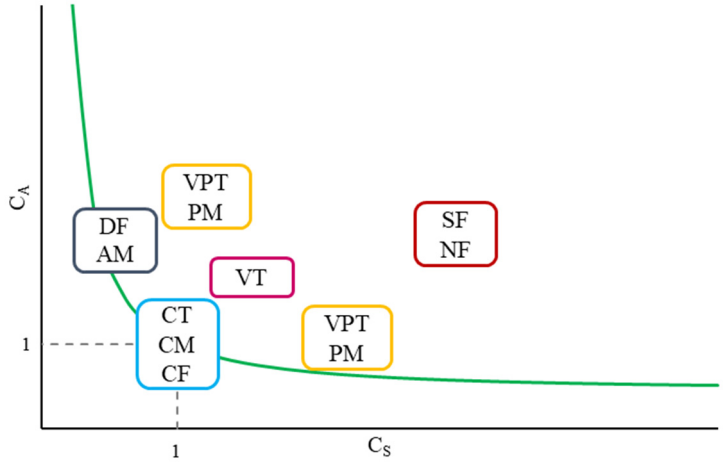

Figure 5.54. Prediction of region for optimal (C_S, C_A) pair range as function of consumption characteristics

5.3.2. Solar radiation effect on the system sizing

Similarly to the energy demand, the irradiation levels on the PV system's location allow to predict the optimal (C_S, C_A) pair region. In previous chapters, the solar radiation components and their relation with the different climates have been discussed. For this section, the diffuse fraction (Eq. 2.15) and the total number of dark days are the variables to consider.

Climates with high diffuse fraction values (Table 3.12) will require a greater array size as its production will be lower. But the DF values also affect to the battery system capacity. The overcast conditions account the number of total dark days, N_{TD}, and are directly applied to the battery system by making $QE=N_{TD}$.

Figure 5.55 shows the estimated region for the optimal (C_S, C_A) pair as function of the solar irradiation characteristics. These values are presented for an LLP=0.1 typical isoreliability curve. After the plot, it can be seen the WMM oversizing.

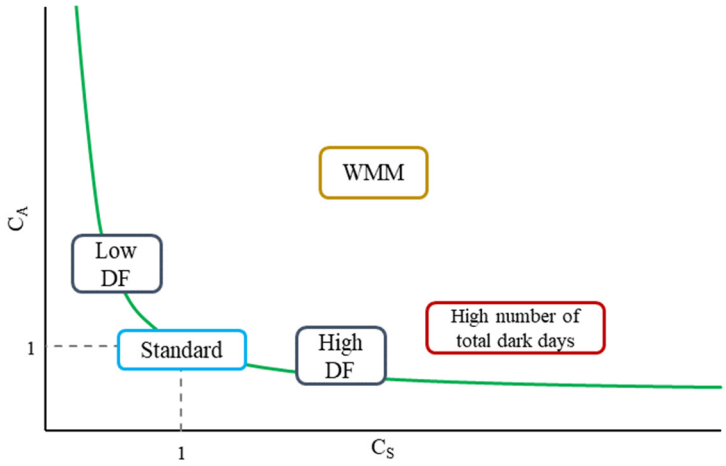

Figure 5.55. Prediction of region for optimal (C_S, C_A) pair range as function of available solar radiation

After the plots, the need of include the power demand variability (Figure 5.54) and the climate seasonality and cloudiness levels (Figure 5.55) in the stand-alone PV sizing procedure is stated. For it, a program to enhance the previous reliability-based LLP methods is developed. The program is used to analyse an experimental stand-alone PV system.

5.3.3. Experimental data source

The experimental power consumption data source is a single-family house in Vedra (Spain, coordinates 42.777; -8.459). The location has a *Cfb* climate (see Chapter 3, Section 3.3.2). The variable energy demand (Figure 5.56a) includes illumination and appliances. The solar radiation data source is the Meteogalicia's Sergude meteorological station in Boqueixón (Spain) [160], located 5 km far from the PV system. For the analysis, solar radiation values from 8 complete years are considered. Figure 5.56b shows the solar GHI values for the location, G_0. The climate seasonality can be seen after the solar radiation values variability.

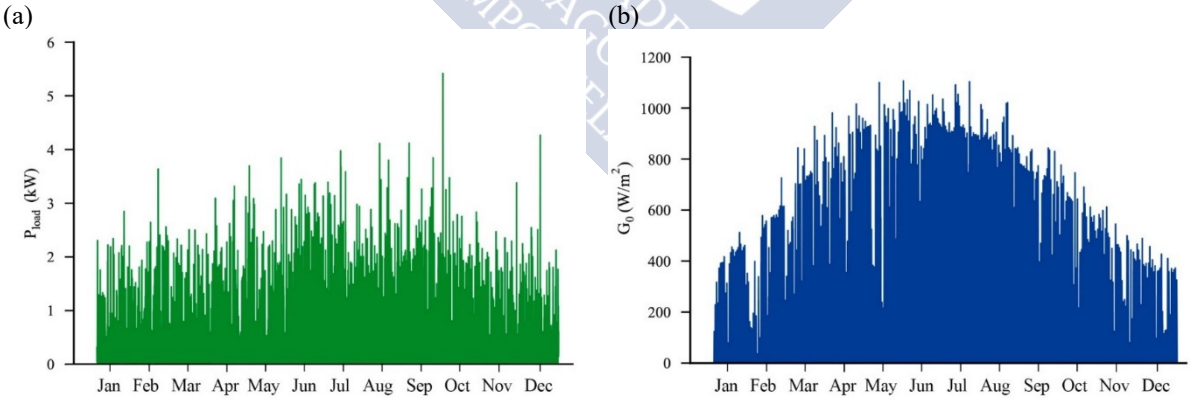

Figure 5.56. (a) Global horizontal radiation daily values and (b) daily experimental power load considered for the analysis

The house, disconnected from the national power grid in December 2015, was initially sized using the WMM with a QE=3 days for the battery system capacity calculation [161]. The PV system is equipped with a control system which provides the system's energy data.

The PV array is ground-mounted and installed with a fixed tilt β of 41º. It consists on 24 UMG modules (see Chapter 4, Section 4.2.1) plus a test unit. The battery system is composed

of 24 OPzS batteries, 660 Ah each, series-connected [142]. Additional information on the experimental setup is available on the published paper (Manuscript IV) [139].

5.3.4. Sizing method modelling

A program is developed to improve the existing LLP sizing methods. The program is based on the battery system's state of charge, SoC, and uses simple calculation procedures. The initial considerations are:

- The PV modules operate on the nominal output voltage, V_{no} (see Chapter 1, Section 1.1.3 for further details).
- The PV array energy production only depends on the incoming solar radiation at the array tilt β. The global radiation data for the analysis corresponds to the G_β value.

The considerations over the PV modules operation voltage and the global irradiation allow calculating the power production as expressed in Eq. 1.1. In addition, no temperature effects, battery ageing-associated or other system losses are considered.

The battery system's state of charge is defined as the ratio between the available energy at a given instant *j* and the total battery system capacity. At the end of a given time interval *t*, the state of charge can be calculated as the minimum value between 1 and the previously stored minus the *t*-interval energy consumption (Eq. 5.44).

$$SoC_t = \min\left(SoC_{t-1} + \frac{E_{DC}(t) - L(t)}{C}\,;1\right) \qquad \text{Eq. 5.44}$$

With this definition, two limit values appear for the battery's state of charge:

- SoC=0 appears when the battery system is in the minimum allowed state of charge to avoid deep discharge processes.
- SoC=1 corresponds to the fully charged battery system.

When the battery system is not able to fulfil the energy demand, the energy deficit for a specific time interval *t*, E_{def}, is defined as Eq. 5.45. This definition allows to calculate the Loss of Load Probability (Eq. 5.46). The simulation allows to obtain the isoreliability curves for the selected LLP values of each defined consumption type.

$$E_{def}(t) = [L(t) - E_{DC}(t)]\,\delta t - SoC_{t-1}\cdot C \qquad \text{Eq. 5.45}$$

$$LLP = \frac{\sum_t E_{def}(t)}{\sum_t L(t)} \qquad \text{Eq. 5.46}$$

The process begins with the irradiation, energy demand and time interval values. With this, the *L* and *G* values for the *t* timestep can be calculated. Starting with fixed C_S and C_A values, the simulation begins as SoC(t=0)=1. With the input data, the program calculates the SoC for every instant *t* as function of the *t-1* value and the energy demand plus the available radiation values on the instant *t*. Four different scenarios may appear depending on the battery system state of charge and the energy production and demand:

a) If $E_{DC}(t) > L(t)$, the SoC increases.
b) If the battery system is fully charged, SoC=1.
c) If $E_{DC}(t) < L(t)$, the SoC decreases.
d) If the battery system has no available energy, SoC=0 and the $E_{def}(t)$ has to be calculated.

The full process diagram is presented in Figure 5.57. The process is developed for 400 C_S values in the (0, 10] range and 200 C_A values in the (0, 5] interval. When the year is completed, the total energy deficits and energy demands can be obtained. With these values, the LLP value can be calculated following Eq. 5.46.

These values allow to build the isoreliability curves for the LLP values of interest of each power consumption type. The program allows to analyse tendencies and, as it allows to consider the economic and environmental constraints, the optimal (C_S, C_A) pair for a fixed reliability can be selected. Since a rude algorithm is used for the economic analysis [139], future market trends in modules and batteries can be analysed.

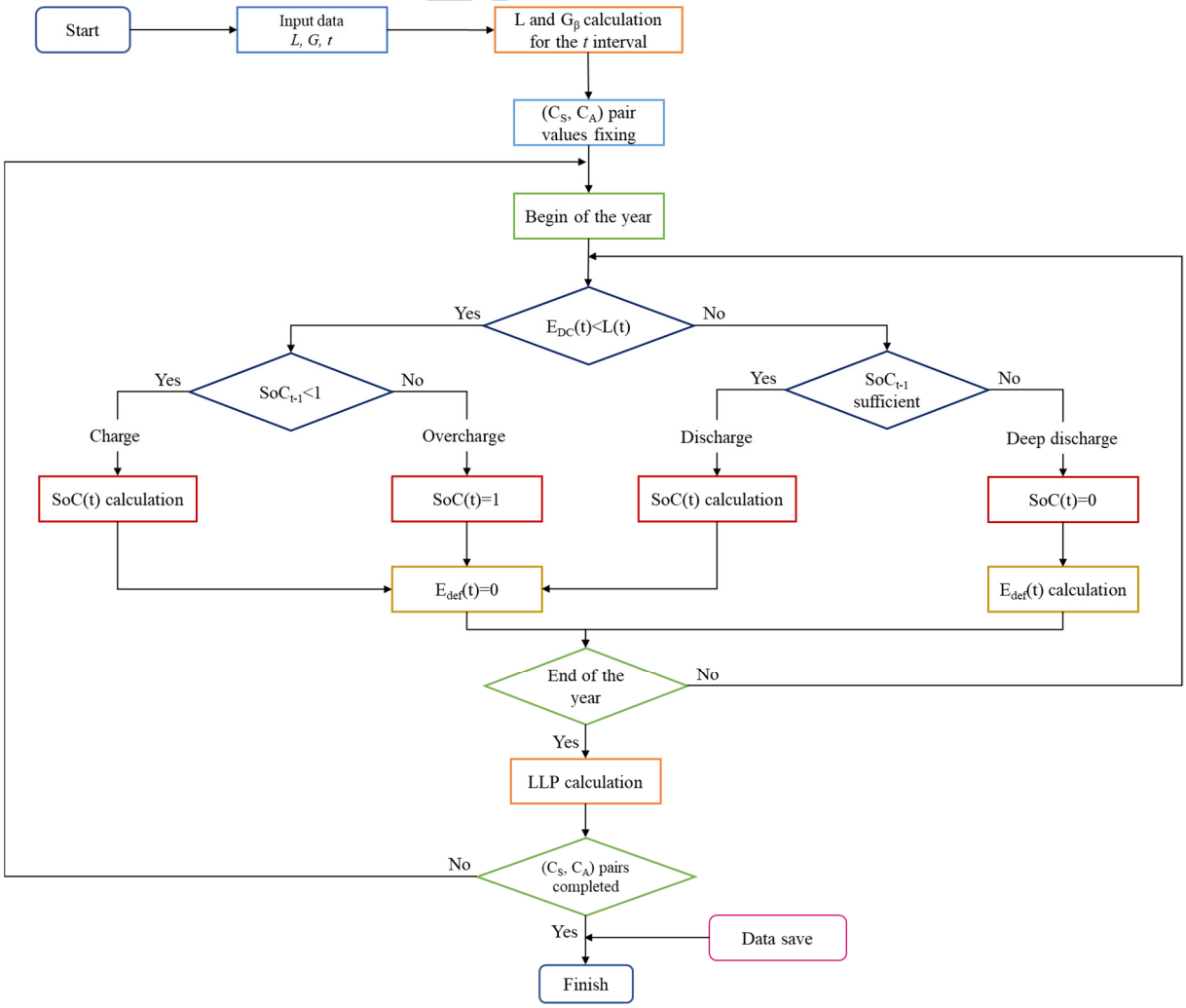

Figure 5.57. Simulation process diagram

As an example, Figure 5.58 shows the L and E_{def} as well as the SoC evolution of a 1-year period for a C_S=2 and C_A=1.5 fixed values. It can be seen how the battery system runs out of

available energy in December, February and June. While the winter energy deficit might be expected, the June deficit is due to a high energy demand after several consecutive overcast days.

From the simulation for a 2 days battery system capacity 50% oversizing in the array capacity with respect to the WMM results, the annual energy demands and solar radiation values are used. With this input data, a 97.5% reliability is calculated, it is, an LLP=0.025.

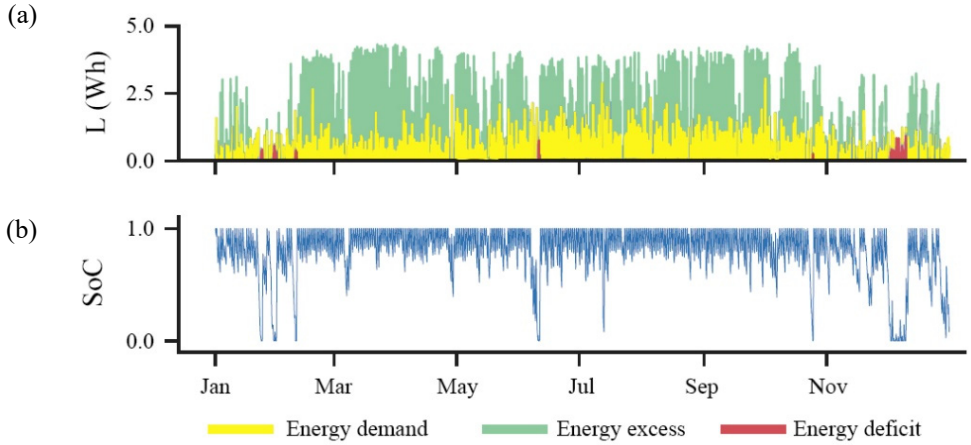

Figure 5.58. (a) Energy demand and production and (b) state of charge along a year

With this reliability, a high energy excess can be seen along almost all the year. This energy is product of the required system oversizing to fulfil the energy demand in low radiation periods. Only the winter season shows low energy surplus production.

The production deficits are related to the climatic variability, which is evaluated with simulations for the 8 years of solar radiation data. With these input data, the isoreliability lines for the selected LLP values are built for the different consumption types.

5.4. ADDITIONAL RESULTS

Besides to the published paper (Manuscript IV) [139], the developed program allowed to obtain additional results to be presented in this section. The proposed method is compared with the analytical methods previously discussed and its timestep limits are analysed. Also, complementary analysis to the published paper on the power consumption and the program application topics are presented.

The developed algorithm allows a rude analysis of the optimal (C_S, C_A) pair using the economic and/or energetic costs as constraint. Therefore, in addition to the published results for the cost analysis [139], the program permits analysing potential future market tendencies as well as evaluate a PV system for a given location using the local associated costs in the sizing moment.

5.4.1. Sizing method comparison with previous LLP methods

The energetic and economic costs analysis led to determine that, in the current energy transition paradigm and for the installation's location, minimizing the C_S value is required to ensure the PV system's sustainability (Manuscript IV) [139]. Against this backdrop, the

optimization of PV systems sizing tends to increasing the array capacity instead of the batteries capacity. This is even more advisable in highly irradiated regions (Figure 5.54). On this section, the low C_S values region is analysed with the developed method and the results are compared with the previously presented methods. It must be noticed that market trends may change the region of interest.

The Egido and Lorenzo method [147] uses model-based irradiation values on a daily basis for a nocturnal energy demand. With these inputs and for different LLP values, the *a* and *b* coefficients are calculated after simulations. These *a* and *b* coefficients are related to climatic variables.

The Zanesco et al. model offers a simplified calculation of *a* and *b* with two different methods [153]. These coefficients are obtained after simulations considering a continuous constant energy demand. The irradiation values are model-based. But this method has an additional model dependence as it uses the clearness index, K_T, a model-dependent value [162].

The isoreliability curves of the experimental setup are calculated for LLP=0.1 and LLP=0.01. The comparison of the Egido and Lorenzo [147] and the Zanesco [153] methods with the developed program is presented in Figure 5.59. While for high C_S values results are compatible, on the low C_S values region of interest, the existing methods do not present an adequate response to $C_S<1$ values. Therefore, even if these expressions [147][153] may appear as valid in a conservative sizing approach, with the current market trends, are inadequate as their associated-costs tend to maximise.

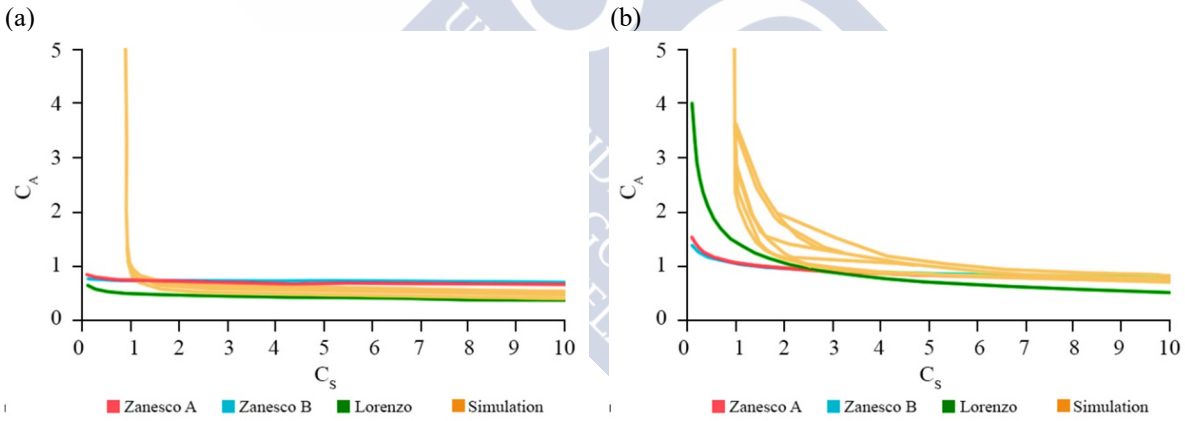

Figure 5.59. Isoreliability curves comparison of simulation and existing methods for (a) LLP=0.1 and (b) LLP=0.01

5.4.2. Iteration frequency

The developed program allows to calculate the isoreliability lines in a minute, 10-minute, hourly and daily time basis. The comparison of the daily isoreliability curves with the other time intervals (Figure 5.60) shows that the results are only compatible with high C_S values.

Therefore, it can be seen that the developed method requires, at least, hourly frequency values. Besides, only time frequencies below daily basis allow to separately analyse the energy demand during day or night-time and analyse the overcast conditions.

To extend this method to any location, the method's time range must be modified to provide the solution with few easily collected values.

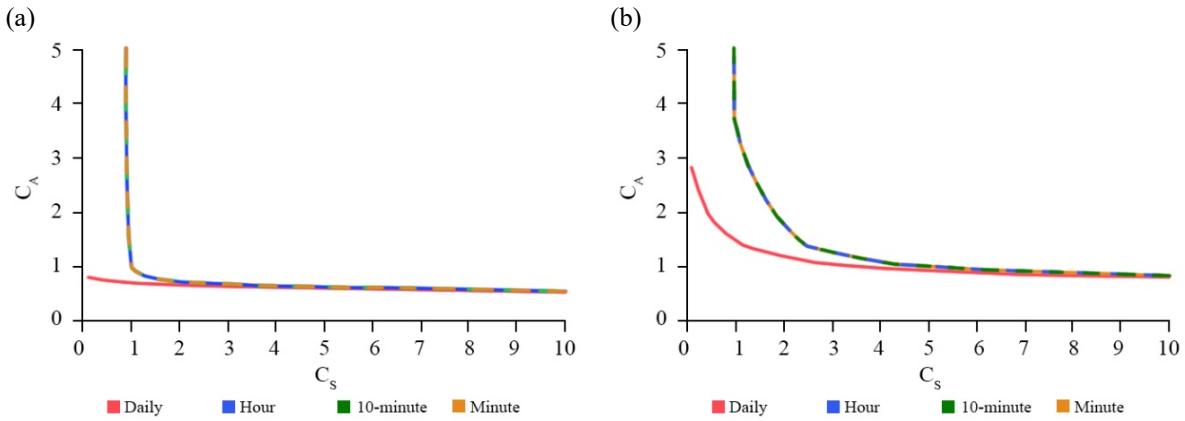

Figure 5.60. Program time basis results comparison for (a) LLP=0.1 and (b) LLP=0.01

5.4.3. Sensitivity to power consumption types

The effect of the different power consumption types in the developed LLP method is evaluated in the published paper (Manuscript IV) [139]. For a 90% system's reliability, the analysis shows a variation in the batteries system capacity of up to 6 times between the diurnal constant and the nocturnal variable consumption on the low C_S values region of interest in the current energy transition paradigm. But this topic deserves a complementary analysis comparing the results with the WMM sizing procedure.

For this analysis, the continuous, diurnal and nocturnal variable consumption type are obtained from the experimental setup. The constant power consumption types are created considering a constant value with a 1.14% noise. All the power consumption scenarios have an equal daily total consumption equal to *L* (Eq. 5.35).

The Figure 5.61, shows the method's capability to analyse different power consumptions in the low C_S region. Also, the increasingly required C_S value for the different power consumption types convergence with the increasing reliability can be visualized. While for a LLP=0.1 the different consumption types response tends to the equal curve with $C_S \approx 2$, this value increases up to $C_S \approx 6$ for the LLP=0.01. This C_S value increases even more when considering higher reliability values, but it has been determined that 99% reliability is the sensitivity limit for the method [139]. Values are presented in Table 5.23.

Table 5.23. C_S values of different reliability values for analysed consumption types

Reliability	C_S value for convergence	C_S variation between consumption types
90%	2	1
99%	6	1.5
99.9%	8	2

Also, the increasing width of the difference between the C_S values for different consumption types for a fixed reliability in the high C_A region can be assessed (Table 5.23). This increasing value shows the relevance of including the consumption type in the PV system's sizing.

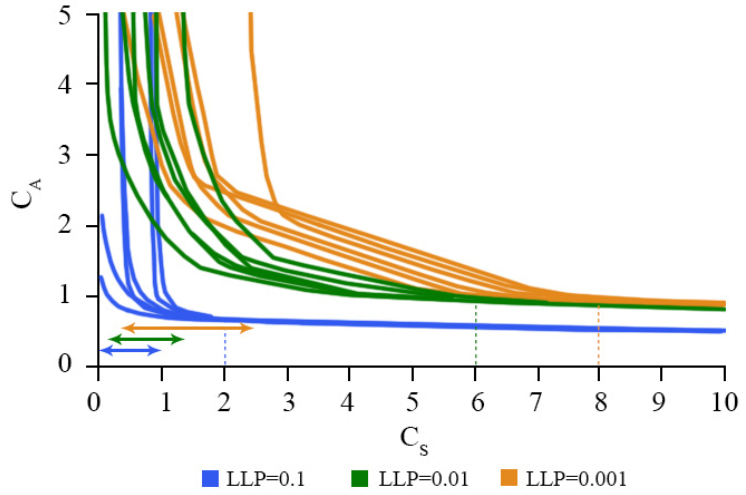

Figure 5.61. Isoreliability curves for (a) the different consumption types with LLP=0.1 and (b) for the consumption types with different LLP values

5.4.4. Additional method application

The developed program can be used for sizing new PV systems or analyse existing installations. When considering the design of a new system, the application of this method will allow increasing its sustainability by selecting the optimal (C_S, C_A) pair which, ensuring the selected reliability, minimizes the system's cost.

In addition to the published results (Manuscript IV) [139], numerically presented in Table 5.24, this method can be used to design the PV system's repowering or the system capability to withstand the ageing-associated losses.

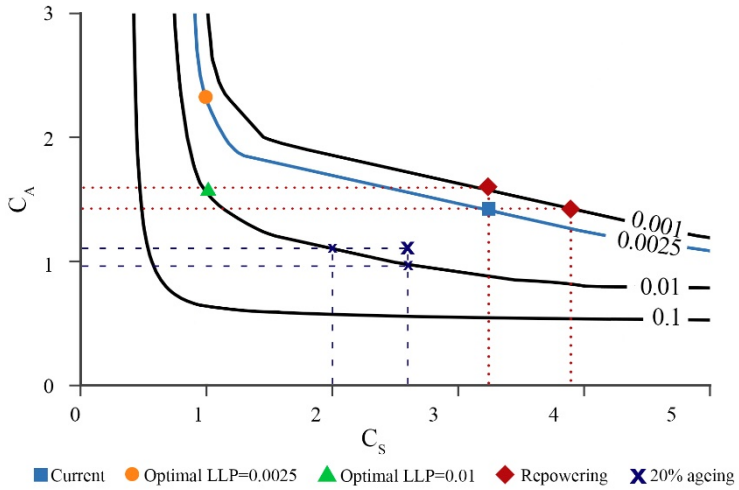

Figure 5.62. Example of optimal equivalent system for different PV system reliabilities

As previously stated, in the current energy transition paradigm and analysing the PV modules and batteries prices evolution, the low battery system capacity is the region of interest. However, this scenario depends on the installation's location technologies availability and is subject of potential variations in the future. Therefore, both C_S and C_A variations are assessed.

The **system repowering** is analysed in terms of the installation's reliability increase. For the analysed experimental setup, increasing the 99.75% reliability to an LLP=0.001 can be done by augmenting the PV array size or the battery system (Figure 5.62, red rhombus):

- Battery system: The (3.90, 1.41) pair increases the PV system reliability to the expected 99.9%. This can be obtained installing a 20% more batteries capacity.
- PV array: In the current energy transition paradigm and for the analysed system, this is the most sustainable approach. The expected 99.9% reliability repowering results in the (3.24, 1.65) pair and requires a 17% array size increase.

The **ageing of the PV system** can be also assessed with this method in terms of reliability after the expected lifetime. A 20% performance decrease for the array production and the batteries capacity at the end of the PV system lifetime is assumed for the analysis. For the analysed experimental setup, the 20% reduction in the array and batteries values lead to the (2.60, 1.13) pair (Figure 5.62, dark blue cross). This pair has a reliability over 99%.

As a 99% reliability is adequate for the experimental system's housing use (Table 5.21), the limit performance reductions in batteries or array size are analysed:

- For a 20% modules production reduction, up to a 38% batteries capacity decrease can be assumed. This reduction corresponds to the (2.00, 1.13) pair.
- For a 20% battery system capacity reduction, up to a 30% array capacity decrease will maintain the 99% reliability. The (0.98, 2.60) represents this reduction.

Therefore, in addition to determine the optimal (C_S, C_A) pair (Manuscript IV) [139], this program allows to find the optimal design for a PV system, analyse the system's repowering configurations and analyse the system's capacity to overcome the ageing process.

Table 5.24. Different available configurations for the experimental PV system in the current energy transition paradigm and for the installation's location

		(C_S, C_A) pair	**LLP value**
Current system configuration	■	(3.24, 1.41)	0.0025 (99.75%)
Same reliability PV design	●	(1.00, 2.35)	0.0025 (99.75%)
Recommended reliability for housing	▲	(1.00, 1.60)	0.01 99%
Reliability increase with modules	◆	(3.24, 1.65)	0.001 99.9%
Reliability increase with batteries	◆	(3.90, 1.41)	0.001 99.9%
20% ageing of PV system	X	(2.60, 1.13)	Over 0.01

Conclusions

The renewable energies play a key role in the climate change mitigation as its use decreases the greenhouse gas emissions and reduce the external energy dependence. The solar energy is one of the best candidates to lead the energy transition, mainly due to the high resource availability and competitive costs with conventional energy sources.

The analysis of the current photovoltaic, PV, market and its future perspectives shows its main strengths and expansion opportunities. The PV technology is characterised by its robustness and maturity level in the energy market. Its price competitiveness favours the PV expansion mainly because of its scalability; PV systems are suitable from small installations to large-scale centralized power generation systems.

However, on this growth scenario, the appearance of new solar panel technologies in early maturity level represent a threat and may pose a weakness for the adequate growth of the PV market. The multiple PV module technologies and increasingly sophisticated designs arising on the market have to be carefully assessed.

The motivation of this work is to provide answers to the questions that emerge from these innovations and its effect on the PV system's sustainability. To that end, and after experimental data, the design of both grid-connected and stand-alone PV systems is evaluated as well as the commercial PV technologies.

For the analysis of the optimal design of grid-connected PV systems, the suitability of installing a solar tracker on a PV system with respect to a fixed-tilt installation is evaluated. With an increasing market share for tracker systems, this analysis assesses the gain, in economic and energetic terms, of a tracker as function of the climate conditions.

The evaluation of the optimal PV technology as function of the climate conditions is crucial to ensure the PV system sustainability. Besides, the selection of the adequate technology minimizes the performance losses and maximizes the system's lifecycle.

The stand-alone PV systems sizing is focused on providing the optimal solution of the energy production-storage pair. This solution must ensure the required system's reliability as function of the consumption type and, the same time has to be economical and environmentally sustainable.

The versatility of PV systems allows multiple applications. Usually, two operation modes are defined; grid-connected systems, it is, centralised as power plants, or stand-alone systems. The second case applies to self-consumption and appears both in developed regions and in third countries.

Currently, the grid-connected centralized PV systems represent the largest portion of the PV systems in operation. On this work, the gain associated to designing a grid-connected PV

system with a tracker system has been assessed. For it, the diffuse fraction, DF, has been defined as the suitable variable for this analysis. The DF measures the cloudiness conditions as the ratio between the diffuse and the solar global radiation.

To avoid model-associated biased results, the work is based on experimental data. These data come from a grid-connected PV field located in Vilalba, Spain. The diffuse fraction values are calculated with experimental data from a close meteorological station.

The balance between the cost increase and the production gain of a tracker-equipped PV system compared to a fixed-tilt limits the maximum DF value to have a net gain for the tracker installation. This limit is, on average, 0.41±0.06. The standard deviation analysis of the experimental values makes that, with an 89% reliability, the DF value is in the [0.14, 0.68] interval.

This study gives rise to the generalization of the gain results of a tracker PV system as function of the climate conditions to any location. Due to the lack of DF experimental values worldwide, values from the NASA-SSE database have been used after validation with experimental data from AEMET.

The annual production of a tracker-equipped PV system compared to a fixed-tilt system has been evaluated. The results show gain values over 25% for all the climates. These values are compatible with the usually published of gains even higher than 40%. Including only the tracker-associated costs, all the climates show a positive response.

As an innovation to the previous studies, and inside the energy transition paradigm, the economic and environmental costs have been assessed. Thereby, the net gain of a tracker varies from a 27% to a -50%. The advised climates are mainly savannah, semi-arid, deserts, Mediterranean with hot summers and continental climates with dry and hot to temperate summers. It is observed that, as a general tendency, the installation of solar tracker systems is not advised for latitudes over 40º.

However, not only the system's design must be analysed for the PV systems optimization. The selection of an adequate PV modules technology is essential to ensure the most positive system's lifecycle. This topic must be analysed for all installation schemes.

To characterize the commercial PV technologies response both standard-operation and laboratory-controlled conditions have been used. For both setups, measurements were done under real sun conditions. The laboratory setup has allowed to separately control the module temperature and the solar irradiation. The other setup has been measured under standard operation conditions. The results comparison has enabled to characterise the analysed PV modules response and cross-check results.

The polycrystalline module technology has been established as optimal for desert and semi-arid climates, as well as for temperate/cold dry hot summer climates. This contradicts the common tendency of installing monocrystalline technologies in this type of climates. Intermediate radiation and temperature values allow both polycrystalline and monocrystalline to be selected. In low temperature and radiation scenarios, in addition to these technologies, the amorphous modules are also adequate. These results allow selecting the optimal PV technology

for any location once known its climate. For the PV technologies visualization, a map has been created to ease the use.

The experimental data analysis allowed to analyse the manufacturer's influence on the performance of same-technology, different-manufacturer PV modules. This evaluation, done for two polycrystalline arrays, showed almost a 9% difference between both arrays.

Despite grid-connected centralised systems are the most frequent PV system type, the current growth tendency is to stand-alone PV systems. These systems use batteries to ensure the power supply and are adequate for any climate, offering energetic independence to users in urban areas or isolated regions.

In addition to the calculation of the PV array and the batteries system, the suitable sizing of a stand-alone PV system requires to analyse the economic and environmental costs.

Two of the most frequent PV systems sizing methods have been evaluated; the worst month method and the Loss of Load Probability method, LLP, based on the system's reliability. Both pose hypotheses that do not allow to distinguish different power consumption types nor assess the PV system's sustainability.

A program has been developed to analyse the different power consumption types influence and the climate seasonality. This method, based on the battery state of charge, allows to calculate the system's reliability after experimental power consumption and irradiation data.

The method has allowed to define the sensitivity limit of the system's reliability as function of the climate conditions in a 99%. Besides, the analysis of different consumption types for a 90% reliability measures a difference of up to 6 times more battery requirements comparing constant diurnal and variable nocturnal energy demands.

The algorithm developed for economic and energetic costs analysis allows to analyse future trends in PV modules and batteries costs, as well as adapt the results to the local constraints for any stand-alone PV system sizing.

In addition, a cost evaluation of the PV system has been done. For a 90% reliability, and comparing with the worst month method solution, the optimal solution for the PV array would be a 25% less and, for the battery system, 1.1 days instead of 3.

Furthermore, this method allows to analyse existing PV systems. For the considered installation, the same reliability solution with a cost reduction of 46% is found. Besides, this method allows to analyse the system's repowering for new demands in existing installations or to measure the PV system's capability to withstand the ageing-associated losses.

USC
UNIVERSIDADE
DE SANTIAGO
DE COMPOSTELA

Conclusiones

Las energías renovables juegan un papel fundamental en la mitigación de cambio climático ya que su uso reduce las emisiones de gases de efecto invernadero y disminuye la dependencia energética externa. La energía solar es una de las mejores candidatas para liderar la transición energética, principalmente debido a la gran disponibilidad de recurso y su coste competitivo respecto de las fuentes de energía convencionales.

Un análisis del actual mercado fotovoltaico, PV, y su previsión de futuro muestra sus principales fortalezas y oportunidades de expansión. La tecnología fotovoltaica se caracteriza por su robustez y su nivel de madurez en el mercado. Su competitividad en términos de precios ha generado la oportunidad de expandir la tecnología fotovoltaica por su capacidad de escalabilidad. Los sistemas PV son adecuados tanto para pequeñas instalaciones como para sistemas de generación centralizados a gran escala.

Pero en este escenario de crecimiento, la aparición de nuevas tecnologías comerciales en fase temprana de maduración representa una amenaza y puede suponer una debilidad para el adecuado crecimiento del mercado fotovoltaico. Las múltiples tecnologías de módulos PV y diseños de sistemas cada vez más sofisticados que han surgido en el mercado han de ser cuidadosamente evaluados.

El objetivo de este trabajo es ofrecer respuesta a las cuestiones que surgen a partir de estas innovaciones y su efecto sobre la sostenibilidad de los sistemas PV. Para ello, y a partir de datos experimentales, se evalúan los diseños de sistemas PV, tanto conectados a red como aislados, así como las tecnologías PV existentes en el mercado.

Para el estudio del diseño óptimo de sistemas PV conectados a red se estudia la idoneidad de la instalación de sistemas equipados con tracker respecto a sistemas instalados a ángulo fijo. Con una creciente presencia de estos sistemas en el mercado PV, este análisis evalúa la rentabilidad, en términos económicos y energéticos, de un tracker en función de las condiciones climáticas.

La evaluación de la selección de la tecnología PV óptima en función de las condiciones climáticas es crucial para asegurar la sostenibilidad del sistema PV. Además, la selección de la tecnología adecuada minimiza las pérdidas de rendimiento y maximiza el ciclo de vida del sistema.

El análisis del dimensionado de sistemas PV aislados se centra en la ofrecer la solución óptima del par producción-acumulación de energía. Esta solución ha de asegurar la fiabilidad requerida para el sistema en función del tipo de consumo y, al mismo tiempo, ha de ser económica y medioambientalmente sostenible.

La versatilidad de las instalaciones PV hace que puedan tener múltiples aplicaciones. En particular suelen establecerse dos modos de funcionamiento; conectadas a red, es decir

centralizadas como una central eléctrica, o aisladas. Este segundo caso se aplica al autoconsumo y se presenta tanto en sociedades desarrolladas como en países terceros.

El mayor porcentaje de sistemas PV instalados en la actualidad corresponde a sistemas conectados a red. En el presente trabajo se ha evaluado la rentabilidad de diseñar un sistema PV conectado a red con seguidor solar. Para ello, se ha utilizado la fracción de difusa, DF, como la variable adecuada para este análisis. La DF mide las condiciones de nubosidad como el cociente entre radiación difusa y global.

Para evitar sesgos asociados al uso de modelos, el trabajo está basado en datos experimentales. Estos datos proceden de una instalación PV conectada a la red eléctrica y ubicada en Vilalba, España. Los valores de fracción de difusa provienen también de datos experimentales de una estación meteorológica cercana.

El balance entre el incremento de costes y la ganancia en producción de un sistema PV equipado con tracker respecto de uno a ángulo fijo limita el valor máximo de DF para tener rentabilidad por instalar un tracker. Esto se produce, en promedio, a un valor de DF de 0.41±0.06. El análisis de la desviación estándar de los datos experimentales hace que, con un 89% de fiabilidad, este valor de DF se encuentre en el intervalo [0.14, 0.68].

Este estudio da pie a la generalización de resultados de rentabilidad de un sistema con tracker en función de las condiciones climáticas a nivel mundial. Debido a la ausencia de valores experimentales de DF a nivel mundial, se han usado valores procedentes de la base de datos NASA-SSE previamente validada con datos experimentales procedentes de AEMET.

Se ha evaluado la producción anual del sistema PV con tracker respecto de uno a ángulo fijo. Los resultados obtenidos son de ganancias superiores al 25% para todos los climas. Estos valores son compatibles con los habitualmente publicados de ganancias superiores incluso al 40%. Incluyendo solo los costes económicos asociados al tracker, todos los climas muestran un comportamiento positivo.

Como innovación a los estudios anteriores, y dentro del nuevo paradigma de transición energética, se han evaluado los costes económicos y medioambientales asociados. Así, la ganancia neta de instalar un tracker varia con los climas desde un 27% a un -50%. Los climas recomendados corresponden principalmente a climas de sabana, semiáridos, desérticos, mediterráneos con veranos cálidos y continentales con veranos secos, tanto cálidos como templados. Se observa que, en general, la instalación de sistemas de seguimiento solar es poco recomendable en latitudes superiores a 40°.

Sin embargo, no solo el diseño del sistema se ha de analizar para optimizar un sistema PV. La adecuada selección de la tecnología de módulos PV es esencial para asegurar el ciclo de vida más positivo del sistema. Este aspecto ha de ser analizado para todo tipo de instalaciones.

Para caracterizar la respuesta de las tecnologías PV comerciales se han utilizado tanto condiciones reales de funcionamiento como condiciones controladas en el laboratorio. En ambos casos las medidas se han realizado en condiciones de sol real. El montaje de laboratorio ha permitido controlar la temperatura de módulo y la irradiación solar de forma separada. El otro sistema se ha medido en condiciones de operación estándar. La comparación de los

resultados ha permitido determinar el comportamiento de los módulos PV analizados y validar los resultados.

Se ha establecido la tecnología policristalina como óptima para climas desérticos y semiáridos, además de para climas con veranos cálidos secos. Esto contradice la tendencia habitual de instalar tecnologías monocristalinas en este tipo de climas. Valores de radiación y temperatura intermedios permiten que tanto la tecnología policristalina como la monocristalina sean aptas. En escenarios de baja temperatura y radiación, además de estas, la tecnología amorfa será adecuada. Estos resultados permiten seleccionar la tecnología óptima para cualquier ubicación conocido su clima. Para la visualización de tecnologías PV se ha realizado un mapa de fácil utilización.

El análisis de los datos experimentales ha permitido ver la influencia del fabricante en el rendimiento de módulos de misma tecnología y distinto fabricante. Esta evaluación, realizada sobre dos arrays de tecnología policristalina, muestra una diferencia de casi un 9% en el rendimiento de ambos arrays.

A pesar de que los sistemas centralizados conectados a red son el tipo de instalación PV más frecuente, actualmente la tendencia de crecimiento es hacia sistemas PV aislados. Estos sistemas utilizan baterías para asegurar el suministro eléctrico y resultan adecuados para cualquier zona climática, ofreciendo independencia energética a los usuarios tanto en entornos urbanos como en regiones aisladas.

Además del cálculo del tamaño del array PV y del sistema de baterías, el adecuado dimensionado de un sistema PV aislado requiere el análisis de los costes económicos y medioambientales.

Se han evaluado dos de los métodos de dimensionado de sistemas PV más comunes; el método del peor mes y el basado en fiabilidad LLP, *Loss of Load Probability*. Ambos plantean hipótesis que no permiten diferenciar distintos tipos de consumo ni evalúan la sostenibilidad del sistema PV.

Se ha desarrollado un programa que permite analizar el efecto de diferentes tipos de consumo y la estacionalidad climática. Este método, basado en el estado de carga de las baterías, permite calcular la fiabilidad del sistema PV a partir de datos experimentales de consumo e irradiación.

Este método ha permitido definir el límite de sensibilidad de la fiabilidad del sistema en función de las condiciones climáticas en un 99%. Además, el análisis de diferentes tipos de consumo para una fiabilidad del 90% determina una diferencia de hasta 6 veces en las necesidades de acumulación entre consumos constantes diurnos y variables nocturnos.

El algoritmo desarrollado para el análisis de costes económicos y energéticos permite analizar futuras tendencias en costes de módulos PV y baterías, así como adaptar los resultados a las restricciones locales para el dimensionado de cualquier sistema PV aislado.

Además, se ha realizado un análisis de los costes del sistema. Para una fiabilidad del 90%, y respecto de la solución definida con el método del peor mes, la solución óptima para el campo de producción PV sería un 25% menor y, para el sistema de baterías, 1.1 en lugar de 3 días.

Adicionalmente al uso para diseño de sistemas PV nuevos, este método permite analizar sistemas PV existentes. Para la instalación considerada, se ha encontrado una configuración con igual fiabilidad con una reducción de costes del 46%. Además, este método permite analizar la repotenciación del sistema para nuevos usos en instalaciones existentes o para evaluar la capacidad del sistema PV para asumir las pérdidas asociadas al envejecimiento.

To be done

The analysis of the optimal design of PV systems as function of the economic and energetic costs provides a simple method to primarily assess the most suitable PV array racking system for a given location. Thus, this method would allow developing an application for the optimal racking system of a PV array after the system's coordinates and a limited number of input values.

The optimal PV technology as function of the climate conditions offers a climate-based decision table for the optimal module technology selection. But, in addition, this analysis shows a clear line of research on the PV modules degradation; the evaluation of the influence of the solar cell's substrate and the epoxy encapsulants on the degradation mechanisms. This research would involve both solar photovoltaics companies and research centres.

The developed LLP sizing method offers promising results both for PV system's sizing and for existing system's analysis. This method offers the possibility of developing a program to improve the current program but maintaining the required variability analysis on climate and consumption. Furthermore, the program should include the additional PV system elements and its costs. Therefore, this would be an interdisciplinary project involving researchers, economists and industrial development centres.

USC
UNIVERSIDADE
DE SANTIAGO
DE COMPOSTELA

Bibliography

[1] G. H. Brundtland, "Our Common Future: Report of the World Commission on Environment and Development," *United Nations Comm.*, vol. 4, no. 1, p. 300, 1987.

[2] United Nations, "History of SD: What is sustainable development - Sustainable Development Commission." [Online]. Available: http://www.sd-commission.org.uk/pages/history_sd.html. [Accessed: 12-Mar-2018].

[3] United Nations, "UN Conference on Environment and Development (1992)," *United*, 1992. [Online]. Available: http://www.un.org/geninfo/bp/enviro.html. [Accessed: 12-Mar-2018].

[4] "World Summit on Sustainable Development," 2002. [Online]. Available: http://www.un.org/events/wssd/summaries/envdevj1.htm. [Accessed: 12-Mar-2018].

[5] United Nations, "The Millennium Development Goals Report," *United Nations*, p. 72, 2015.

[6] UNDP (United Nations Development Programme), "Sustainable Development Goals."

[7] UNDP (United Nations Development Programme), "Transforming our world: The 2030 agenda for sustainable development," 2015.

[8] O. Edenhofer, R. Pichs Madruga, and Y. Sokona, *Renewable Energy Sources and Climate Change Mitigation (Special Report of the Intergovernmental Panel on Climate Change)*, vol. 6, no. 4. 2012.

[9] IEA (International Energy Agency), "Chapter 1: Introduction and scope," in *World Energy Outlook 2017*, 2017, p. 782.

[10] "Download free solar resource maps | Solargis." [Online]. Available: http://solargis.com/products/maps-and-gis-data/free/download/world. [Accessed: 04-Feb-2017].

[11] NASA, "Earth at Night," 2017. [Online]. Available: https://www.nasa.gov/topics/earth/earthday/gall_earth_night.html. [Accessed: 19-Dec-2017].

[12] R. M. Swanson, "A Vision for Crystalline Silicon Photovoltaics," *Prog. Photovoltaics Res. Appl.*, vol. 14, pp. 443–453, 2006.

[13] IRENA, *Renewable Power Generation Costs in 2017*. 2018.

[14] ISE (Fraunhofer Institute for Solar Energy Systems), "Photovoltaics Report 2017," 2017.

[15] "Price Quotes - EnergyTrend PV." [Online]. Available: https://pv.energytrend.com/pricequotes.html. [Accessed: 28-Feb-2018].

[16] Zachary Shahan, "Solar Panel Cost Trends," 2014. [Online]. Available: https://cleantechnica.com/2014/09/04/solar-panel-cost-trends-10-charts/. [Accessed: 28-Feb-2018].

[17] V. V. Tyagi, N. A. A. Rahim, N. A. Rahim, and J. A. L. Selvaraj, "Progress in solar PV technology: Research and achievement," *Renew. Sustain. Energy Rev.*, vol. 20, pp. 443–461, 2013.

[18] J. Y. Ye, T. Reindl, A. G. Aberle, and T. M. Walsh, "Performance degradation of various PV module technologies in tropical Singapore," *IEEE J. Photovoltaics*, vol. 4, no. 5, pp. 1288–1294, 2014.

[19] M. E. Başoŀlu, A. Kazdaloŀlu, T. Erfidan, M. Z. Bilgin, and B. Cąkir, "Performance analyzes of different photovoltaic module technologies under ̄zmit, Kocaeli climatic conditions," *Renewable and Sustainable Energy Reviews*, vol. 52. pp. 357–365, 2015.

[20] A. Öztürk, S. Alkan, U. Hasirci, and S. Tosun, "Experimental performance comparison of a 2-axis sun tracking system with fixed system under the climatic conditions of Düzce, Turkey," *Turkish J. Electr. Eng. Comput. Sci.*, vol. 24, no. 5, pp. 4383–4390, 2016.

[21] M. De Simón-Martín, C. Alonso-Tristán, and M. Díez-Mediavilla, "Sun-trackers profitability analysis in Spain," *Prog. Photovolt Res. Appl.*, vol. 22, no. February 2013, pp. 1010–1022, 2013.

[22] United Nations, "Paris Agreement," *Conf. Parties its twenty-first Sess.*, no. December, p. 32, 2015.

[23] OECD/IEA and IRENA, "Perspectives for the Energy Transition: Investment Needs for a Low-Carbon Energy System," *Int. Energy Agency*, p. 204, 2017.

[24] REN21, "Renewables 2017 Global Status Report," Paris, 2017.

[25] C. Honsberg and S. Bowden, "The photovoltaic effect | PVEducation." [Online]. Available: http://pveducation.org/pvcdrom/solar-cell-operation/the-photovoltaic-effect. [Accessed: 19-Feb-2018].

[26] R. Nave, "Photoelectric Effect." [Online]. Available: http://hyperphysics.phy-astr.gsu.edu/hbase/mod2.html. [Accessed: 19-Feb-2018].

[27] A. R. Jordehi, "Parameter estimation of solar photovoltaic (PV) cells: A review," *Renew. Sustain.*

Energy Rev., vol. 61, pp. 354–371, 2016.
[28] "Curso de Energía Solar Fotovoltaica: La célula solar." [Online]. Available: https://www.ujaen.es/investiga/solar/07cursosolar/home_main_frame/03_celula/01_basico/3_celula_04.htm. [Accessed: 19-Feb-2018].
[29] P. G. V. Sampaio and M. O. A. González, "Photovoltaic solar energy: Conceptual framework," *Renew. Sustain. Energy Rev.*, vol. 74, no. December 2016, pp. 590–601, 2017.
[30] J. Subtil Lacerda and J. C. J. M. Van Den Bergh, "Diversity in solar photovoltaic energy: Implications for innovation and policy," *Renew. Sustain. Energy Rev.*, vol. 54, pp. 331–340, 2016.
[31] J. Cormican, "Solar panels and voltage." [Online]. Available: http://www.sunforceproducts.com/Support Section/Solar Panel & Charge Controllers/The Basics of Solar Power for Producing Electricity.pdf. [Accessed: 13-Nov-2016].
[32] C. Honsberg and S. Bowden, "Short-Circuit Current | PVEducation." [Online]. Available: http://www.pveducation.org/pvcdrom/short-circuit-current. [Accessed: 16-Nov-2016].
[33] R. Arndt and R. Puto, "Basic understanding of IEC standard testing for photovoltaic panels," *... [2012]. Http//Tuvamerica. Com/Services/Photovoltaics/ ...*, no. 978, pp. 1–15, 2010.
[34] E. Lorenzo and E. L. Pigueiras, *Electricidad solar: Ingeniería de los sistemas fotovoltaicos*. Universidad Politécnica de Madrid, 1994.
[35] F. Lasnier and T. G. Lang, *Photovoltaic Engineering Handbook*. CRC Press, 1990.
[36] D. D. Milosavljević, T. M. Pavlović, and D. S. Piršl, "Performance analysis of a grid-connected solar PV plant in Nis, republic of Serbia," *Renew. Sustain. Energy Rev.*, vol. 44, pp. 423–435, 2015.
[37] A. M. Khalid, I. Mitra, W. Warmuth, and V. Schacht, "Performance ratio - Crucial parameter for grid connected PV plants," *Renew. Sustain. Energy Rev.*, vol. 65, pp. 1139–1158, 2016.
[38] SMA Solar Technology AG, "Performance ratio," pp. 1–9, 2015.
[39] Masakazu Ito, "Life Cycle Assessment of PV Systems," in *Crystalline Silicon - Properties and Uses*, P. S. Basu, Ed. 2011, p. 17.
[40] V. M. Fthenakis *et al.*, "Methodology Guidelines on Life Cycle Assessment of Photovoltaic Electricity," *Methodol. Guidel. Life Cycle Assess. Photovolt. Electr.*, vol. IEA PVPS T, no. 5454, p. International Energy Agency Photovoltaic Power Sys, 2011.
[41] A. Stoppato, "Life cycle assessment of photovoltaic electricity generation," *Energy*, vol. 33, no. 2, pp. 224–232, 2008.
[42] F. Cucchiella and I. Dadamo, "Estimation of the energetic and environmental impacts of a roof-mounted building-integrated photovoltaic systems," *Renew. Sustain. Energy Rev.*, vol. 16, no. 7, pp. 5245–5259, 2012.
[43] R. H. E. M. Koppelaar, "Solar-PV energy payback and net energy: Meta-assessment of study quality, reproducibility, and results harmonization," *Renew. Sustain. Energy Rev.*, vol. 72, no. August 2016, pp. 1241–1255, 2017.
[44] K. P. Bhandari, J. M. Collier, R. J. Ellingson, and D. S. Apul, "Energy payback time (EPBT) and energy return on energy invested (EROI) of solar photovoltaic systems: A systematic review and meta-analysis," *Renew. Sustain. Energy Rev.*, vol. 47, pp. 133–141, 2015.
[45] D. L. Talavera, G. Nofuentes, and J. Aguilera, "The internal rate of return of photovoltaic grid-connected systems: A comprehensive sensitivity analysis," *Renew. Energy*, vol. 35, no. 1, pp. 101–111, 2010.
[46] A. Audenaert, L. De Boeck, S. De Cleyn, S. Lizin, and J. F. Adam, "An economic evaluation of photovoltaic grid connected systems (PVGCS) in Flanders for companies: A generic model," *Renew. Energy*, vol. 35, no. 12, pp. 2674–2682, 2010.
[47] N. Jungbluth, M. Tuchschmid, and M. de Wild-Scholten, "Life Cycle Assessment of Photovoltaics: Update of ecoinvent data v2. 0," *ESU-services Ltd., 2008*, pp. 1–22, 2008.
[48] "GTM Research | Solar, Energy Storage, and Grid Edge Analysts | Greentech Media." [Online]. Available: https://www.greentechmedia.com/research/analysts#gs.uIkwAH8. [Accessed: 21-Jan-2018].
[49] S. Moskowitz, "The Global PV Tracker Landscape 2016: Prices , Forecasts , Market Shares and Vendor Profiles Table of Contents List of Figures," 2016.
[50] "Solar Tracker Market size worth over USD 27bn by 2024." [Online]. Available: https://www.gminsights.com/pressrelease/solar-tracker-market. [Accessed: 20-Jan-2018].
[51] J. Simon and G. Mosey, "Feasibility Study of Economics and Performance of Solar Photovoltaics at the Kerr McGee Site in Columbus , Mississippi," no. January. p. 47, 2013.
[52] B. Hammad, A. Al-Sardeah, M. Al-Abed, S. Nijmeh, and A. Al-Ghandoor, "Performance and economic comparison of fixed and tracking photovoltaic systems in Jordan," *Renew. Sustain. Energy Rev.*, vol. 80, no. September 2016, pp. 827–839, 2017.
[53] I. Sefa, M. Demirtas, and I. Çolak, "Application of one-axis sun tracking system," *Energy Convers.*

Manag., vol. 50, no. 11, pp. 2709–2718, 2009.
[54] G. C. Lazaroiu, M. Longo, M. Roscia, and M. Pagano, "Comparative analysis of fixed and sun tracking low power PV systems considering energy consumption," *Energy Convers. Manag.*, vol. 92, pp. 143–148, 2015.
[55] A. Bahrami, C. O. Okoye, and U. Atikol, "Technical and economic assessment of fixed, single and dual-axis tracking PV panels in low latitude countries," *Renew. Energy*, vol. 113, pp. 563–579, 2017.
[56] A. Bahrami, C. O. Okoye, and U. Atikol, "The effect of latitude on the performance of different solar trackers in Europe and Africa," *Appl. Energy*, vol. 177, pp. 896–906, 2016.
[57] F. M. Hoffmann, R. F. Molz, J. V. Kothe, E. Oscar Benitez Nara, and L. P. C. Tedesco, "Monthly profile analysis based on a two-axis solar tracker proposal for photovoltaic panels," *Renew. Energy*, 2017.
[58] C. O. Okoye, A. Bahrami, and U. Atikol, "Evaluating the solar resource potential on different tracking surfaces in Nigeria," *Renew. Sustain. Energy Rev.*, vol. 81, no. March 2016, pp. 1569–1581, 2018.
[59] C. Cabo Landeira and Á. López-Agüera, "PV Tracker System Net Gain Associated o the Local Climatic Conditions," *Int. J. Res. Appl. Sci. Eng. Technol.*, vol. 6, no. I, pp. 185–193, 2018.
[60] A. Braña Lopez, C. Cabo Landeira, A. Lopez Aguera, and R. Pernas Leiro, "Optimal PV technology selection depending on climatic conditions," *Int. J. Res. Appl. Sci. Eng. Technol.*, vol. 5, no. XI, pp. 2962–2970, 2017.
[61] Charles R. Landau, "Optimum Tilt of Solar Panels," 2015. [Online]. Available: http://www.solarpaneltilt.com/. [Accessed: 20-Jun-2017].
[62] M. J. Clifford and D. Eastwood, "Design of a novel passive solar tracker," *Sol. Energy*, vol. 77, no. 3, pp. 269–280, 2004.
[63] V. Sumathi, R. Jayapragash, A. Bakshi, and P. Kumar Akella, "Solar tracking methods to maximize PV system output – A review of the methods adopted in recent decade," *Renew. Sustain. Energy Rev.*, vol. 74, no. February, pp. 130–138, 2017.
[64] H. Mousazadeh, A. Keyhani, A. Javadi, H. Mobli, K. Abrinia, and A. Sharifi, "A review of principle and sun-tracking methods for maximizing solar systems output," *Renew. Sustain. Energy Rev.*, vol. 13, no. 8, pp. 1800–1818, 2009.
[65] "Solar tracker market expected to grow | Evolve India." [Online]. Available: http://evolveindia.in/blog/2015/10/24/solar-tracker-market-expected-to-grow/. [Accessed: 07-Feb-2018].
[66] "Norvento NED Factory - Google Maps." [Online]. Available: https://www.google.es/maps/place/NORVENTO+nED+FACTORY/@43.3138257,-7.664484,617m/data=!3m1!1e3!4m5!3m4!1s0x0:0xabf60b1d78967799!8m2!3d43.3151251!4d-7.6652384?hl=es. [Accessed: 01-Mar-2017].
[67] Ingeteam, "Ingecon Sun Smart 10 - 12,5 - 15 - 20 - 25 - 30." .
[68] Sunways, "Sunways Solar Inverter NT 10000 - NT 12000." .
[69] LiCor, "LI-COR LI-200S Pyranometer Sensor." p. 2, 2014.
[70] Meteogalicia, "Estacións meteorolóxicas: Consulta históricos." [Online]. Available: http://www2.meteogalicia.es/galego/observacion/estacions/estacionsHistorico.asp?Nest=10124&red=102&tiporede=&idprov=0. [Accessed: 20-Sep-2016].
[71] D. Y. Goswami, F. Kreith, and J. F. Kreider, *Principles of solar engineering (Second edition)*. Taylor & Francis Group, 2000.
[72] John A. Duffie and William A. Beckman, *Solar engineering of thermal processes (Third edition)*. John Wiley & Sons, 2006.
[73] S. A. S. Eldin, M. S. Abd-Elhady, and H. A. Kandil, "Feasibility of solar tracking systems for PV panels in hot and cold regions," *Renew. Energy*, vol. 85, pp. 228–233, 2016.
[74] Y. Hu and Y. Yao, "A methodology for calculating photovoltaic field output and effect of solar tracking strategy," *Energy Convers. Manag.*, vol. 126, pp. 278–289, 2016.
[75] B. Y. H. Liu and R. C. Jordan, "The interrelationship and characteristic distribution of direct, diffuse and total solar radiation," *Sol. Energy*, vol. 4, pp. 1–19, 1960.
[76] D. G. Erbs, S. A. Klein, and J. A. Duffie, "Estimation of the diffuse radiation fraction for hourly, daily and monthly-average global radiation," *Sol. Energy*, vol. 28, no. 4, pp. 293–302, 1982.
[77] R. E. Basher, "The correction of diffuse radiation measurements made with shade band apparatus," *Sci. Rep.*, vol. 5, p. 14, 1984.
[78] G. Stanhill, "Observation of shade-ring corrections for diffuse sky radiation measurements at the Dead Sea," *Q. J. R. Meteorol. Soc.*, vol. 111, no. 470, pp. 1125–1130, 1985.
[79] E. W. Weisstein, "Bessel's correction - Calculating the standard deviation with n-1 method." [Online]. Available: http://mathworld.wolfram.com/BesselsCorrection.html. [Accessed: 07-Nov-2017].
[80] S. Kivrak, M. Gunduzalp, and F. Dincer, "Theoretical and experimental performance investigation of a

two-axis solar tracker under the climatic condition of Denizli, Turkey," *Prz. Elektrotechniczny*, vol. 88, no. 2, pp. 332–336, 2012.
[81] N. A. Kelly and T. L. Gibson, "Improved photovoltaic energy output for cloudy conditions with a solar tracking system," *Sol. Energy*, vol. 83, no. 11, pp. 2092–2102, 2009.
[82] R. Fu *et al.*, "U.S. Solar Photovoltaic System Cost Benchmark: Q1 2016," *Natl. Renew. Energy Lab.*, no. September, p. 37, 2016.
[83] I. Edinbarough, "Experimental study on the optimum harvesting of sunlight for an efficient solar energy system," in *120th ASEE Annual Conference & Exposition*, 2013, p. 12.
[84] L. Guillon and D. Rousse, "An Experimental Validation of the Concept Critical Solar Radiation for Solar," *Int. J. Appl. Sci. Technol.*, vol. 5, no. 3, pp. 1–11, 2015.
[85] "GIS data and maps | Solargis." [Online]. Available: https://solargis.com/products/maps-and-gis-data/. [Accessed: 19-Dec-2017].
[86] NASA, "NASA SSE: Surface meteorology and Solar Energy." [Online]. Available: https://eosweb.larc.nasa.gov/sse/. [Accessed: 06-Jul-2017].
[87] "NASA Langley - POWER."
[88] AEMET, "Agencia Estatal de Meteorología - AEMET- Gobierno de España." [Online]. Available: http://www.aemet.es/es/portada. [Accessed: 07-Dec-2017].
[89] M. Kottek, J. Grieser, C. Beck, B. Rudolf, and F. Rubel, "World map of the Köppen-Geiger climate classification updated," *Meteorol. Zeitschrift*, vol. 15, no. 3, pp. 259–263, 2006.
[90] C. Cabo Landeira and Á. López-Agüera, "Net benefit evaluation method for solar tracker connected PV systems," *Int. J. Res. Appl. Sci. Eng. Technol.*, vol. 6, no. I, pp. 2638–2645, 2018.
[91] Norvento Enerxía, "NORVENTO – Un paso hacia tu independencia energética." .
[92] A. J. Arnfield, "Climate classification." [Online]. Available: https://www.britannica.com/topic/classification-1703397#ref284593. [Accessed: 21-Jan-2018].
[93] J. E. Oliver, *Encyclopedia of World Climatology*. Springer Science & Business Media, 2008.
[94] M. Belda, E. Holtanová, T. Halenka, and J. Kalvová, "Climate classification revisited: From Köppen to Trewartha," *Clim. Res.*, vol. 59, no. 1, pp. 1–13, 2014.
[95] "Thornthwaite's Classification." [Online]. Available: http://www.meteotemplate.com/template/plugins/climateClassification/thornthwait.php. [Accessed: 19-Jan-2018].
[96] R. E. Ricklefs, "The Biome Concept in Ecology," *Econ. Nat.*, pp. 87–112, 2008.
[97] D. Chen and H. W. Chen, "Using the Köppen classification to quantify climate variation and change: An example for 1901–2010," *Environ. Dev.*, vol. 6, pp. 69–79, Apr. 2013.
[98] M. Paulescu *et al.*, "Ångström-Prescott equation: Physical basis, empirical models and sensitivity analysis," *Renew. Sustain. Energy Rev.*, vol. 62, pp. 495–506, 2016.
[99] NREL, "NSRDB - National Solar Radiation Dababase Data Viewer." [Online]. Available: https://maps.nrel.gov/nsrdb-viewer/?aL=UdPEX9%255Bv%255D%3Dt%268VWYIh%255Bv%255D%3Dt%268VWYIh%255Bd%255D%3D1&bL=groad&cE=0&lR=0&mC=31.653381399664%2C-3.1640625&zL=2. [Accessed: 08-Dec-2017].
[100] PVgis, "PVGIS: Europe PV potential estimation utility." [Online]. Available: http://re.jrc.ec.europa.eu/pvg_tools/en/tools.html. [Accessed: 28-Aug-2017].
[101] The World Bank Group, "Global Solar Atlas." [Online]. Available: http://globalsolaratlas.info/?c=11.027472,9.448242,5&s=16.804541,0.74707. [Accessed: 08-Dec-2018].
[102] "Physical Solar Model (PSM) v3 API | NREL: Developer Network." [Online]. Available: https://developer.nrel.gov/docs/solar/nsrdb/psm3_data_download/. [Accessed: 08-Dec-2018].
[103] R. Perez *et al.*, "A new operational model for satellite-derived irradiances: Description and validation," *Sol. Energy*, vol. 73, no. 5, pp. 307–317, 2002.
[104] ECMWF, "ERA5 climate reanalysis." [Online]. Available: https://www.ecmwf.int/en/forecasts/datasets/reanalysis-datasets/era5. [Accessed: 08-Dec-2018].
[105] Hans-Ertel-Centre for Weather Research, "COSMO Regional Reanalysis - COSMO-REA6." [Online]. Available: http://reanalysis.meteo.uni-bonn.de/?Download_Data___COSMO-REA6. [Accessed: 08-Feb-2018].
[106] P. W. Stackhouse, W. S. Chandler, T. Zhang, D. Westberg, A. J. Barnett, and J. M. Hoell, "Surface meteorology and Solar Energy (SSE) Release 6.0 Methodology Version 3.2.0," *Nasa*, p. 76, 2016.
[107] C. H. Whitlock, P. W. Stackhouse, W. S. Chandler, J. M. Hoell, and T. Zhang, "Renewable energy applications from NASA satellite analysis and modeling," pp. 2–7, 2004.
[108] J. Sancho, J. Riesco, and C. Jiménez, *Atlas de Radiación Solar en España*. Ministerio de Agricultura,

Alimentación y Medio Ambiente, 2012.
[109] "CMSAF - Data Access." [Online]. Available: http://www.cmsaf.eu/EN/Data_Access/Data_Access_node.html;jsessionid=C633F596C5B29B342F0D2C680A8BE41D.live11293. [Accessed: 19-Jan-2018].
[110] CantyMedia, "Weatherbase - Travel Weather Averages." [Online]. Available: http://www.weatherbase.com/. [Accessed: 07-Sep-2017].
[111] CantyMedia, "Geoba.se: Gazetteer - The World at Your Fingertips." [Online]. Available: http://geoba.se/index.php. [Accessed: 08-Sep-2017].
[112] A. K. Pandey, V. V. Tyagi, J. A. Selvaraj, N. A. Rahim, and S. K. Tyagi, "Recent advances in solar photovoltaic systems for emerging trends and advanced applications," *Renew. Sustain. Energy Rev.*, vol. 53, pp. 859–884, 2016.
[113] ISE (Fraunhofer Institute for Solar Energy Systems), "Fraunhofer Institute for Solar Energy Systems Photovoltaic Report," 2017.
[114] E. Elibol, Ö. T. Özmen, N. Tutkun, and O. Köysal, "Outdoor performance analysis of different PV panel types," *Renew. Sustain. Energy Rev.*, vol. 67, pp. 651–661, 2017.
[115] G. Makrides, B. Zinsser, M. Norton, G. E. Georghiou, M. Schubert, and J. H. Werner, "Potential of photovoltaic systems in countries with high solar irradiation," *Renew. Sustain. Energy Rev.*, vol. 14, no. 2, pp. 754–762, 2010.
[116] C. L. de A. Dias, D. A. Castelo Branco, M. C. Arouca, and L. F. Loureiro Legey, "Performance estimation of photovoltaic technologies in Brazil," *Renew. Energy*, vol. 114, no. PB, pp. 367–375, 2017.
[117] I. de la Parra, M. Muñoz, E. Lorenzo, M. García, J. Marcos, and F. Martínez-Moreno, "PV performance modelling: A review in the light of quality assurance for large PV plants," *Renew. Sustain. Energy Rev.*, vol. 78, no. April, pp. 780–797, 2017.
[118] S. R. Williams, T. R. Betts, P. Vorasayan, R. Gottschalg, and D. G. Infield, "Actual PV module performance including spectral losses in the UK," *Photovolt. Spec. Conf.*, pp. 4–7, 2005.
[119] D. Sarti and R. Einhaus, "Silicon feedstock for the multi-crystalline photovoltaic industry," *Sol. Energy Mater. Sol. Cells*, vol. 72, no. 1–4, pp. 27–40, 2002.
[120] HT, "HT I-V400w Curve Tracer Datasheet." p. 3, 2015.
[121] Agencia Estatal de Meteorología, Ministerio de Medio Ambiente y Medio Rural y Marino de España (State Agency of Meteorology, and Ministry of the Environment and Rural and Marine Affairs of Spain), *Atlas Climático Ibérico (Iberian Climate Atlas)*. 2017.
[122] FLIR, "FLIR E50 Thermal Imaging Camera." .
[123] D. C. Jordan and S. R. Kurtz, "Photovoltaic degradation rates - An Analytical Review," *Prog. Photovoltaics Res. Appl.*, vol. 21, no. 1, pp. 12–29, 2013.
[124] "Photovoltaic Module Testing and Certification | WO | TÜV Rheinland." [Online]. Available: https://www.tuv.com/world/en/photovoltaic-modules.html. [Accessed: 17-Jan-2018].
[125] Wurth Solar, "The Haute Couture of Photovoltaics CIS Solar Modules Technical Data Sheet General technical data." .
[126] S. Saraiva, R. Melício, J. C. O. Matias, C. M. P. Cabrita, and J. P. S. Catalão, "Simulation and experimental results for a photovoltaic system formed by monocrystalline solar modules," *IFIP Adv. Inf. Commun. Technol.*, vol. 372 AICT, pp. 329–336, 2012.
[127] Suntech, "Suntech STP280-24/Vd datasheet." p. 2, 2011.
[128] M. Köntges *et al.*, *Review of Failures of Photovoltaic Modules*. 2014.
[129] I. Rodríguez Cabo, "El Proyecto Pierre Auger como Red de Sistemas Fotovoltaicos Aislados de Alta Estadística," *Tesis Dr. USC*, 2014.
[130] J. Sidawi *et al.*, "The effect of reverse current on the dark properties of photovoltaic solar modules," *Energy Procedia*, vol. 6, pp. 743–749, 2011.
[131] L. Cristaldi *et al.*, "Simplified method for evaluating the effects of dust and aging on photovoltaic panels," *Meas. J. Int. Meas. Confed.*, vol. 54, pp. 207–214, 2014.
[132] A. Rao, R. Pillai, M. Mani, and P. Ramamurthy, "Influence of dust deposition on photovoltaic panel performance," *Energy Procedia*, vol. 54, pp. 690–700, 2014.
[133] M. Almazroui, "Climatology and Monitoring of Dust and Sand Storms in the Arabian Peninsula." p. 31, 2013.
[134] J. Hoppmann, J. Volland, T. S. Schmidt, and V. H. Hoffmann, "The economic viability of battery storage for residential solar photovoltaic systems - A review and a simulation model," *Renew. Sustain. Energy Rev.*, vol. 39, pp. 1101–1118, 2014.
[135] E. McKenna, M. McManus, S. Cooper, and M. Thomson, "Economic and environmental impact of lead-acid batteries in grid-connected domestic PV systems," *Appl. Energy*, vol. 104, pp. 239–249, 2013.

[136] M. Hiremath, K. Derendorf, and T. Vogt, “Comparative life cycle assessment of battery storage systems for stationary applications,” *Environ. Sci. Technol.*, vol. 49, no. 8, pp. 4825–4833, 2015.
[137] E. Alsema, “Energy Payback Time and CO2 Emissions of PV Systems,” *Pract. Handb. Photovoltaics*, vol. 25, no. June 1999, pp. 1097–1117, 2012.
[138] K. Bataineh and D. Dalalah, “Optimal Configuration for Design of Stand-Alone PV System,” *Smart Grid Renew. Energy*, vol. 3, no. 2, pp. 139–147, 2012.
[139] C. Cabo Landeira, Á. López-Agüera, and F. Núñez Sánchez, “Loss of Load Probability method applicability limits as function of consumption types and climate conditions in stand-alone PV systems,” *Int. Res. J. Eng. Technol.*, vol. 5, no. 3, pp. 2036–2043, 2018.
[140] A. E. Pascual, “Sizing of stand - alone PV systems based on the ‘ worst month .’” ISF-Engineering without Borders, p. 13, 1998.
[141] IDAE, *Pliego de Condiciones Técnicas de Instalaciones Aisladas de Red*. Ministerio de Industria, Energía y Turismo, 2009.
[142] Victron Energy, “Off-Grid, Back-Up & Island Systems.” p. 96, 2017.
[143] *Instalaciones de Energía Solar - Tomo V: Sistemas de Conversión eléctrica*. CENSOLAR, 2008.
[144] N. H. Reich, E. A. Alsema, W. Van Sark, W. C. Turkenburg, and W. C. Sinke, “Greenhouse gas emissions associated with photovoltaic electricity from crystalline silicon modules under various energy supply options,” *Prog. Photovolt Res. Appl.*, vol. 19, no. January 2011, pp. 603–613, 2011.
[145] C. Breyer *et al.*, “Solar photovoltaics demand for the global energy transition in the power sector,” *Prog. Photovoltaics Res. Appl.*, no. September, pp. 1–19, 2017.
[146] Y. Lin, J. X. Johnson, and J. L. Mathieu, “Emissions impacts of using energy storage for power system reserves,” *Appl. Energy*, vol. 168, no. 784, pp. 444–456, 2016.
[147] M. Egido and E. Lorenzo, “The sizing of stand alone PV-system: A review and a proposed new method,” *Sol. Energy Mater. Sol. Cells*, vol. 26, no. 1–2, pp. 51–69, 1992.
[148] J. M. Gordon, “Optimal sizing of stand-alone photovoltaic solar power systems,” *Sol. Cells*, vol. 20, no. 4, pp. 295–313, 1987.
[149] L. Barra, S. Catalanotti, F. Fontana, and F. Lavorante, “Ananalytical method to determine the optimal size of a photovoltaic plant,” *Sol. Energy*, vol. 33, no. 6, pp. 509–514, 1985.
[150] B. Bartoli, V. Cuomo, F. Fontana, C. Serio, and V. Silvestrini, “The design of photovoltaic plants: An optimization procedure,” *Appl. Energy*, vol. 18, no. 1, pp. 37–47, 1984.
[151] A. Benatiallah, R. Mostefaoui, and M. Boubekri, “A Comparison of Simplified and Statistical Methods of Sizing Photovoltaic Installation for a Remote Dwelling in the Saharan Region,” *J. Human-Environmetal Syst.*, vol. 8, no. 1, pp. 1–6, 2005.
[152] I. Zanesco and D. E. Adriano Moehlecke, Tiago C. Severo, Silvio L.R. Santos Junior, Eduardo A. Zenzen, “Implementaçao e Análise de Sistemas Fotovoltaicos Autonomos,” *X Congr. Bras. Energ.*, vol. 1, pp. 530–541, 2004.
[153] I. Zanesco, A. Moehlecke, G. S. Medeiros, A. P. Mallmann, and S. Ponce-Alcantara, “Analytic Method for Sizing Stand-Alone PV Systems in Brazil,” no. January, 2004.
[154] L. L. Bucciarelli, “Estimating loss-of-power probabilities of stand-alone photovoltaic solar energy systems,” *Sol. Energy*, vol. 32, no. 2, pp. 205–209, 1984.
[155] T. Hove, “A method for predicting long-term average performance of photovoltaic systems,” vol. 21, 2000.
[156] D. Clark, S. Klein, and W. Beckman, “A method for estimating the performance of photovoltaic systems,” *Sol. Energy*, vol. 33, no. 6, pp. 551–555, 1984.
[157] S. A. Klein and W. A. Beckman, “Loss-of-Load probabilities for stand-alone photovoltaic systems,” vol. 39, no. 6, pp. 499–512, 1987.
[158] G. Notton, M. Muselli, P. Poggi, and A. Louche, “Autonomous photovoltaic systems : Influences of some parameters on the sizing : Simulation timestep, input and output power profile,” *Renew. Energy*, vol. 7, no. 4, pp. 353–369, 1996.
[159] A. N. Celik, “Effect of different load profiles on the loss-of-load probability of stand-alone photovoltaic systems,” *Renew. Energy*, vol. 32, no. 12, pp. 2096–2115, 2007.
[160] Meteogalicia, “Estacións meteorolóxicas: Consulta históricos Sergude (A Coruña).” [Online]. Available: http://www2.meteogalicia.gal/galego/observacion/estacions/estacionsHistorico.asp?Nest=10095&prov=A Coruña&tiporede=automaticas&red=102&idprov=0. [Accessed: 19-Jan-2018].
[161] J. Urrestarazu Olmos, “Estudio de un sistema fotovoltaico autónomo,” *Trab. Fin Máster. Máster en Energías Renov. y Sostenibilidad Energética. Fac. Física. Univ. Santiago Compost.*, p. 54, 2016.
[162] S. Dervishi and A. Mahdavi, “Computing diffuse fraction of global horizontal solar radiation: A model comparison,” *Sol. Energy*, vol. 86, no. 6, pp. 1796–1802, 2012.

Figure list

Table list